Developing Superhydrophobic Coatings for Mitigating Aircraft Icing using Plasma Spray Processes

Navid Sharifi

A Thesis

In the Department

of

Mechanical, Industrial and Aerospace Engineering

Presented in Partial Fulfillment of the Requirements

For the Degree of

Doctor of Philosophy (Mechanical Engineering) at

Concordia University

Montreal, Quebec, Canada

February 2018

CONCORDIA UNIVERSITY

School of Graduate Studies

This is to certify that the thesis prepared

By: *Navid Sharifi*

Entitled: *Developing Superhydrophobic Coatings for Mitigating Aircraft Icing using Plasma*
            Spray Processes

And submitted in partial fulfilment of the requirements for the degree of

Doctor of Philosophy (Mechanical Engineering)

Complies with the regulations of the University and meets the accepted standards with respect to originality and quality.

Signed by the final Examining Committee:

_____ Chair
Dr. S. Samuel Li

_____ External Examiner
Dr. Mohammad Jahazi

_____ External to Program
Dr. Michelle Nokken

_____ Examiner
Dr. Robin Drew

_____ Examiner
Dr. Mamoun Medraj

_____ Thesis Co-Supervisor
Dr. Ali Dolatabadi

_____ Thesis Co-Supervisor
Dr. Christian Moreau

_____ Thesis Co-Supervisor
Dr. Martin Pugh

Approved by: _____
               Dr. Ali Dolatabadi, Graduate Program Director

March 22nd, 2018   _____
                          Dr. Amir Asif, Dean
                          Faculty of Engineering and Computer Science

ABSTRACT

Developing Superhydrophobic Coatings for Mitigating Aircraft Icing using Plasma Spray Processes

Navid Sharifi, PhD
Concordia University, 2018

In-flight icing due to the presence of super-cooled water droplets is a major problem for aircraft operators. Accumulation of ice on the surface of wings, control parts and sensors can result in a range of problems including navigation issues, decreased efficiency, increasing fuel consumption, forced flight delays and cancelation and, if neglected or mismanaged, even fatal flight incidents. A significant potential solution for mitigating the icing problem is the use of superhydrophobic coatings i.e. coating that are extremely water repelling. Superhydrophobic coatings, by repelling the water droplets, can delay and in some cases prevent ice accumulation. Additionally, superhydrophobic coatings can facilitate ice removal by heating or vibration due to their non-stick properties. The superhydrophobicity of a surface is a result of the combination of the surface micro-texture and its surface energy which is determined by the chemistry of the surface. The major challenge facing the use of superhydrophobic coatings is the fact that low surface energy materials are mainly organic, polymeric compounds that suffer from poor durability, and in addition, micro-textured coatings are typically made by complex and expensive techniques. In this work atmospheric plasma spray (APS) and suspension plasma spray (SPS) which are flexible, scalable and efficient surface engineering techniques, are employed to develop micro-textured superhydrophobic coatings for anti-icing applications.

In this research, APS and SPS TiO_2 micro-textured coatings are developed. After treatment by a stearic acid solution in order to lower their surface energy, these coatings demonstrate hydrophobicity and superhydrophobicity to different extents. APS coatings that are produced using 10-80 micron-sized particle feedstock, although highly hydrophobic, lack the extreme water repellency known as water mobility, due to their relatively coarse micro-texture. In the SPS process, submicron-sized TiO_2 particles in the form of a suspension are used as feedstock. The SPS coatings typically show superhydrophobicity with water contact angles higher than 150°. The

coatings produced using an ethanol-based suspension demonstrated extreme hydrophobicity and a water droplet impacting on their surface bounces back and detaches from them easily. The parameters influencing the SPS process are further studied and optimized to achieve coatings with hierarchical surface micro-texture i.e. a surface with a primary micron-sized and a secondary submicron-sized micro-texture. After optimization of the process, the SPS TiO_2 coatings show extreme superhydrophobicity with water contact angles as high as 170°, water sliding angles as small as 1.3° and a contact angle hysteresis as small as 4°. The best of the SPS coatings is then tested to evaluate its performance in icing and deicing conditions as well as its durability. It is demonstrated that the SPS TiO_2 coating developed in this work can decrease the ice accretion up to 62% compared to the uncoated surface for certain icing conditions. This coating can also significantly decrease the deicing time and the amount of heat required to maintain an ice-free surface. Most notably, the SPS TiO_2 superhydrophobic coating shows remarkably better resistance to dry particle erosion and icing/deicing cycles compared to commercial superhydrophobic spray coatings. Furthermore, it is demonstrated that even if the superhydrophobicity of the SPS coating is reduced due to water droplet erosion, it is easily recoverable due to the durability of the hierarchically micro-textured TiO_2 ceramic base.

To Bahareh, love of my life;

who is my best friend, and my "partner in crime"!

Acknowledgement

First and foremost, I would like to express my deepest appreciation to my thesis supervisors; Professor Ali Dolatabadi, Professor Christian Moreau and Professor Martin Pugh for their continuous guidance, encouragement and support during the course of my PhD program. Their contribution to my life expands beyond their invaluable scientific input and academic advice. I learnt from them inspiring lessons of professionalism, commitment, creativity and compassion, among many other things.

I am grateful to Professor Jolanta Sapieha from Polytechnique Montreal, Professor Mohammad Jahazi from École de Technologie Supérieure (ETS), Professor Rolf Wuthrich, Professor Mamoun Medraj, and Professor Robin Drew from Concordia University for permitting me to use their research facilities.

Thanks are due to Concordia University's research staff, particularly Robert Oliver and Mazen Samara and administrative staff including Maureen Thuringer, Leslie Hosein, Sophie Merineau and Arlene Zimmerman.

I am greatly thankful to my amazing friends and colleagues, Fadhel Ben Ettouil, Maniya Aghasibeig, Ali Alem, Reza Attarzadeh, Marc Roche, Hani Jazaerli and Lucas Hof for their friendship and support. Furthermore I would like to thanks all past and present members of Thermal Spray and Multiphase Flow Laboratory including Sadegh, Milad, Mehdi, Fariba, Alex L, Maria, Damir, Ali, Shahin, Omid, Alex N, Fernanda, Elnaz, Siavash, Tahmineh and Hafez.

I extend my appreciation to the Fonds de recherche du Québec – Nature et technologies (FRQNT), Canada Research Chair Program and all members of the Phobic2Ice project for the support of my research.

This work could not have been completed without endless understanding, patience and encouragement of my lovely wife Bahareh, and I am very lucky to share my life with her.

I am forever indebted to my mom, Mozhgan, my dad, Abbas and my brother Nima for their unconditional love and ever-lasting support.

Last, but not least, many thanks to my friends Ali, Shagha, Farnaz and Sya who were always there for me, especially in hardest moments.

Contribution of Authors

This thesis includes coauthored work in Chapters 3, 4, 5 and 6. Therefore, the contribution of each coauthor other than the author of this thesis is detailed below:

Chapter 3: M. Pugh, C. Moreau and A. Dolatabadi supervised the research and revised the manuscript.

Chapter 4: M. Pugh, C. Moreau and A. Dolatabadi supervised the research and revised the manuscript.

Chapter 5: F. Ben Ettouil helped with preparation of coating samples. C. Moreau, A. Dolatabadi and M. Pugh supervised the research and revised the manuscript.

Chapter 6: A. Dolatabadi, M. Pugh and C. Moreau supervised the research and revised the manuscript.

Table of Contents

List of Figures

List of Tables

List of Abbreviations

Abbreviation	Meaning (unit)
ACA	Advancing Contact Angle (°)
AOI	Angle of Impact
APS	Atmospheric Plasma Spray
CAH	Contact Angle Hysteresis (°)
CLSM	Confocal Laser Scanning Microscopy
COR	Coefficient of Restitution
CVD	Chemical Vapor Deposition
DOE	Design of Experiments
HVOF	High Velocity Oxygen Fuel
LWC	Liquid Water Content (g/m^3)
MVD	Median Volume Diameter (μm)
NW	NeverWet®
PAA	Polyacrylic Acid
PTA	Plasma Transferred Arc
PTFE	Polytetrafluoroethylene
PVD	Physical Vapor Deposition
PVP	Polyvinylpyrrolidone
RCA	Receding Contact Angle (°)
SA	Sliding Angle (°)
SD	Standard Deviation
SEM	Scanning Electron Microscopy
SPS	Suspension Plasma Spray
UED	Ultra EverDry®
WCA	Water Contact Angle (°)
XRD	X-ray Diffractometer

List of Symbols

Symbol	Meaning (unit)
D_{32}	Sauter mean diameter (μm)
D_{10}	10% of particles are this particles size
D_{50}	50% of particles are this particles size
D_{90}	90% of particles are this particles size
f_{LA}	Fraction of total contact area in between liquid and air
R_a	Arithmetic mean height of the surface on a line (μm)
R_f	Ratio of real surface area to projected surface area
R_{ku}	Kurtosis of the height distribution of the surface on a line
R_q	Arithmetic mean height of the surface on a line (μm)
R_{sk}	Skewness of the height distribution of the surface on a line
R_z	Maximum height of the surface on a line (μm)
S_a	Arithmetic mean height of the surface (μm)
S_{ku}	Kurtosis of the height distribution of the surface
S_q	Arithmetic mean height of the surface (μm)
S_{sk}	Skewness of the height distribution of the surface
S_z	Maximum height of the surface (μm)
γ_{LA}	Liquid/air interfacial energy (mJ/m^2)
γ_{SA}	Solid/air interfacial energy (mJ/m^2)
γ_{SL}	Solid/liquid interfacial energy (mJ/m^2)
θ_0	Intrinsic water contact angle on an ideally smooth surface (°)
θ_A	Advancing contact angle (°)
θ_C	Apparent contact angle of a rough surface (°)
θ_R	Receding contact angle (°)
θ_S	Sliding angle (°)

Chapter 1. Introduction

1.1.   In-flight icing

Ice formation on aerodynamic surfaces of aircraft is regarded as a major problem in the aerospace industry [1]. Ice accumulation may cause jamming and damage to parts, sensors and controllers and alter the aerodynamics of the airplane. Build-up of thick ice layers reduces lift and increases drag which can result in premature stall [2]. The combination of all these effects can lead to a range of undesired consequences including, but not limited to, flight delays, emergency landings, damaged parts and increased energy consumption to control the situation [3].

In-flight ice accretion occurs due to the presence of super-cooled water droplets i.e. a water droplet with a temperature below its freezing point. Such droplets impinge on the leading surfaces of the airplane and freeze either immediately or after spreading due to the relative velocity of the airplane and the surrounding air [4]. Gradual accumulation of ice over time, resulting from consecutive impingement of multiple water droplets can result in buildup of relatively thick and heavy ice layers [5].

Historically, a wide range of solutions have been employed to deal with this icing problem. Such solutions vary from using weather forecasts to avoid icing conditions and specialized training aimed to increase awareness of pilots and staff through to the use of mechanical and thermal deicing systems [6]. A significant potential solution to this icing problem is to apply superhydrophobic coatings on the airplane surfaces that are susceptible to icing. Superhydrophobic coatings, which are coatings with extreme water repellence, have been shown to delay ice formation [7] and facilitate ice removal [8] in certain icing conditions.

A major challenge for any practical application of superhydrophobic coatings on aircraft is their mechanical durability. Currently, superhydrophobic coatings are typically made using polymeric materials due to their low surface energies [9]. However, these materials are not durable by nature and can deteriorate easily when exposed to erosion and wear. Recent research has also

led to the manufacture of micro-textured superhydrophobic coatings that rely on a distinctive surface morphology to provide water repelling characteristics [10]. Such surface morphology has two scales of roughness features: a primary, micron-sized roughness and a secondary, submicron or nano-sized roughness. This micro-texture (known as hierarchical morphology), if created on an intrinsically hydrophobic material can render the surface of the material superhydrophobic [11]. However, the majority of the surface engineering processes that can produce this type of morphology are rather complicated, expensive and impractical to apply to large surfaces such as the wings of an airplane [12].

The main objective of this research is to use thermal spray processes as a flexible in terms of variety of materials that can be deposited, scalable and commercially viable surface engineering technique to develop and optimize superhydrophobic coatings for anti-icing applications in aircraft. Before presenting a comprehensive literature review in Chapter 2 of this thesis, a more in-depth perspective on the in-flight icing phenomenon and its consequences is provided herein. Additionally, some of the common practices used to deal with this icing problem in the aerospace industry are introduced and ultimately the idea of using superhydrophobic coatings to mitigate the icing problem is explored. At the end of this chapter, the main objectives of this research and the organization of this thesis are presented.

1.1.1. Hazards and consequences of aircraft icing

Icing-related damage is commonly reported and can cause considerable expense to airline companies. For example, in 2002 alone, the total damage of twelve icing-related incidents to United Airlines aircraft cost over $2 million dollars [13]. According to a study [14], there have been 2,212 icing-related reports from 1978 to 2002, of which 693 incidents are considered aerodynamically significant. Icing has been the main reason for $96 million per year in terms of personal injuries and damage in the USA [15].

By disturbing the air flow, ice can cause loss of lift, increase in drag force, and consequently damage or jamming of control surfaces or mechanical parts [16]. To compensate for the further drag caused by ice accumulation, more power is needed which itself results in an increase of the angle of attack and causes even more ice to form on the airfoil [17]. Accumulation of ice disturbs the air flow and consequently deviates the aircraft from optimal flight conditions. This leads to higher fuel consumption as well as the possibility of damage and jamming of critical parts of the aircraft [18,19].

2

1.1.2. Icing conditions and parameters

As mentioned before, in-flight ice forms due to the presence of super-cooled water droplets in the atmosphere and their impact on the surfaces of the aircraft. In other words, the icing risk drastically decreases either when the temperature is high enough so that water droplets are above their freezing temperature or the temperature is so low that only ice crystals exist. A schematic of the status of water droplets at different altitudes and the corresponding icing risk level and ice types is presented in Figure 1.1. As demonstrated in this Figure, at lower altitudes where the temperature is greater than 0°C, water droplets are not in a super-cooled state and their impact on the aircraft does not result in any ice formation. On the other hand, at high altitudes, due to the extremely low temperatures (lower than ≈ -40°C) only ice crystals exist which do not cause a risk of icing. In fact, it is at intermediate altitudes that the icing risk is considerably higher.
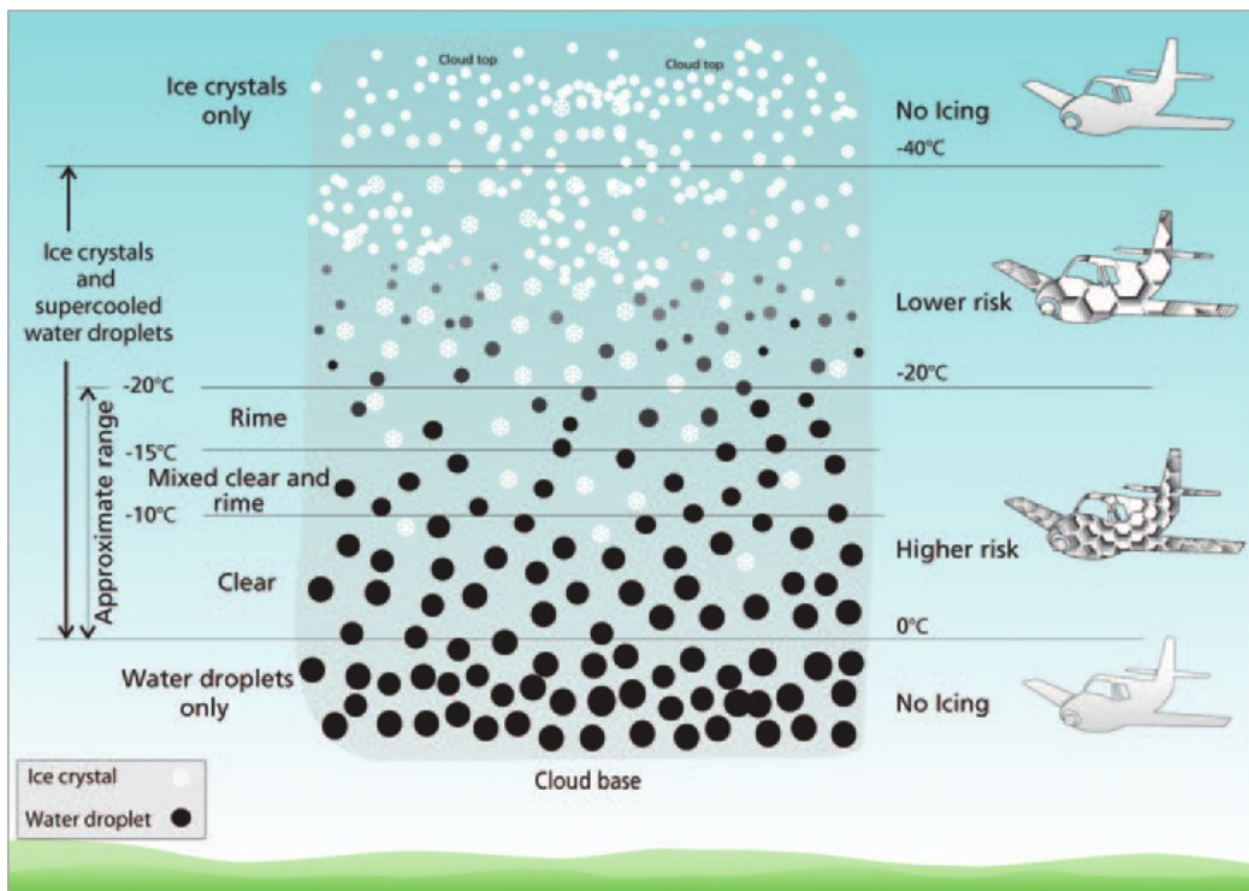
Figure 1.1. Icing risk and types of ice at various altitudes [20].

3

In addition to the ice formation, the type of ice that is formed plays an important role in determining the icing risk. Typically, in-flight ice is classified into three different types based on formation mechanism and characteristics of the ice. It is important to note that all three ice types form through the impact of super-cooled water droplets on the surfaces of the aircraft. The formation conditions and characteristics of each ice type is briefly described below.

The first ice type is *clear* or *glaze* ice. This type of ice forms when a super-cooled water droplet impacts on the surface but does not immediately and completely freeze upon impact. This happens when the temperature is typically between 0 to -10°C, the droplets are relatively large and liquid water content is relatively high. Liquid water content (LWC) is an indicator of humidity, in terms of grams of water per a cubic meter of air and is commonly used in aeronautics and related literature. In such condition, the droplets do not completely freeze upon impact resulting in what is known as wet growth of the ice [21]. Relatively higher temperatures (close to 0°C) and larger volume causes the droplet to retain a liquid form and spread backwards. This phenomenon is known as runback flow and causes the glaze ice to form on places other than the point of impact of the droplet. As the name *'clear ice'* suggest, this type of ice is mostly transparent and smooth. Clear ice has high adhesion to the surface and is considered to be the most undesirable type of ice [22].

The second type of ice is *rime ice*. Rime ice forms in different conditions to that of clear ice, i.e. at temperatures typically between -15 to -40°C, relatively small droplet size and lower liquid water contents. In the case of rime ice, the droplets immediately freeze in place upon impact, causing air pockets to be entrapped between them resulting in what is known as dry growth of the ice [21]. The rime ice is white and has low adhesion to the surface thus it is easier to remove.

The third type of ice is *mixed ice* which forms typically between -10 to -15°C and has mixed characteristics of both clear and rime ice. A schematic representing the different ice types is presented in Figure 1.2.
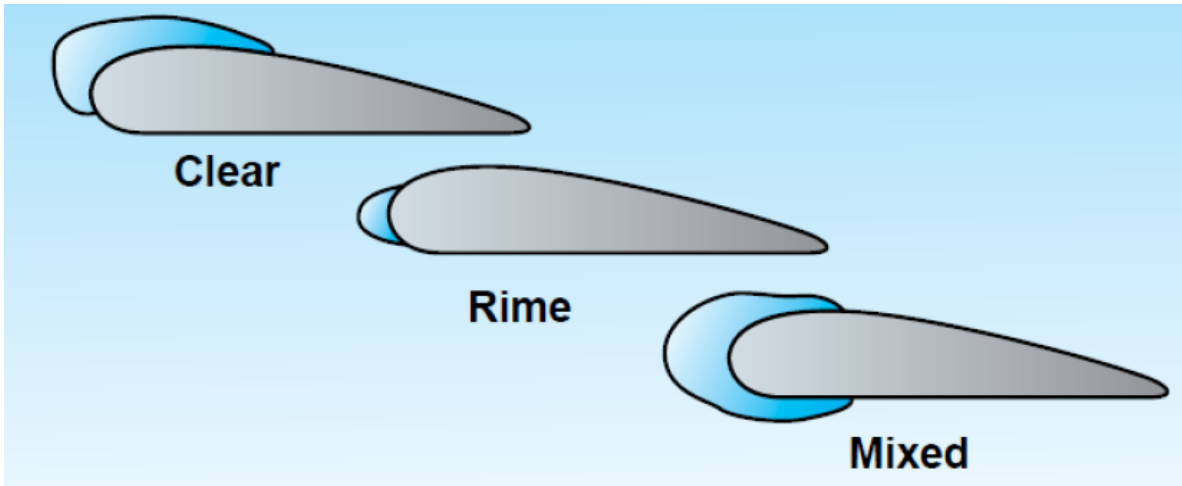
Figure 1.2.Types of ice formed on an aircraft wing [23].

A summary of the parameters influencing the type of ice and the risk of icing is introduced in Table 1.1. As mentioned before the most undesirable type of ice is clear ice due to the fact that it is harder to detect because of being transparent and also has high adhesion to the surface. Clear ice is also more detrimental to flight conditions as it can affect many areas due to runback flow and can grow large enough to negatively affect the aerodynamics of the airplane [24].

Table 1.1. Conditions of formation of different ice types [25].

Parameters	Glaze (Clear) ice	Mixed ice	Rime ice
Temperature	0°C to -10°C	-10°C to -15°C	-15°C to -40°C
Droplet size	Large	Small to large	Small
Liquid water content	High	Low to high	Low
Risk	High	Intermediate	Low

In Table 1.2 the conditions that are typically considered as an icing risk for aviation are presented [26]. As demonstrated in this table, icing risk conditions are not limited to sub-zero temperatures. Even at slightly warmer temperatures, there is a risk of icing since the temperature of the body of the airplane may still be lower than the freezing point. Additionally, it is important

to note that although icing risk conditions are usually assumed in the presence of water droplets smaller than 50 μm, the presence and effect of larger droplets cannot be ignored [27].

Table 1.2. Icing risk conditions [26].

Parameter	Icing risk conditions
Liquid water content (LWC) of water in air	From 0.1 to 3 g/m^3
Temperature	From +4°C to -40°C
Droplet diameter (MVD)	Usually from 1-50 μm but also up to 400 μm

1.1.3. Icing protection systems

To deal with icing problems, weather forecast information is used as well as special training to improve the pilot's awareness and skills [22]. Some automatic systems have also been developed for detection of icing and evaluation of aircraft icing performance in icing conditions [28]. Such systems provide information to the pilot and can control the operation of an aircraft's anti-icing systems. Simulation tools have been developed to predict, control and optimize the aircraft's response to flight in icing conditions [29]. Moreover, pre-flight preparations include deicing (removal of the ice) and anti-icing (providing protection against ice formation) procedures [30]. In addition, recent in-flight anti-icing and deicing systems based on heating or mechanical ice removal have been developed [31]. This approach may be effective in preventing ice accumulation on the leading edge. However, it is impractical to place heating elements below all surfaces that are prone to icing. Furthermore, the efficiency of such systems can be further improved by modifying the surface characteristics.

1.1.4. Superhydrophobic coatings for icing protection

A remarkable potential solution to the icing problem is to treat the prone surfaces in such a way that they are immune to icing i.e. ice does not easily form on them. Investigations have shown that if a surface is superhydrophobic, under certain icing conditions, it can effectively reduce the chance of ice accumulation or even completely prevent ice formation [32]. Even in the case of ice formation, the amount of thermal energy needed to remove the ice from a

superhydrophobic surface has been reported as being significantly reduced [33]. Superhydrophobic surfaces are surface with extremely water-repelling properties. Such surfaces are typically identified by high water repellence (manifested through water contact angles higher than 150°) and high water mobility (manifested through a water sliding angle smaller than 10°). The characteristics, properties and types of superhydrophobic surfaces are discussed in details in Chapter 2. Here, the potential of superhydrophobic surfaces for anti-icing applications is discussed.

Figure 1.3 shows two surfaces, one an uncoated aluminum alloy and the other, the same alloy with a superhydrophobic surface coating, that have been exposed to the same icing conditions for a certain period of time. As clearly demonstrated in the photo, ice accumulation is observed on the untreated aluminum surface while no significant amount of ice has been formed on the superhydrophobic surface. This figure clearly showcases the potential of superhydrophobic surfaces to mitigate the icing problem in these specific icing conditions. It is believed that ice formation on superhydrophobic surfaces is alleviated because super-cooled water droplets do not easily stick on these surfaces and mainly bounce off and detach from the surface before they start to freeze [34]. Studies have also shown that in the case of ice formation on a surface, superhydrophobic surfaces are additionally beneficial since ice detachment from these surfaces required less heating compared to conventional surfaces [35].

Figure 1.3. Comparison of a superhydrophobic surface (right/front) to a hydrophilic surface (left/back) in icing conditions [1].

---

[1] Courtesy of A. Dolatabadi, 2010.

Although it is widely accepted that superhydrophobic coatings can reduce ice accretion particularly in the case of clear ice, some studies have opposed this idea by arguing that surface roughness which is an important factor in superhydrophobic surface can contribute to ice nucleation as well as increasing ice adhesion to the surface [36,37]. This issue signifies the importance of testing and evaluating icing performance of every new superhydrophobic coating in expected icing conditions to determine whether such coatings are in fact advantageous i.e. to determine the relationship between superhydrophobicity and icephobicity.

Another important challenge of dealing with superhydrophobic coatings for anti-icing purposes is the issue of durability. Many novel superhydrophobic surfaces that are described in the literature either demonstrate poor mechanical durability [38,39] or are made with complex and expensive processes and as such have limitations in terms of being practically applied to surfaces of aircraft components [40,41]. This is the main motivation of this work in selecting and working with a surface engineering technique which is capable of developing durable coatings with flexibility and scalability to be used in aerospace anti-icing and deicing applications.

In this work, the main objective is to address the aforementioned issues by using thermal spraying as a versatile, scalable and flexible coating technique to develop, optimize and functionalize superhydrophobic coatings. Regarding the durability of these coatings, the aim is to develop coatings with adequate durability to withstand potential erosion and ice/deicing cycles for a reasonable amount of time with the possibility to restore and renew their functionality in a simple and quick way.

1.2. Objectives

The main objectives of this research are presented here with respect to the sequence of the chapters of this thesis:

- To develop micro-textured ceramic coatings with a dual-scale hierarchical surface morphology using thermal spray techniques. These coatings must be designed in such a way that after treatment for lowering their surface energy, they demonstrate superhydrophobic characteristics.

- To optimize the coating process to control and tailor the surface micro-texture in order to achieve the maximum water repellency and mobility for the coatings. This objective is to be achieved using a parametric study and "design of experiment" methods to determine the

influence of various deposition parameters on coating morphology and wetting characteristics.

- To investigate the anti-icing functionality of the coatings in different icing conditions and to determine the contribution of the superhydrophobic coatings developed in this work to the mitigation of ice accretion, and the facilitation of ice removal.

- To improve the practical application of thermal sprayed superhydrophobic coatings by improving the durability and providing easy reparability compared to polymer-based superhydrophobic coatings.

- To investigate the relationship between superhydrophobicity and icephobicity, and how superhydrophobic coatings can contribute to mitigating the aircraft icing.

1.3. Thesis organization

This thesis comprises seven chapters. Each chapter is briefly described herein. The first chapter introduced the in-flight icing problem and formulated the challenges that icing imposes on aircraft and aviation. Various ice accretion conditions and mechanisms were explained and some of the current approaches to mitigate in-flight icing were described. At the end, the objectives of this work were presented.

Chapter 2 provides a comprehensive literature review of the different surface engineering techniques that are employed to manipulate the wetting characteristics of engineering materials. In this chapter, first the fundamentals of surface wetting are reviewed and the different wetting behaviors of surfaces are introduced. Afterwards, the concept of superhydrophobicity is presented and the effect of surface roughness on apparent wetting behavior and wetting regimes is explored. Some of the techniques that are used in the scientific literature to develop superhydrophobic surfaces are introduced and the potential strengths and deficiencies of each technique is discussed. Additionally in Chapter 2, thermal spraying is introduced and two techniques used in this research, atmospheric plasma spraying (APS) and suspension plasma spraying (SPS) are briefly explained. At the end, a comprehensive review of the efforts that have employed thermal spraying to develop superhydrophobic coatings is presented.

Chapter 3 presents a comprehensive investigation of the atmospheric plasma spray (APS) process as a promising method to develop scalable and economically reasonable coatings with tailored micro-texture and wettability. In this chapter, various deposition conditions in the APS

process are explored to determine the optimum conditions that result in the most desired coating morphology and consequently, wetting behavior.

Chapter 4 focuses on developing new coatings with improved water repellency and mobility using the suspension plasma spray process (SPS). The SPS process allows the use of submicron-sized feedstock material to generate micro and nano-scale hierarchical roughness which can lead to superhydrophobicity. The results are then compared to that of the APS process and other natural and manufactured superhydrophobic surfaces.

Chapter 5 presents a rigorous investigation of the influence of SPS process parameters on coating morphology and consequently the wetting behaviors of the coatings. A test matrix is developed and experiments are designed accordingly to determine the most important and influential deposition conditions. This approach contributes to obtaining finer and more uniform morphological features on the coatings. These results are used to control and tailor the hierarchical micro-texture of the coatings which in turn results in enhanced water repellence and mobility.

Chapter 6 focuses on evaluation of the icing performance and durability of the SPS superhydrophobic coatings. Firstly, the coatings are tested in various icing conditions. Their icing performance and their contribution to delayed ice accretion and facilitation of deicing is compared to uncoated samples as well as commercially available, polymer-based superhydrophobic spray coatings. Secondly, the durability of the coatings is evaluated by exposing them to erosive and destructive environments including solid particle erosion, high velocity water droplet erosion, cloud-sized water droplet erosion and icing/deicing cyclic tests. The durability tests results are also compared to that of commercially available superhydrophobic spray coatings.

Chapter 7 summarizes the findings, conclusions and contributions of this work and suggests some recommendations for future work.

Chapter 2. Literature Review

2.1. Fundamentals of surface wetting

The static wetting behavior of the surface of a solid material in interaction with water is typically characterized by its static water contact angle, or for short, its contact angle (also known as wetting angle). The contact angle is the angle between solid/liquid and liquid/gas interfaces when a solid, a liquid and a gas phase are in contact. The water *contact angle* of an ideally smooth surface, denoted here by θ_0 is determined by the interfacial energies between the three phases as given in Eq. (2.1), Young's equation [42]:

$$\cos\theta_0 = \frac{\gamma_{SA} - \gamma_{SL}}{\gamma_{LA}} \qquad \text{Eq. (2.1)}$$

where γ_{SL}, γ_{SA}, and γ_{LA} are solid/liquid, solid/air and liquid/air surface tensions. For water, based on Young's equation, the contact angle of an ideally smooth solid surface depends on its interfacial energies, γ_{SL} and γ_{SA} and as a result on the surface chemistry demonstrated in Figure 2.1.

According to Eq. (2.1), when γ_{SA} is larger than γ_{SL} i.e. the droplet tends to spread across the surface, the water contact angle is smaller than 90°. This means that the surface tends to be wet by water. Materials that tend to be wet by water are called hydrophilic (literally, lover of water). Hydrophilic materials are sometimes referred to as high surface energy materials. A schematic of a water droplet sitting on a hydrophilic surface is demonstrated in Figure 2.1.a.

On the other hand, when γ_{SL} is larger than γ_{SA}, the contact angle is larger than 90°. Consequently, the surface tends not to be wet by water. These materials with a tendency to repel water are called hydrophobic (literally, scared of water). Hydrophobic materials are sometimes referred to as low surface energy materials. A schematic of a water droplet sitting on a hydrophobic surface is demonstrated in Figure 2.1.b.
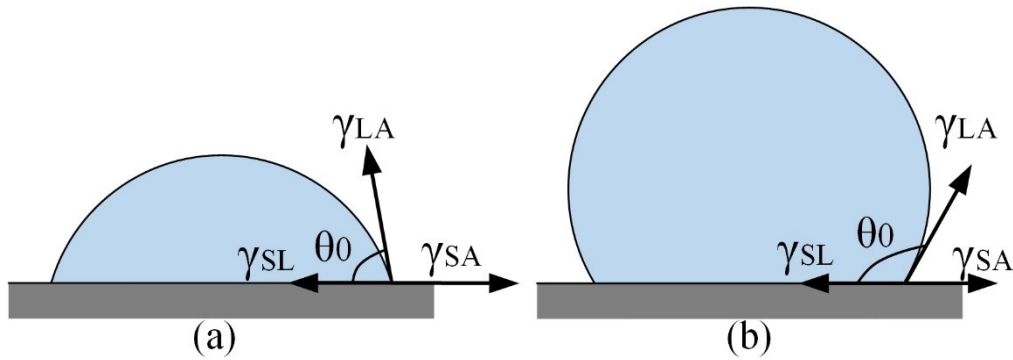
Figure 2.1. Schematic of (a) a hydrophilic and (b) a hydrophobic surface.

In addition to static contact angle, there are other parameters that quantify the interaction of a moving water droplet on a solid surface. Three of these parameters, advancing contact angle (θ_A), receding contact angle (θ_R), and sliding angle (θ_S) are presented in Figure 2.2. When a water droplets starts to move on a surface, the contact angle on the forward moving or advancing side of the droplet is called its *advancing contact angle*, denoted here as θ_A. On the other hand, the contact angle on the backward or receding side of droplet is called the *receding contact angle*, denoted here as θ_R. Theoretically, the advancing and receding contact angles are respectively the largest and smallest contact angle values that can be measured on that surface [43,44]. The difference between these two values is called the *contact angle hysteresis* and is an indication of the energy that is dissipated during the movement of droplet on the solid surface. In view of that, a surface with a relatively large contact angle hysteresis value has a tendency to adsorb water whilst a surface with a relatively small contact angle hysteresis has a tendency to repel water.

An additional parameter that is commonly used to characterize the wetting behavior of a surface is the *sliding angle*, denoted here as θ_S. The sliding angle is the angle to which a surface must be tilted for a water droplet to start to move on that surface. The sliding angle is relevant only for highly water repellent surfaces because on otherwise water adsorbing surfaces, a sufficiently small water droplet can be pinned and not move, even if the surface is turned upside down. The sliding angle of a surface is another indication of water repellency because the smaller the sliding angle, less force is required to move the droplet on the surface. In fact, for a water repelling surface, contact angle hysteresis and sliding angle represent a similar notion. The smaller the value of these two parameters, the more water repellent the surface is. However, it is important to note that the values of contact angle hysteresis and sliding angle are not necessarily the same.
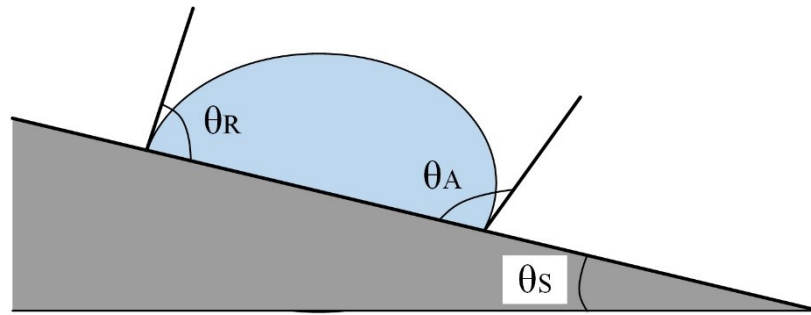
Figure 2.2. Sliding angle, advancing and receding contact angles of a droplet on a tilted surface.

2.2. Superhydrophobicity

The term superhydrophobic is widely used to describe surfaces that are extremely water repellent and show highly hydrophobic behavior. The lotus leaf is a well-known example of a natural superhydrophobic surface [45]. The criterion for superhydrophobic behavior is conventionally considered to be a contact angle value larger than 150° [46]. However, sometimes additional conditions such as contact angle hysteresis or a sliding angle smaller than 10° are also used for determining superhydrophobicity [47]. The term "ultra-hydrophobicity" is sometimes used interchangeably with superhydrophobicity [48] while sometimes it is used to refer to even higher contact angles, for example higher than 170° [49]. In the context of superhydrophobicity, high contact angle values are sometimes considered to represent "water repellence" or "water repellency" of the surface [50], whereas low contact angle hysteresis or sliding angle values represent "water mobility" [51]. Thus, a superhydrophobic surface is assumed to have both high water repellency and high water mobility [52].

Regarding superhydrophobic surfaces, there are two other parameters that are commonly used to characterize and quantify the extent of superhydrophobicity of the surface: contact time and coefficient of restitution. Measuring these two parameters is possible due to the fact that an impinging droplet of water recoils and rebounds from a superhydrophobic surface if it has the proper impact velocity and the surface has sufficiently high water mobility [53]. The contact time is the duration of time from when an impinging water droplet comes into contact with the surface until it is completely detached from the surface. Obviously, a shorter contact time indicates higher water repellency and shorter interaction between the water droplet and the surface [54,55].

The coefficient of restitution which was originally defined for collision of two solid objects is defined as the ratio of the velocity before and after the impact [56]. The coefficient of restitution

has a value between 0 and 1 and represents dissipation of energy during the impact. The closer the value is to 1, the less energy is dissipated during the impact of a droplet onto a solid surface. Consequently, values closer to 1 are considered more desirable for superhydrophobic surfaces [57]. It is important to note that upon impact of a water droplet on a surface, the droplet usually goes through considerable deformation in the form of spreading and recoil [58–60]. If the impact velocity is high enough, the droplet may even experience breakup [61]. Therefore, the measurement of coefficient of restitution needs to be carried out carefully and in a controlled manner in order to obtain repeatable and comparable results for various solid surfaces.

Superhydrophobic surfaces have been the subject of great attention for potential applications where minimal interaction between a solid surface and a liquid is desired. Such applications include but are not limited to; anti-icing [62–64], self-cleaning [65–67], drag reduction [68–70], and corrosion resistance [71–73]. Since in this work the main focus is on anti-icing and deicing properties and application of superhydrophobic coatings, a comprehensive literature review on anti-icing and deicing of superhydrophobic surfaces will be presented further in this chapter. However, before discussing this topic, it is important to further explore another factor that plays a major role in wetting behavior of solid surfaces. This factor is the roughness or surface micro-texture of the solid surface.

2.3. Effect of surface roughness on wetting

Surface chemistry is not the only factor effecting the wetting behavior of solid surfaces. It is shown repeatedly in the literature [74] that the surface morphology (roughness) also has a great impact on the wetting behavior of solids. The lotus leaf has been known as a symbol of purity and cleanliness for thousands of years. This is because of the lotus leaf's "self-cleaning" capability which allows the plant to survive in muddy and polluted environments. The lotus leaf is a typical natural superhydrophobic surface. Scanning Electron Microscopy (SEM) imaging of the surface of lotus leaf [74,75], as a natural superhydrophobic surfaces shows that there is a "hierarchical" microstructure (dual-scale roughness) on this surface. This microstructure, shown in Figure 2.3, contains micro asperities 20–40 μm apart, each covered with a smaller scale roughness of "epicuticular wax crystalloids" [76]. The superhydrophobicity of this surface originates in these crystalloids both chemically and structurally. Many other natural superhydrophobic surfaces have been reported to have a more or less similar hierarchical micro-texture [77–79].
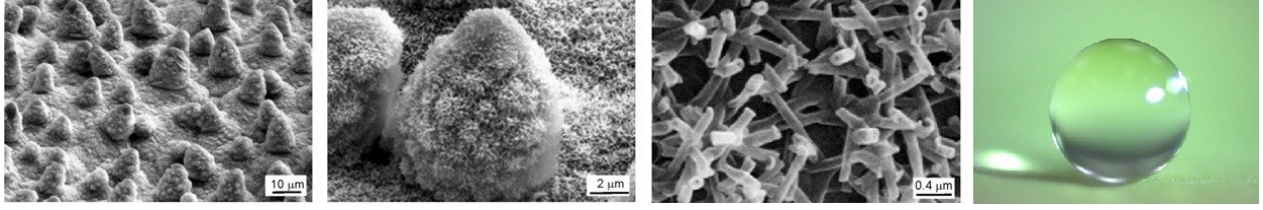
Figure 2.3. SEM images of lotus leaf in three different magnifications (first three pictures from left), and image of water droplet sitting in almost full sphere shape on the lotus leaf [74,75].

On superhydrophobic surfaces with hierarchical micro-texture, the primary, micro-scale roughness of the surface results in the formation of air pockets between the solid and the liquid. The water droplet sits partially on these air pockets which leads to a decrease of the actual contact area of the droplet with the solid surface and results in increased "apparent contact angle" and reduced contact angle hysteresis of the surface [80]. The term "apparent contact angle" in this context indicates that the contact angle which is practically measured on a rough surface is different from the contact angle on a smooth sample of the same material.

There are two models to explain the influence of roughness on the wetting and contact angle of a rough solid surface. One model, suggested by Wenzel [81], assumes a smooth, homogenous water-solid interface called the Wenzel state. The other model, proposed by Cassie and Baxter [82], assumes a composite water-solid-air interface called the Cassie-Baxter state. A schematic of the two models is illustrated in Figure 2.4. The effect of Wenzel and Cassie-Baxter wetting regimes on the contact angle of a rough solid surface is manifested through Eq. (2.2) and Eq. (2.3) respectively:

$$\cos \theta_c = R_f \cos \theta_0 \qquad \text{Eq. (2.2)}$$

$$\cos \theta_c = R_f \cos \theta_0 - f_{LA}\left(R_f \cos \theta_0 + 1\right) \qquad \text{Eq. (2.3)}$$

where θ_c is the apparent water contact angle on a rough surface, θ_0 is the contact angle on the smooth surface (intrinsic contact angle), R_f is non-dimensional surface roughness factor which is equal to the ratio of real surface area to projected surface area, $(R_f > 1)$, and f_{LA} is the fraction of the total contact area in between liquid and air.
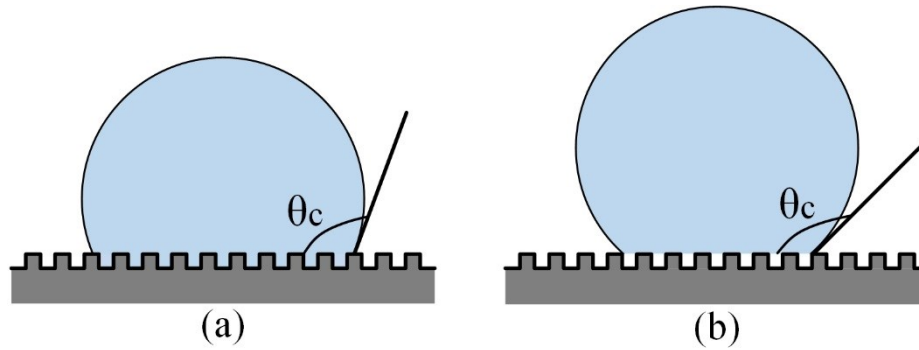
Figure 2.4. Schematic of (a) Wenzel and (b) Cassie-Baxter wetting state.

In the Wenzel state (Figure 2.4.a and Eq. (2.2)), surface roughness amplifies the wetting behavior of the solid. Thus when roughened, an intrinsically hydrophilic surface becomes more hydrophilic and an intrinsically hydrophobic state becomes more hydrophobic when the dominant wetting state is Wenzel. However, it must be noted that in the case of the Wenzel wetting regime, since water penetrates through pores and asperities of the surface, generally the adhesion between water and solid surface is high. Therefore, even highly hydrophobic surfaces have typically poor water mobility in the Wenzel state [83].

On the other hand, the Cassie-Baxter wetting state generally reduces the wettability of a surface regardless of intrinsic wetting behavior due to the presence of air pockets between the solid and liquid phases. Therefore an intrinsically hydrophilic surface may show hydrophobic behavior when roughened in a proper manner to have a Cassie-Baxter wetting regime [84]. As a result, a Cassie-Baxter wetting regime is favorable for developing superhydrophobic surfaces with improved water repellency and mobility. The governing wetting regime on a surface is determined by various geometrical parameters of its roughness including the height of the features, the width of the gap between features and the presence of secondary scale roughness [85,86].

In Figure 2.5, the wettability behavior for smooth, micro-textured, nano-textured and hierarchically textured solid surfaces is shown. The largest contact area between the droplet and the surface occurs on smooth and micro-textured surfaces. The contact area decreases when using nanostructured surfaces and is minimized in the case of a hierarchical structure [87–89]. Consequently, the apparent contact angle also progressively increases.
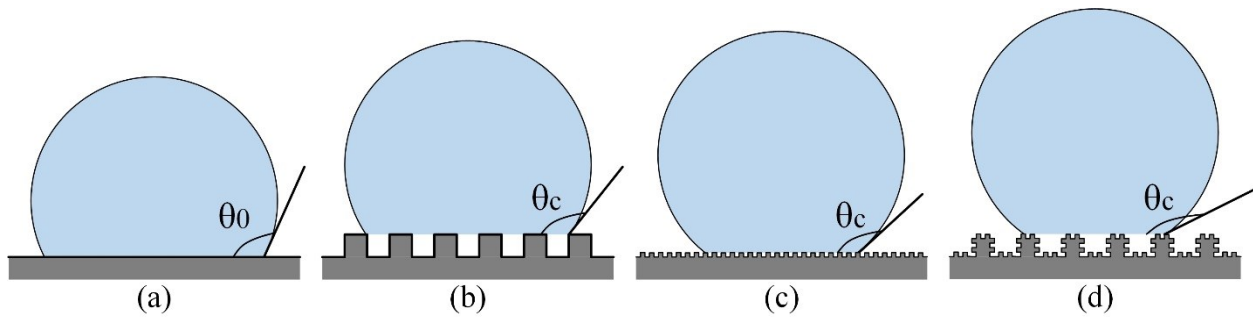
Figure 2.5. Schematic for wetting of (a) smooth, (b) micro-textured, (c) nano-textured and (d) hierarchically textured solid surfaces.

Multiple studies [90–93] have confirmed that the wettability of a surface is governed by both its surface micro-texture and chemical composition. A hierarchical surface structure similar to the one observed on the lotus leaf and other natural superhydrophobic surfaces seems to be crucial to make sure that a Cassie-Baxter (composite) interface is most likely to occur and is stable on a surface. It is speculated that in such a micro-texture, the micron-sized roughness provides air pockets, assuring the formation of a composite interface. Additionally, the smaller-scaled (nano-sized) roughness helps stabilize the composite interface by pinning the liquid and preventing it from filling the cavities which could result in the transition from the Cassie-Baxter to the Wenzel state. In other words, the combination of the hierarchical roughness alongside an intrinsically hydrophobic material with relatively small surface free energy results in a superhydrophobic surface. It can be concluded that in the presence of an appropriate hierarchical surface micro-texture, extremely low surface energy materials such as fluorocarbons are not necessarily required to obtain a superhydrophobic surface. This fact has been widely used by researchers to produce biomimetic superhydrophobic surfaces inspired by nature [94–96].

2.4. Bio-inspired superhydrophobic surfaces

As mentioned before, there are several potential applications for superhydrophobic surfaces that have been investigated in the literature, such as anti-icing, self-cleaning surfaces, corrosion resistance surfaces, biomedical devices, liquid separation, and the reduction of turbulent flow in water-bearing pipes. A list of applications studied in various publications for superhydrophobic surface is presented in Table 2.1. As a result, the topic of developing functional superhydrophobic surfaces has gained widespread popularity and interest in recent years, and has been the subject of extensive research. This is evident by the increasing number of publication on

the topic over the past few years [97–99]. A basic search on the 'web of knowledge' website shows that there have been 266 publications related to superhydrophobicity in 2006. This number rose to 715 in 2011. Many of these publications present novel techniques and processes for developing superhydrophobic surfaces.

Table 2.1. Potential applications sought for superhydrophobic surfaces in the literature.

Application	Anticipated Mechanisms	Examples
Anti-icing	Delay freezing by repelling super-cooled droplets Reduced ice adhesion	[100–103]
Anti-fogging	Repelling water micro-droplet; Preventing deposition of water on surface	[104–106]
Self-cleaning	Repelling contaminating liquid Droplets removing contamination and leaving surface	[107–109]
Corrosion resistance	Repelling corrosive liquids	[110–113]
Liquid separation	Different wetting behavior towards various liquids	[114–116]
Fluid drag reduction	Reduced fluid adhesion on the interface	[117–119]
Drop-wise condensation	Forming drops on surface which are easily removed	[120–122]
Biomedical devices	Controlled wetting and selective interaction	[123,124]

As previously mentioned the wetting behavior of a solid surface is a function of both its surface energy, which is in turn influenced by surface chemistry, and its micro-texture. If a material has very low surface energy it means it is intrinsically extremely hydrophobic. Very low surface energy materials are typically some families of hydrocarbons and polymers such as fluorosilanes [125]. There are several problems associated with these materials for practical applications including durability, safety and practicality concerns [38,126]. Due to such challenges, many of the recently developed superhydrophobic surfaces take inspiration from the roughness-induced superhydrophobicity of the lotus leaf and other natural superhydrophobic surfaces and therefore, are sometimes known as "bio-inspired superhydrophobic surfaces".

In the case of so-called "bio-inspired superhydrophobic surfaces", the extreme hydrophobicity of the surface is not only due to its surface chemistry and intrinsic water repellency,

but also the presence of some type of surface micro-texture similar to what is observed on the lotus leaf and other natural superhydrophobic surfaces. In other words, this approach relies on a rough and textured surface in order to promote a Cassie-Baxter wetting regime and consequently a superhydrophobic behavior. It is important to note that in order to improve the outcome of such an approach, it is necessary to have an intrinsically hydrophobic (but not necessarily superhydrophobic) surface wetting behavior.

Typically, there are two approaches to fabricate roughness-induced superhydrophobic surfaces: one is to roughen a surface which is made from hydrophobic material; and the other is to chemically modify a hydrophilic rough surface to become hydrophobic. Many conventional surface engineering techniques have been employed to develop superhydrophobic surfaces. These techniques include, but are not limited to; lithography, etching, deposition techniques such as chemical vapor deposition (CVD) and electrodeposition, sol-gel, layer-by-layer (LbL), self-assembly and laser treatment. Multiple comprehensive reviews of these methods can be found in review papers such as [10,12,39,127,128]. It should be mentioned that each of these methods has their particular advantages and disadvantages. Take for instance lithography techniques that are relatively accurate and applicable to large areas, but they are also slow and costly processes. On the other hand, etching techniques are fast but less controllable with the possibility of chemical contamination. Self-assembly methods are flexible and relatively inexpensive processes but using them requires accessibility and availability of suitable precursors. A summary of these techniques and the respective wetting characteristics of the coatings developed by these techniques is presented in Table 2.2. It is important to note that in this table, the thermal spray processes are excluded since they are to be discussed in further detail in the following sections.

Generally, the majority of existing superhydrophobic surface treatments suffer from one of the two main limitations for practical anti-icing application: firstly, lack of durability and secondly, complexity and scalability of the techniques. The first limitation is due to the fact that some of these surface treatments rely on polymers as low surface energy, intrinsically hydrophobic materials to deliver the hydrophobicity of the surface. However polymers are materials with secondary bonding between the molecules, and therefore typically demonstrate poor mechanical performance and especially, a very low resistance to wear and abrasion. Additionally, many polymeric materials are susceptible to environmentally degrading factors such as ultra-violet exposure and temperature variation.

Table 2.2. A list of surface engineering techniques used in recent research publications for developing superhydrophobic surfaces.

Surface modification technique	Examples	Highest contact angle (°)	Lowest contact angle hysteresis-(CAH) or sliding angle (SA) (°)
Lithography	[129]	170	30 (CAH)
	[130]	169	2 (CAH)
Etching	[131]	155	5 (CAH)
	[132]	166	2 (CAH)
CVD	[133]	160	Not reported
	[134]	> 160	~ 2 (SA)
Electrodeposition	[135]	154	Not reported
Sol-gel	[136]	168	1 (SA)
	[111]	155	7 (SA)
Layer-by-layer	[137]	157	1 (SA)
Self-assembly	[138]	165	4 (CAH)
Laser treatment	[139]	160	3 (CAH)
	[140]	166	4 (SA)
	[141]	166	10 (CAH)

To-date the only known materials with intrinsic hydrophobicity i.e. the static contact angle of a smooth sample of these materials that is larger than 90°, are hydrocarbon and polymeric materials with the arguable exception of rare-earth oxides. In some recent publications [142–144], some or all of the rare-earth oxides have been reported to be intrinsically hydrophobic. However these reports have been disputed in other publications [145,146] by arguing that environmental contamination is the main reason for apparent hydrophobicity of rare-earth oxides. The first such observation have been reported by Lawrence et al. [147] of cerium dioxide (CeO_2) membranes showing a contact angle of around 120°. Martinez et al. [148] have reported contact angle ranging from 94° to 134° for electrodeposited CeO_2.

Maybe the most prominent report of intrinsic hydrophobicity of rare-earth oxides has been made by Azimi et al. [149] about pressed and sintered samples of all rare-earth oxides. However, in this work the reported wetting parameter is the advancing contact angle and not the static contact angle and it must be noted that having an advancing contact angle of larger than 90° does not necessarily mean that the static contact angle is also larger than 90°. Preston et al. [150] have made a counterargument that once properly cleaned and contamination-free, rare-earth oxides are in fact hydrophilic and their apparent hydrophobicity is due to adsorption of hydrocarbon groups from exposure to ambient air. In a later publication, coauthored by Azimi, Khan et al. [151] respond to Peterson et al. [150] by claiming that rare-earth oxides demonstrate hydrophilicity due to surface oxygen content exceeding the stoichiometric ratio. They demonstrate this by showing that a freshly sputtered CeO_2 with a surface O/Ce ratio of around 3 is hydrophilic, but after being left in ultra-high vacuum, the surface O/Ce ratio reduces to around 2.2, showing hydrophobicity.

Even though the subject of intrinsic hydrophobicity of rare-earth oxides seems debatable, it could potentially offer a significant solution to the issue of durability of superhydrophobic coatings. A ceramic material such as a rare-earth oxide is naturally much more durable compared to polymeric and hydrocarbon alternatives. However, as mentioned before it is not clear whether or not rare-earth oxide demonstrate hydrophobicity at all or just in some conditions and therefore this topic is further investigated and the results are reported in the Appendix section of this thesis.

A second limitation of some of the surface engineering techniques employed to develop superhydrophobic surface by researchers is the complexity and limited scalability of these methods. Controlled environment, long and costly production processes and limited controllability of surface engineering process are examples of such limitations. Many of these techniques successfully generate fine and uniform hierarchical patterns on the surface which result in extremely high water repellency and in some cases reasonably durable superhydrophobic surfaces. However, these methods are basically impractical for treating for instance the wings and other large surfaces of an aircraft.

A list of superhydrophobic surface modifications aimed for mitigating the icing problem are presented in Table 2.3. In this list, different superhydrophobic surfaces are classified according to their respective contributions to mitigating the icing problem. As also mentioned in Chapter 1, this contribution can be in terms of delaying ice nucleation, preventing ice or frost formation and reducing ice adhesion or a combination of them.

Table 2.3. A list of various superhydrophobic and icephobic surfaces for anti-icing applications and their respective contributions to the icing problem.

Examples	Surface Modification Technique	Type of contribution to icing mitigation	Durability	Complexity (Scalability)
Mishchenko et al. [152]	Ion etching	Delaying ice/frost formation	Not reported	Complex
Wang et al. [153]	Chemical etching		Not reported	Scalable
Liao et al. [154]	Etching		Durable	Complex
Arianpour et al. [155]	Self-assembly		Not reported	Moderate
Jung et al. [37]	Spray casting		Not reported	Scalable
Li et al. [156]	Deposit and dry		Not reported	Scalable
Zhu et al. [157]	Spin coating	Reducing ice adhesion	Not durable	Scalable
Sojoudi et al. [158]	iCVD		Durable	Complex
Susoff et al. [159]	Sol-gel		Durable	Complex
Wang et al. [101]	Etching	Delay ice/frost formation and reducing ice adhesion	Durable	Complex
Varanasi et al. [160]	Photolithography		Not reported	Complex

In examples provided in Table 2.3, it is important to note that the supposed icing delay reported for some of the cases is not necessarily for in-flight icing conditions. The in-flight icing condition tests need to be performed in real flight tests or icing wind tunnels. However, sometimes (for example [103,154]) the icing delays have been reported for a static water droplet ; in other cases (for example [161,162]) the icing delay has been reported for droplets falling on the surface from a certain vertical distance. Such studies, although informative and useful, do not represent in-flight icing conditions, in the sense that droplet size and impact velocity are considerably different from that of in-flight cases. To reiterate from Chapter 1, the main icing hazard condition for in-flight icing is micro-droplets with an average size ranging from 20-50 μm in diameter, temperatures of 0 to -40°C and impact velocities of 50-100 m/s.

As previously mentioned, the superhydrophobic surfaces developed using the aforementioned techniques have a variety of potential applications. Here, we mainly focus on the

application of superhydrophobic surfaces for anti-icing applications. The most challenging issue in producing these surfaces for aerospace is the fact that these surfaces need to survive harsh and abrasive environments. In fact, the most critical problem with bio-inspired superhydrophobic surfaces for use at the industrial scale is their poor mechanical properties. On one hand, we need to make a relatively complex hierarchical micro/nano structure on the surface to obtain the desired stable superhydrophobicity, while on the other hand we must make sure that these surfaces have the proper mechanical properties required for the particular applications (i.e. anti-icing surfaces). These two expectations are to some extent opposite in nature.

So far, according to what has been discussed, there is a lack of a surface engineering technique that is capable of developing micro-textured surfaces with hierarchical roughness which is commercially viable and easily applicable and scalable to large surfaces, and moreover, is reasonably controllable, repeatable and capable of producing durable coatings. This brings us to the motivation of this work which is to employ thermal spray processes to produce these coatings. In the next section, a brief introduction to thermal spray techniques is presented followed by a more detailed discussion of atmospheric plasma spraying (APS) and suspension plasma spraying (SPS) which are the two thermal spray techniques used in this work. In the following section a literature review of thermally-sprayed, highly hydrophobic and superhydrophobic state-of-the-art coatings is presented.

2.5. Thermal spray processes

As previously mentioned, there are two requirements to produce a superhydrophobic surface: a hierarchical micro/nano texture, and a low surface energy material. Plasma spray processes (APS and SPS) are shown to be capable of producing microstructured functional coatings using various types of materials. In addition, thermal spray processes are considered efficient, versatile and cost effective methods of surface engineering. As a result, thermal spray process can be considered as a potential solution to fabricate superhydrophobic surfaces for industrial applications.

In thermal spray processes, the feedstock material is injected into a high temperature jet created by a heat source. The heat source could be a combustion or a non-combustion source such as an electric arc or a plasma. The heat source partially or fully melts the feedstock materials and propels the feedstock particles towards a substrate. The feedstock material is typically in powder,

wire, or rod form. Upon impact, the fully or partially molten particles form splats, rapidly cool down, solidify and adhere to the surface. The splat undergoes extremely high cooling rates (typically in the order of 10^6 K/s)[163]. Collection of these splats forms a layer of coating on the surface of the substrate. The deposition, usually with a raster pattern, scans the entire surface of the substrate and the process continues until the desired coating thickness is achieved. Figure 2.6 demonstrates a schematic of thermal spray process [164].
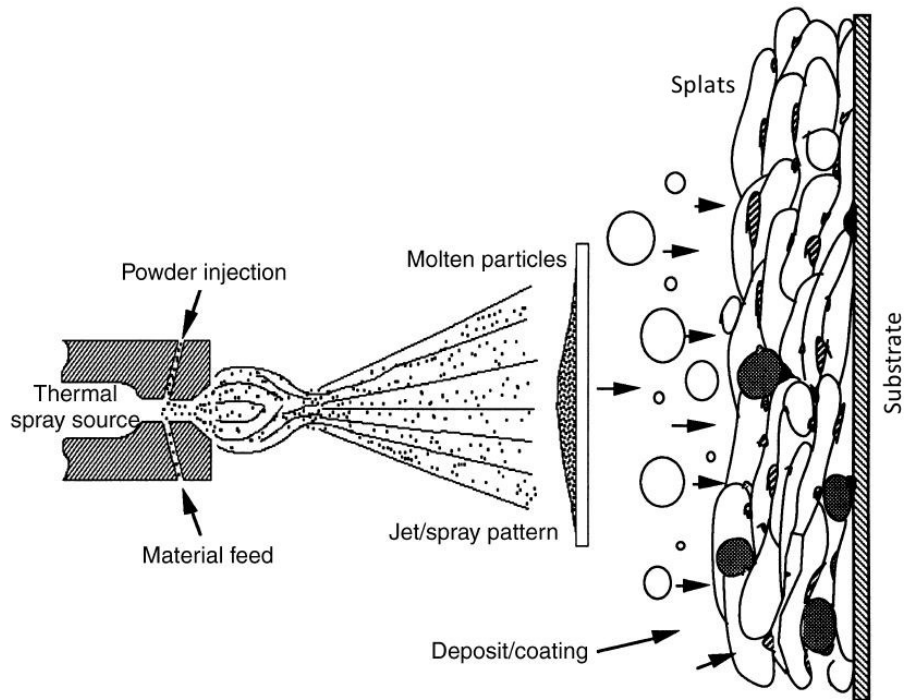
Figure 2.6. Formation of the coating in a thermal spray process [164].

In thermal spray, there are numerous process parameters affecting the coating deposition, microstructure and characteristics [165]. By controlling and carefully adjusting these parameters, it is possible to achieve a wide range of surface textures and morphologies. However, this requires meticulous examination of these parameters for different processes and coating materials. Different sub-classes of thermal spray processes include flame spray, wire arc spray, plasma transferred arc (PTA) deposition, induction plasma, high velocity oxygen-fuel (HVOF), detonation-gun and DC plasma spray. In Figure 2.7 [166] a comparison between different thermal spray techniques in terms of temperature and velocity of particles is presented. This range of temperatures and velocities allows deposition of virtually any material that does not decompose before reaching its melting point using the thermal spray process. In this work, the coating development stage has been carried out using a DC plasma system.
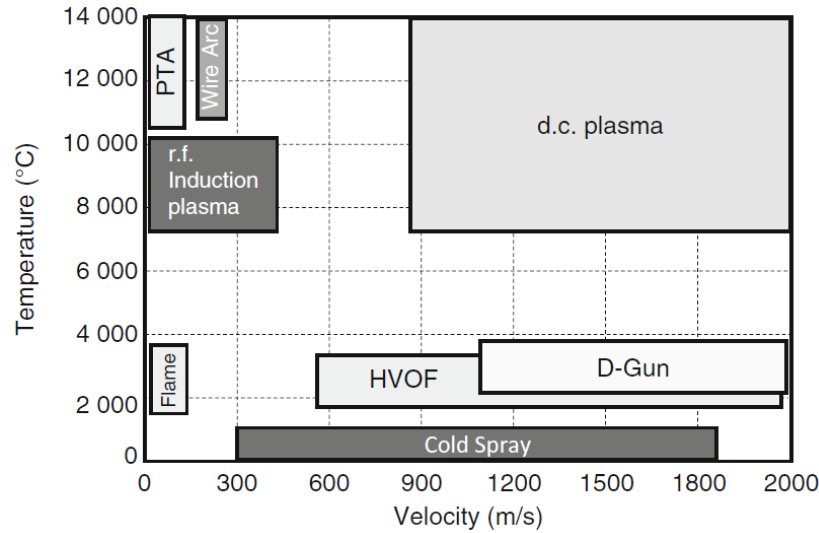
Figure 2.7. Gas temperatures and velocities obtained with different thermal spray systems [166].

One of the most important, widely used types of thermal spraying is atmospheric plasma spraying (APS). In this process, a high-temperature high-velocity plasma jet is used to heat and accelerate particles towards the substrate. The most important advantage of the APS process is its versatility. A wide variety of materials can be deposited on different substrate materials [167]. A second major advantage of this method of coating is that it is relatively cost efficient in comparison to some other surface modification methods [163,168], and thus it has found several industrial applications for developing functional coatings. Another benefit of atmospheric plasma spraying is the limited heat input to the substrate material that minimizes the thermal impact on the substrate. This means that typically the microstructure and physical properties of the substrate will remain unchanged. The plasma spraying method has been widely used to apply coatings on materials to provide them with resistance to wear, heat, erosion, and/or corrosion as well as some other desired surface properties [169–172].

Most powders used as feedstock in APS range in size from a few tens to a few hundreds of micrometers. Using conventional APS powders will result in microstructured coatings [173]. In order to produce nanostructured coatings, submicron or nano-size powders must be used. However, it is not practical to use such small particles in APS. Generally, particles smaller than 10 μm are difficult to be deposited using the APS technique. Very fine particles have very low mass, limiting their penetration in the high speed plasma jet so that they will not gain enough momentum to reach and impact the substrate [174]. Additionally clogging problems may occur in the powder feeder, powder line or injector. Therefore, the deposition of submicron or a nano

structured coatings in APS is very challenging. A solution to this problem is a relatively new variety of plasma spraying called suspension plasma spraying (SPS). This method allows one to deposit submicron and nano-scaled materials since feedstock materials are injected in the form of a suspension. A schematic of suspension plasma spray technique is presented in Figure 2.8.
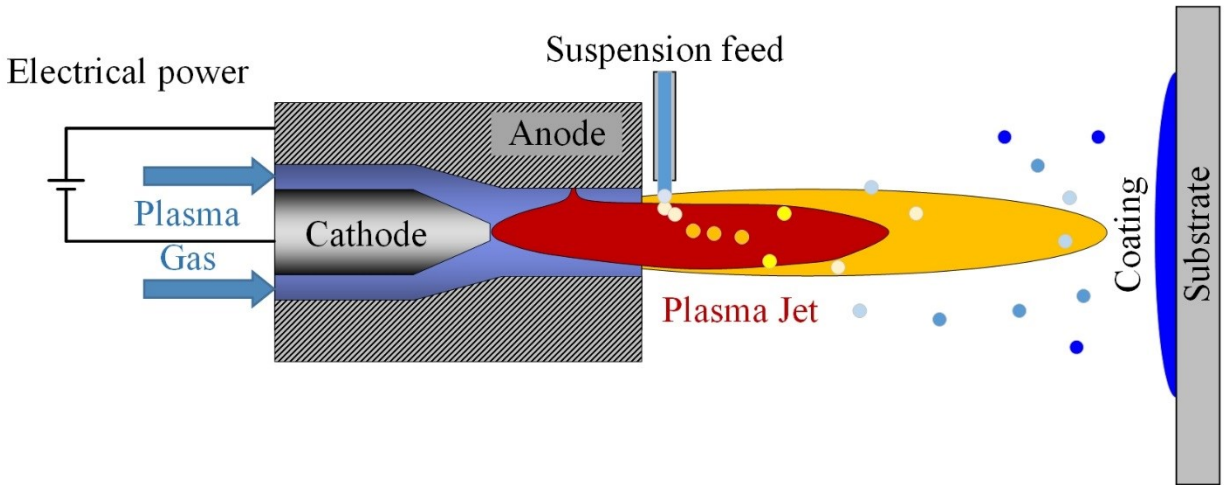
Figure 2.8. A schematic of suspension plasma spray technique.

In the SPS technique, the feedstock suspension usually contains a solvent (most of the time water or ethanol), the powder, and a dispersing agent that helps stabilize the suspension. When the suspension is injected into the plasma plume, it undergoes one, or sometimes multiple, breakup and atomization phases [175]. Then the solvent evaporates due to the heat from the plasma, leaving aggregates of powder. Sometimes these aggregates explode due to the jet and form smaller aggregates. These clusters of fine particles fully, or partially, melt depending on the condition and temperature and impact onto the substrate, creating splats. These stages are schematically demonstrated in Figure 2.9.
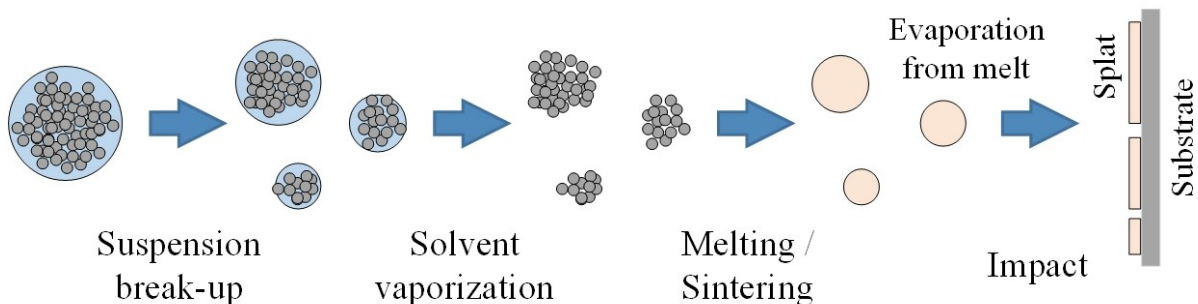
Figure 2.9. Various stages of coating formation in SPS technique.

According to Fauchais et al. [165,175,176], there are numerous parameters (up to nearly 50) that control APS and SPS processes and subsequently the coating structure. As a result, it can be concluded that plasma spraying processes (both APS and SPS) are capable of producing quite a wide variety of microstructures and coatings. The surface morphology of two plasma sprayed coatings is shown in Figure 2.10 [177]. In these examples, the parameters controlling the spraying/deposition process (in particular the deposition temperature), are modified in order to achieve such structures through deposition of semi-molten particles on a preheated substrate. Thermal spray techniques have occasionally been employed to develop coatings with special or controlled wetting properties including superhydrophobic coatings. In the next section a review of published research work that used thermal spraying to develop highly hydrophobic or superhydrophobic coatings is presented.
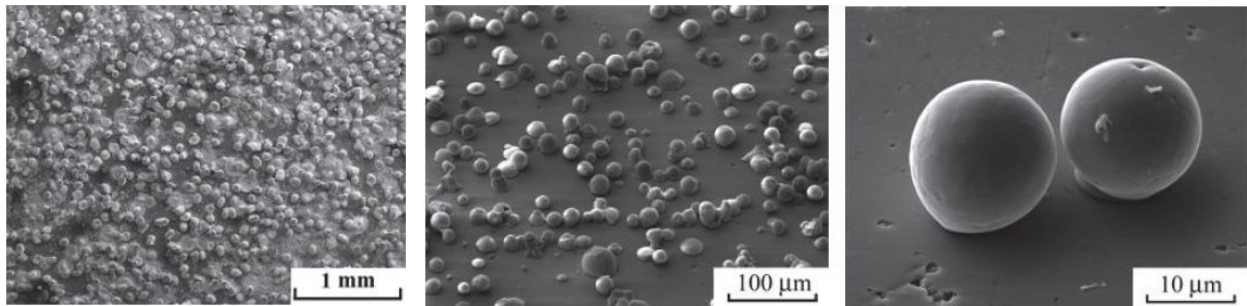
Figure 2.10. SEM images of microstructure of deposited Mo particles (LEFT), and Yttria stabilized Zirconia (MIDDLE and RIGHT) [177].

2.6.   Wetting behavior and superhydrophobicity of thermally sprayed coatings

Plasma spray coatings are widely used today for a variety of applications. Suspension plasma spray (SPS) process is particularly employed to produce thermal barrier coatings (TBCs) for aerospace applications [178–180]. However, the wettability of the thermally sprayed coatings has not been fully investigated.

The wetting behavior of a plasma sprayed oxide coating has been studied by Harju et al [181]. All studied oxide coatings showed hydrophilicity and surface preparation methods showed a great influence on the surface wettability. Additionally, surface contamination from exposure to the atmosphere has been found to increase the contact angle of the coatings. A liquid flame spray process was used to develop a polymer-based coating with high contact angle on a paperboard surface [182]. In this study, the coating showed low mobility which is not interesting for water repellency applications.

Eigenbrod et al. [183] introduced a multilayer coating process with thermal spraying as a base for air-sprayed polymeric top surface. The coatings demonstrate high water mobility but the multilevel process is complicated and the top layer is not very durable. The HVOF process has also been used to develop hydrophobic coatings [184]. Li et al. [185] showed that an atmospheric plasma sprayed mixture of Fe, Ni, and Cr, although hydrophilic as deposited, will gradually become hydrophobic due to adsorption of hydrocarbon groups when left in ambient air in the laboratory. After 35 days, the coatings have contact angles higher than 150° and sliding angles lower than 10 (Figure 2.11). Gou et al. [186] employed a vacuum cold spray process to deposit agglomerated nano-size titanium oxide on glass substrates. After being treated by a fluoroalkylsilane solution the coatings demonstrate superhydrophobicity. Obviously, a vacuum-based technique is not very practical for the large surfaces of aircraft.
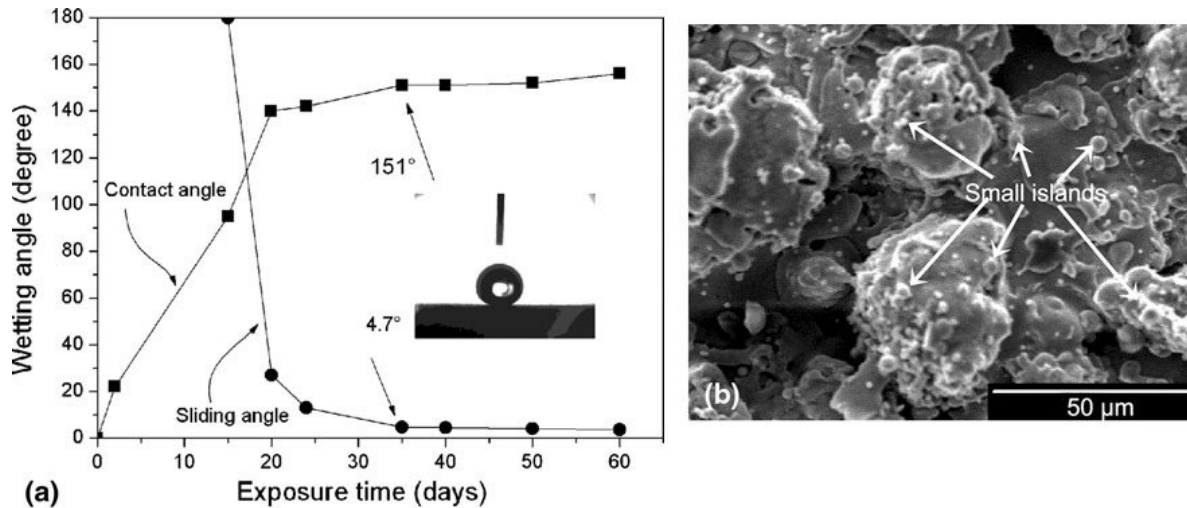
Figure 2.11: Change of the surface contact angle and sliding angle versus exposure time (a); and the microstructure of the coating (b) [185].

As mentioned before, there are reports of the hydrophobicity of rare-earth oxides. Gentleman et al. [187] claim observing hydrophobicity in thermally sprayed mixtures of various rare-earth oxides. Cai et al. [188] used solution precursor plasma spraying (SPPS) to deposit CeO_2 coatings. These coatings are not hydrophobic as-sprayed, but become superhydrophobic after being left in a vacuum chamber for 48 hours. Although no information about the carbon content of the surface is given, one could speculate that this change of behavior could be due to contamination of the coating surface in the vacuum chamber from exposure to the oil from the vacuum pump.

Leblanc, Bidkar et al. [189,190] are the first to report the development of superhydrophobic coatings using suspension plasma sprayed coatings that are further treated by a polymeric chemical for reducing surface energy. Although these coatings are mainly aimed for drag-reduction, they also demonstrate reduced ice adhesion.

In two different works, Chen et al. [73] and Koivuluoto et al. [191] reported developing polyurethane-based thermally sprayed coatings with reduced ice adhesion. Chen et al. [192] used a mesh as a shield to generate a patterned thermally sprayed coatings. A secondary top layer of polymer-based coating render these coatings superhydrophobic. The coatings demonstrate poor abrasion resistance. Schematic of the method used by Chen et al [192] is presented in Figure 2.12.
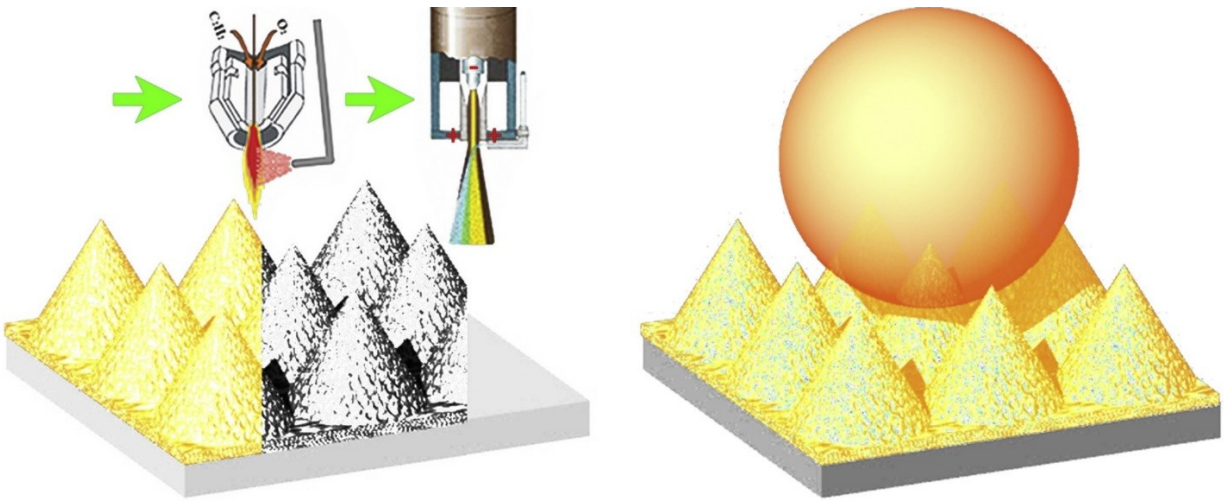
Figure 2.12. Schematic of a plasma sprayed superhydrophobic coating with multiscale topographical features achieved by shielding and then treating by PTFE [192].

In conclusion, as discussed above, there is a significant demand for a scalable, efficient, durable and easily reparable surface engineering solution to develop superhydrophobic coatings and test them in icing conditions. Thus the motivation of this work, which was described in detail in Chapter 1, is to address these gaps and shortcomings by using plasma spraying techniques for the development of durable, anti-icing superhydrophobic coatings.

Preface to Chapter 3.

As it was discussed in the previous chapters, one of the main objectives of this work is to investigate the capability of thermal spray processes to generate micro-textured coatings that can be treated to become superhydrophobic and to be used in anti-icing applications. In view of that, the atmospheric plasma spraying (APS) was the first technique that was investigated. APS process has various advantages to be employed for this purpose. Firstly, it is a scalable technique and can be easily applied to large surface. Additionally, APS is an atmospheric process that does not require any controlled environment. Moreover, the feedstock of APS process is typically micron-sized dry particles and poses smaller safety concerns compared to suspension feedstock which will be investigated later in this work. As a result, the next chapter in this thesis is entirely devoted to investigating the potential of APS process to created micro-textured coatings and how the process parameters can be controlled to optimize the wetting behavior of the resulting coatings.

Chapter 3. Morphology and Wetting Behaviour of Atmospheric Plasma Sprayed Titanium Dioxide [2]

Navid Sharifi, Martin Pugh, Christian Moreau and Ali Dolatabadi

Department of Mechanical and Industrial Engineering, Concordia University
Montreal, QC H3G 1M8, Canada

Abstract

The wettability of a solid surface is an important factor in the interaction of the surface with liquids. The wetting behaviour of a solid surface is a result of both its surface free energy and its morphology. Water wettability of solid surfaces is typically measured by their water contact angle. Low-wetting surfaces (hydrophobic) and extremely low-wetting surfaces (superhydrophobic) have various potential applications such as anti-icing coatings. In this paper, the wetting behaviour of atmospheric plasma sprayed (APS) titanium dioxide coatings and its dependence on the morphology of the coatings is investigated. The temperature and the velocity of the particles forming the coating are considered as the determining parameters for deposition conditions. By altering the two parameters, different surface morphologies were produced and their wetting behaviour was studied. The surface energy of the coatings was reduced using stearic acid treatment. It was found that within the range of particle velocity and temperature studied in this work, it is possible to produce surfaces with water contact angles close to a superhydrophobic state and as high as 144° as a combining result of both reduced surface energy and accomplished surface morphology. These high contact angle values were achieved through decreasing the temperature of the particles whilst increasing their velocity. Such coatings have a rough and irregular surface morphology which contributes to an increase in hydrophobicity of these coatings.

3.1. Introduction

The wettability of a solid surface by a liquid is governed by Young's Equation [42]:

$$\gamma_{sg} - \gamma_{sl} - \gamma_{lg} \cos \theta_0 = 0$$

Based on Young's Equation, the liquid contact angle (θ_0) is determined by the balance of interfacial energies of the solid, liquid and gas phases. The liquid is considered to "wet" the surface if its contact angle is smaller than 90°. In the case of the liquid phase being water, surfaces with water contact angles below 90° are called hydrophilic and surfaces with water contact angles above 90° are called hydrophobic.

In addition to the interfacial energies, the roughness of a surface can also effect its wettability. There are two models that explain the wetting behaviour of rough solid surfaces. The Wenzel model [81], assumes that the wetting region is a homogeneous interface between the solid and liquid phases. The apparent contact angle of a rough surface (θ) can be determined by the Wenzel equation:

$$\cos \theta = r \cos \theta_0$$

In this equation, the roughness ratio, r, is the ratio of the real surface area to the apparent surface area. According to the Wenzel model, the roughness amplifies the wetting behaviour of a surface. Thus, an intrinsically hydrophilic surface becomes more hydrophilic when roughened while an intrinsically hydrophobic surface becomes more hydrophobic when roughened.

On the other hand, the Cassie-Baxter model [82] assumes that the liquid-solid contact area is heterogeneous due to small gas bubbles entrapped between the liquid and solid phases. The apparent contact angle of a surface in the Cassie-Baxter wetting regime can be determined by:

$$\cos \theta = r_f f \cos \theta_0 + f - 1$$

In this equation, r_f is the roughness ratio of the wet region and f is the area fraction of wet region. The effect of roughness on the wettability of the surface under the Cassie-Baxter regime is more complicated than that under the Wenzel regime.

The wetting behaviour of a surface becomes especially important when it comes to interactions of liquid with the surface. For instance, when extended interaction of a surface with water is desirable, a hydrophilic surface is desirable. On the other hand, hydrophobicity is beneficial when minimum interaction of the solid surface with water is required.

When a surface is highly hydrophobic, it is typically referred to as a superhydrophobic surface. In the literature the criterion for superhydrophobicity is commonly considered to be a water contact angle greater than 150° [52]. The concept of superhydrophobicity is often associated with the structure of lotus leaves as natural superhydrophobic surfaces [193]. The non-wetting behaviour of a lotus leaf is a result of the combination of a low surface energy material with a special morphology, known as hierarchical or dual-scale micro-nano roughness [75].

There are several potential applications for highly hydrophobic and superhydrophobic surfaces including self-cleaning, low-friction and anti-icing surfaces [194]. There have been several techniques developed in recent years to produce bio-mimetic superhydrophobic surfaces [195]. The majority of these techniques combine the use of a low surface energy material and a type of surface roughness to achieve low water wettability [98]. However, many of these surfaces either lack good mechanical durability or have very high production costs [41]. Therefore, these surfaces are not appropriate for applications such as anti-icing on aeroplane external surfaces or power lines.

Atmospheric plasma spraying (APS) is a promising technique for producing coatings with special applications. APS can be used to produce mechanically durable coatings on relatively large engineering surfaces such as an aeroplane wing. It is a relatively fast, economical and versatile surface modification method that provides the possibility of producing desired morphologies by controlling deposition parameters such as power of the plasma torch and size of the feedstock.

The aim of this work is to investigate the capability of the APS technique to produce coatings with micro roughness to develop highly hydrophobic coatings with low water wetting behaviour. In this study, the focus is on adjusting the process parameters in order to control the temperature and velocity of the particles to produce different morphologies. The surface energy of the coatings is reduced using stearic acid treatment. The coatings are further studied and compared based on their morphologies and their apparent water contact angle.

3.2. Experimental

3.2.1. Materials

Titanium dioxide was chosen for this study due to its relative availability and low price as well as its relative durability and wear resistance as a ceramic. Also, the experiments were partially based on another study by the same authors [196]. Titanium dioxide, like the majority of ceramics

33

and metals is intrinsically hydrophilic with a water contact angle of 72° [197]. A commercial sintered and crushed titanium dioxide powder (Metco 102, Sulzer Metco) with a nominal size of 11 to 45 µm was used as the feedstock for producing the coatings. The SEM micrograph and the XRD pattern of the feedstock are presented consecutively in Figure 3.1 and Figure 3.2. In the SEM micrograph, feedstock particles are shown to have random shapes with sharp corners and edges. This might contribute to increasing the roughness of the coating, especially for partially molten particles. The XRD pattern shows that the feedstock powder mainly consists of rutile phase and Magneli phases. Magneli phases are reduced titanium dioxide and will transform to TiO_2 if they are exposed to high temperatures and oxygen [198].
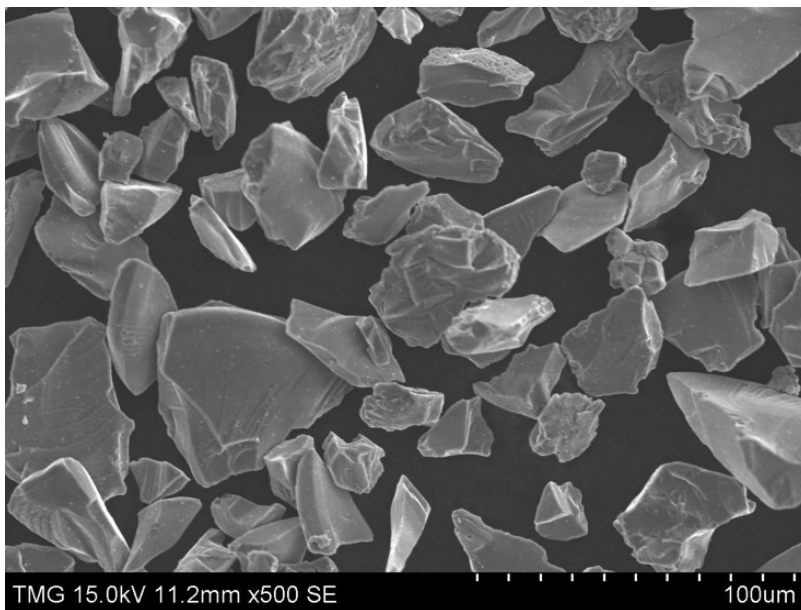
Figure 3.1. SEM micrograph of the feedstock powder.
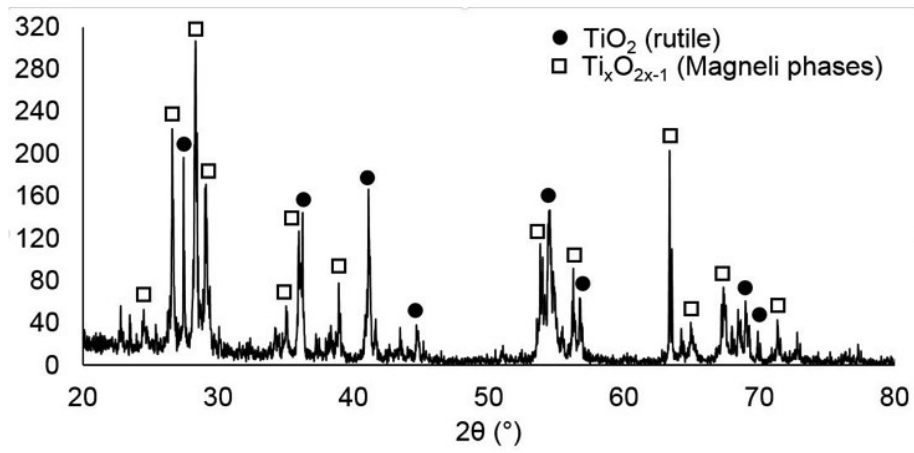
Figure 3.2. XRD pattern of the feedstock powder.

3.2.2. Selecting Deposition Parameters

It is widely acknowledged by scholars [165] that there are numerous parameters affecting the structure, phase distribution and morphology of APS coatings. This limits the repeatability of APS coatings. In order to deal with this problem, it was decided to focus on the temperature and velocity of the particles upon impact with the substrate. The effect of many deposition parameters can be represented by these two factors. Thus, optimization of a coating structure and performance is highly facilitated.

To select the deposition parameters in such a way that the effect of change in temperature and velocity of the particles is easily observed, a number of experiments were carried out using a DPV-2000 (Tecnar) APS diagnosis system. A set of spraying conditions suggested by the feedstock provider (Sulzer Metco) was used as a basis. Since the suggested commercial spray conditions are normally designed to achieve a dense coating and the purpose of this work was to achieve a rough and porous coating, the suggested conditions by the provider were used as the highest average particle temperature and velocity and all the other conditions were selected to have relatively lower particle temperature and velocity.

The final conditions that were chosen for this work are shown in terms of particle temperature and velocity in Figure 3.3. For the reader's convenience, these five spray conditions will be referred as HT/HV (for high temperature and high velocity), LT/LV (for low temperature and low velocity), HT/LV, LT/HV and MT/MT (for medium temperature and medium velocity) throughout the rest of this article.

In order to alter the particle temperature and velocity, the spraying conditions that were changed were plasma gas (argon) flow rate, secondary gas (hydrogen) flow rate and plasma current. Plasma gun stand-off distance was kept constant (9 cm) in order to have a relatively constant heat input to the substrates. The plasma torch travel speed (1 m/s), spraying pattern, plasma gasses pressure, feeding rate (10 g/min), carrier gas (also argon) flow and pressure were other parameters that were kept constant in order to have a valid comparison between the five coatings. The spraying parameters for the five conditions are given in Table 3.1.
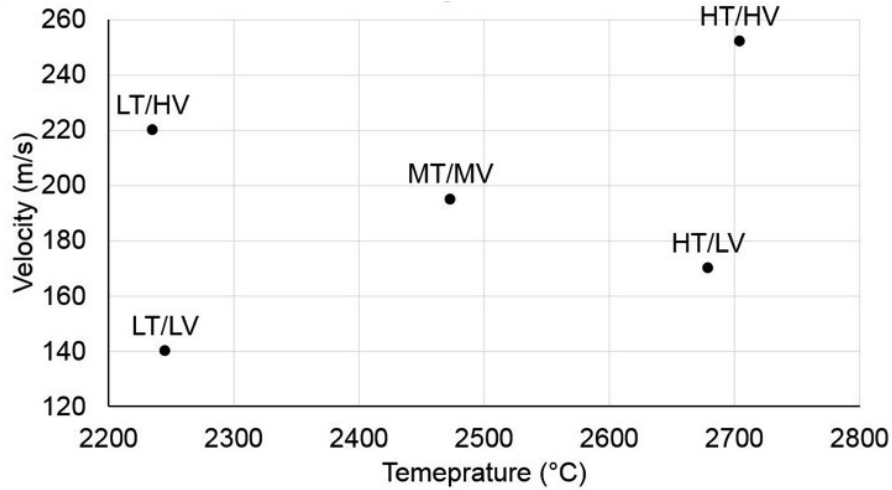
Figure 3.3. Average particle temperature and velocity for the five deposition conditions.

Table 3.1. Spraying Conditions.

	HT/HV	HT/LV	MT/MV	LT/HV	LT/LV
Ar flow rate (L/min)	40	20	40	60	30
H_2 flow rate (L/min)	6.5	6.5	2	1	1
Plasma current (A)	500	500	500	500	300

3.2.3. Coating Process

The coatings were carried out using a 3MB Sulzer Metco plasma torch. A 9MP Sulzer Metco powder feeder was used to inject the particles. All the coatings were deposited on 25 × 25 × 3 mm low carbon steel substrates. Prior to coating, all the substrates were grit-blasted and then ultrasonically cleaned in acetone. During the coating process, the temperature of the substrates was monitored using an A320 ThermoVision (FLIR Systems) infra-red camera. Pre-heating and air-cooling were used to make sure that the temperature of the substrates remain in the range of 100 to 200°C throughout the deposition process for all samples.

3.2.4. Reducing the Surface Energy

After the coating process, all samples were ultrasonically cleaned in acetone. Since the wetting behaviour of such coatings is very sensitive to surface contamination [199], the samples were boiled in deionised water for 10 minutes and then dried with compressed air to ensure the

samples are free from contamination to a satisfactory level. Then the samples were dipped into a 0.5 wt.% solution of stearic acid in 1-propanol and left at room temperature to dry [200].

3.2.5. Characterization of the Coatings

The XRD pattern of the coatings was obtained in order to identify the phases present in the coatings. The water contact angle of the coatings were measured using a sessile droplet method at room temperature and humidity. The setup consisted of a Photron Fastcam SA1 camera (Photron, USA), a manual droplet generator and a backlight LED. A schematic of the water contact angle measurement setup is shown in Figure 3.4. In order to achieve reliable results, the water contact angle measurements were carried out five times on three separate samples for each spraying condition and the presented results are an average of 15 measurements for each case.
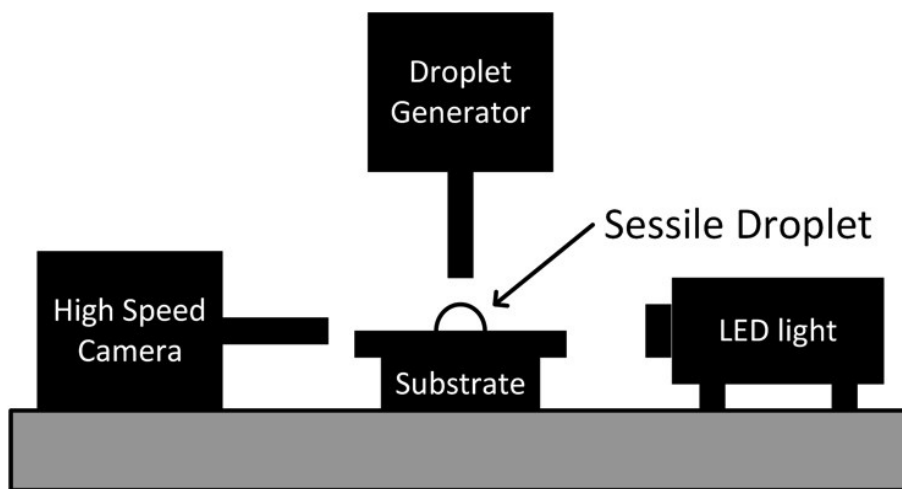
Figure 3.4. Schematic of the contact angle measurement setup.

A Hitachi S-3400N VP scanning electron microscopy (SEM) equipped with an energy dispersive X-ray spectrometer (EDX) was used to study the morphologies and the elemental distribution of the coatings.

3.3. Results and Discussion

The XRD patterns of the coatings that underwent the highest temperature (HT/HV) and the lowest temperature (LT/LV) are consecutively shown in Figure 3.5 and Figure 3.6. According to the XRD patterns, both coatings mainly consist of titanium dioxide in rutile form which is the common polymorph of titanium dioxide at ambient temperature. It is known that in thermally sprayed titanium dioxide coatings, rutile is more likely to form compared to the other polymorphs

of titanium dioxide, anatase and brookite [198]. It is also notable that some traces of iron from the substrates are shown in both XRD patterns due to the relatively small thickness of the coatings.
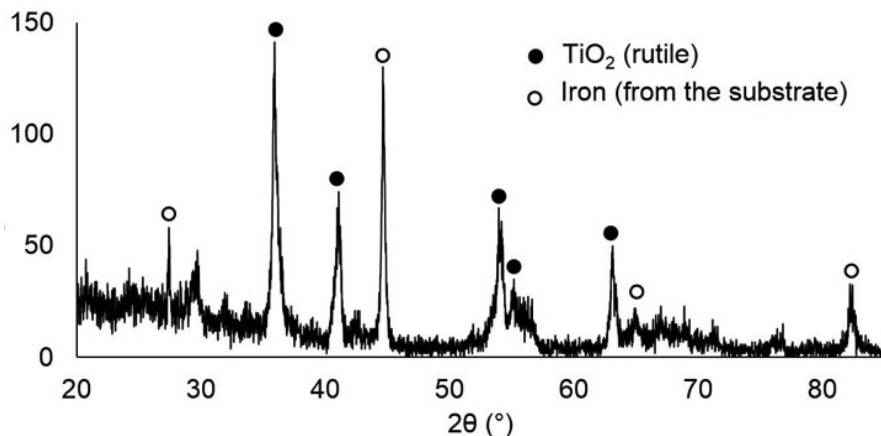
Figure 3.5. XRD pattern of coating HT/HV.

In order to have a better understanding of the net effect of the stearic acid treatment of the coatings, a smooth flat glass sample was treated in a similar manner that the coatings were treated. After treating the fairly flat sample with stearic acid solution, its contact angle was 94° making it slightly hydrophobic.
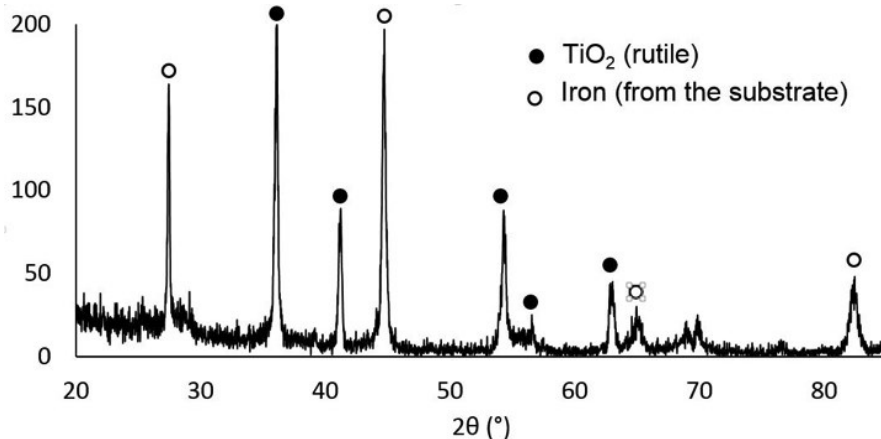
Figure 3.6. XRD pattern of coating LT/LV.

As mentioned before, after the deposition process, the samples were ultrasonically cleaned in acetone to get rid of dust, contamination and residue from the process. These samples were then boiled in deionised water, in order to make sure all the contamination, particularly the carbon species were removed from the surface. It is noteworthy that after this procedure, due to the intrinsic hydrophilicity of titanium dioxide and the fact that the coatings are very porous, a drop of water does not rest on the surfaces but rather is absorbed into the pores of the surface. Therefore

it is impossible to measure the water contact angle of the coatings after this cleaning process (i.e. very small intrinsic contact angle).

After the coated samples were subsequently treated in the stearic acid solution, their water contact angle was measured and the results are illustrated in the Figure 3.7. As was mentioned, the intrinsic contact angle of titanium dioxide is 72° and the contact angle of smooth glass treated by stearic acid solution is 94°. However it is seen that the water contact angle of titanium dioxide APS coatings treated with stearic acid solution range from 125° to 144°. This is attributed to the morphology of the surface of these coatings.
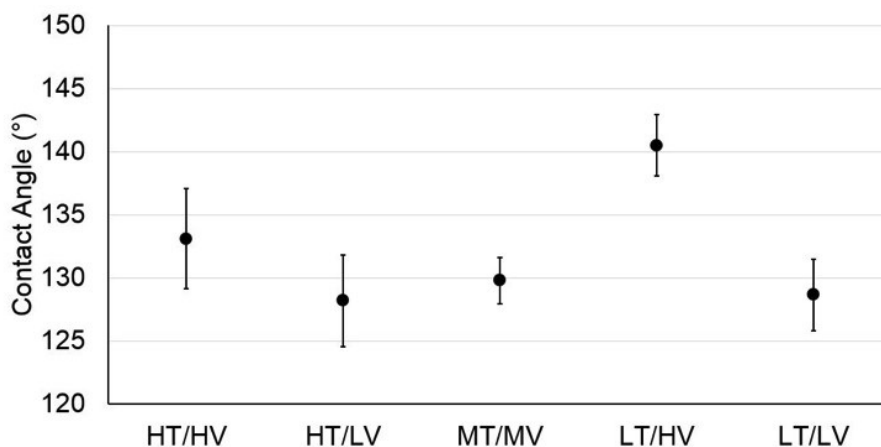
Figure 3.7. Measured water contact angle of the coatings.

An SEM micrograph of the five coatings with an inset image of sessile droplet sitting on their surfaces is shown in Figure 3.8 to Figure 3.12. The first important thing to be mentioned is that, as shown in these micrographs, the stearic acid treatment has not significantly changed the morphology of the coatings. The layer deposited from stearic acid treatment is very thin. In the SEM micrographs, the only visible sign of the stearic acid treatment is a slight colour alteration (and possible build-up) on the relatively flat parts of the coatings. This fact suggests that the difference between the wetting behaviour of the coatings is mainly as a result of the difference in their morphology.

As mentioned earlier, an SEM micrograph of the HT/HV coating is given in Figure 3.8. This coating shows the second highest water contact angle. In this coating, particles with relatively high temperature impacted on the substrate with relatively high velocity. Splats overlapped on their edges and formed the asperities seen in the micrograph. It is very difficult to distinguish single splats in this image. This is due to the high temperature and velocity of the impacting particles that

caused them to splash, split and form erratic shapes. As a result of splashing, there are some small satellite droplets spread on the surface of the coating. Theses satellite droplets can contribute to the desired morphology of the coatings if they are homogenously dispersed.
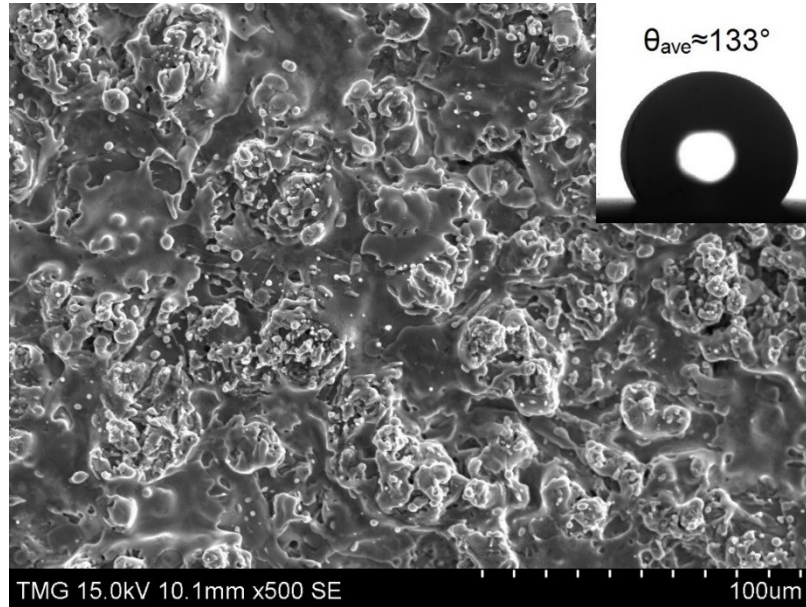
Figure 3.8. An SEM micrograph of the coating HT/HV. Inset: a sessile drop of water on this surface.

The SEM micrograph of the HT/LV coating is shown in Figure 3.9. Compared to the previous image, here the single splats are more distinguishable. Also, there are considerably more satellite droplets dispersed on the surface as a result of splashing and spreading of the molten particles. This coating apparently has the flattest surface among the five coated samples as well as the lowest average water contact angle. This is attributed to the relatively large splats forming several smooth areas in the morphology of the coating.

The surface morphology of the MT/MV coating is shown in Figure 3.10. This surface shows a morphology that can be considered between the morphology of the two previous coatings. Its surface roughness is not as erratic as the HT/HV coating, and not as flat as HT/LV coatings.

The surface morphology of the LT/HV coating is demonstrated in the Figure 3.11. This is the most interesting of the coatings because it is associated with the highest value of water contact angle. In this coating, the temperature of the particles was relatively lower thus more viscous and less mobile, giving less splashing. However, the relatively high velocity of the particles cause them to jam, split and overlap. As a result, this coating has the most erratic morphology among all the

40

other coatings. The high water contact angle of this coating compared to the other coatings is attributed to its morphology and roughness.
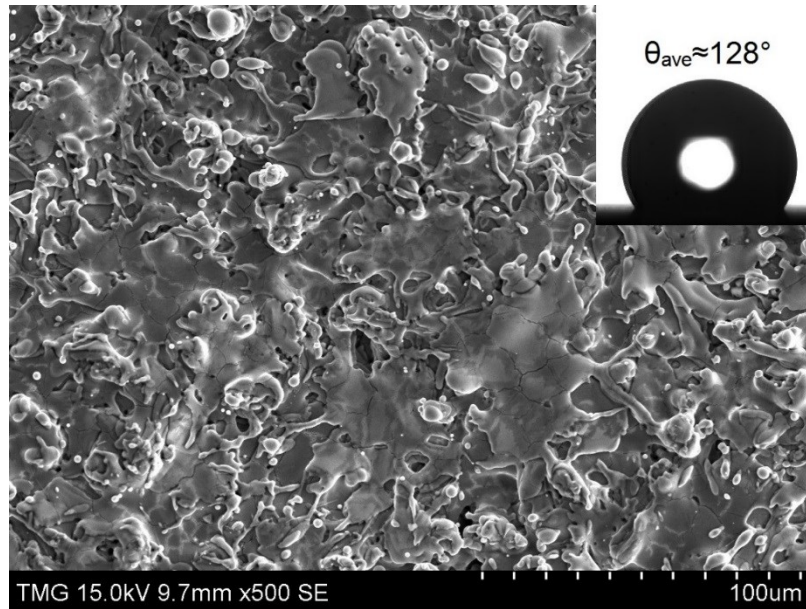
Figure 3.9. An SEM micrograph of the coating HT/LV. Inset: a sessile drop of water on this surface.
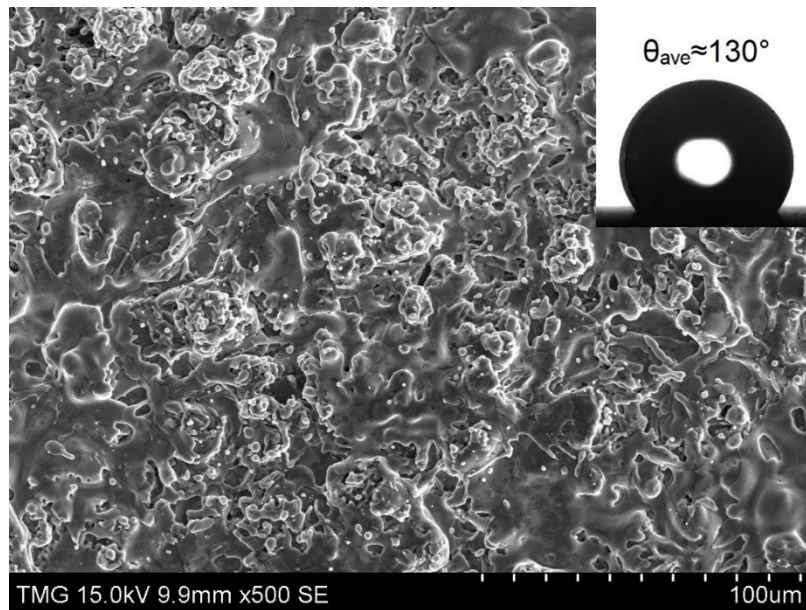
Figure 3.10. An SEM micrograph of the coating MT/MV. Inset: a sessile drop of water on this surface.

The SEM micrograph of the LT/LV coating is shown in the Figure 3.12. Contrary the fact that it might have been predicted prior to this study that the lowest temperature and velocity of the

particles would result in the roughest surface and therefore the lowest wettability, it is shown that the surfaces of LT/LV coatings have less erratic roughness features and therefore give a smaller water contact angle.
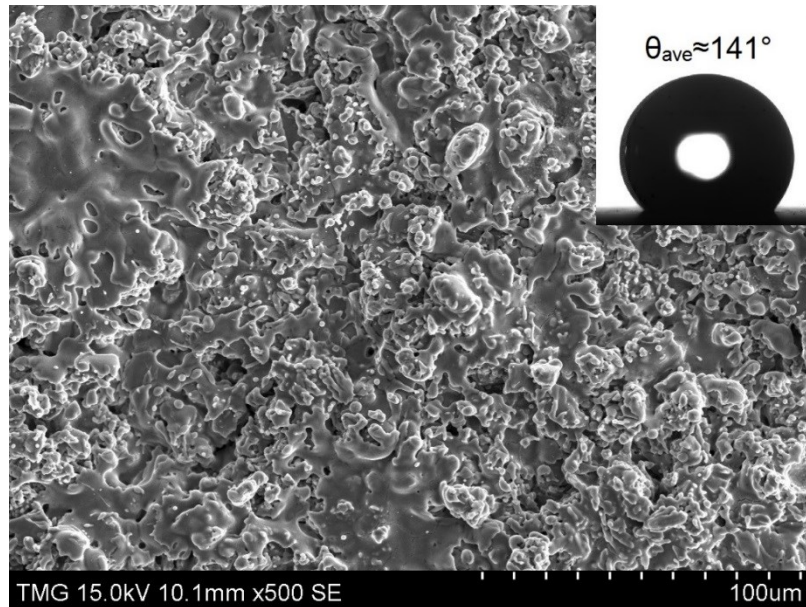
Figure 3.11. An SEM micrograph of the coating LT/HV. Inset: a sessile drop of water on this surface.

Nevertheless, one interesting feature of this coating is the few, nearly spherical, asperities that are seen on the surface and are apparently a result of semi-molten particles impacting onto the substrate with relatively low velocity. These features are reported to improve hydrophobicity [201] in thermally sprayed coatings. However, in this case this spherical shapes are too few in number to significantly affect the hydrophobicity. It is expected that by controlling the deposition conditions, the number and distribution of such features can be adjusted in a way that hydrophobicity of the coating increases significantly.
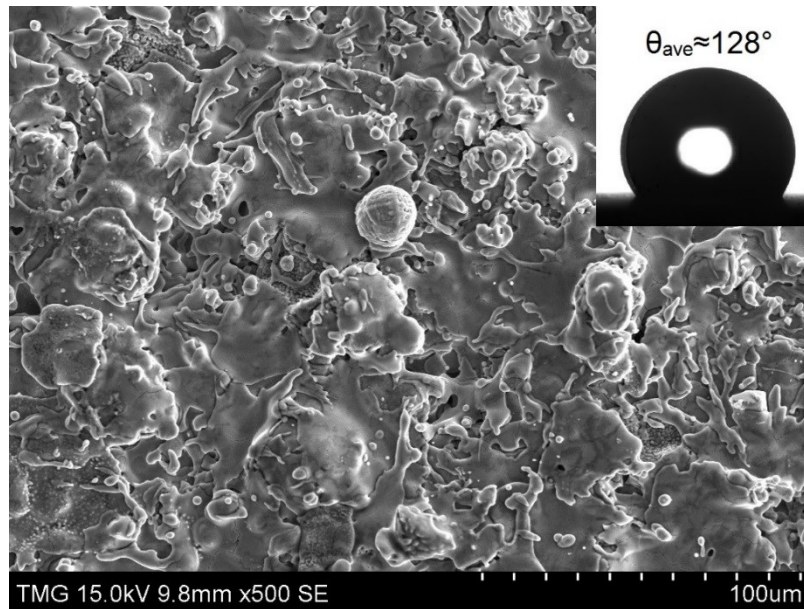
Figure 3.12. An SEM micrograph of the coating LT/LV. Inset: a sessile drop of water on this surface.

According to the results of this study, it can be concluded that with further increase in the particle velocity and decreasing the temperature to the lowest possible value, higher roughness and therefore lower wettability of the coatings may be produced. However, there are two points worth mentioning at this point. First, the temperature and the velocity of the particles in thermal spraying are to some extent coupled. This means that usually when one deposition parameter is changed, the other also changes. In order to increase one of these parameters and decrease the other one, it is necessary to alter the deposition parameters beyond their typical amounts. The second point is that, as there are several parameters affecting the morphology of the thermally sprayed coatings, there are also many morphological features that can change the wettability of a surface. In this sense, the conclusion from the results of this study can hardly be extended to a range of the parameters (i.e. temperature and velocity of the particles) significantly different from the ones investigated in this work.

3.4. Summary and Conclusion

In this work, the wettability of titanium dioxide APS coatings is studied. The various deposition conditions were determined based on measuring the temperature and the velocity of the particles. XRD tests showed that coatings are almost entirely made of rutile phase. Measurements showed that the water contact angle of the coatings increased from the intrinsic contact angle of

43

hydrophilic titanium dioxide (72°) to a hydrophobic state with a water contact angle of between 125° to 144°. The highest contact angle and therefore the lowest wettability was achieved through the coating with lowest particle temperature and highest particle velocity.

The SEM imaging revealed that high particle temperature, especially if accompanied by low particle velocity will result in a relatively flat and plane morphology. This type of morphology is not favoured when a low wetting behaviour is desired. The most erratic and rough coating morphology is achieved for a coating with relatively low particle temperature and high particle velocity. The cooler particles split and solidified in a random shaped manner upon impact to form this morphology. This is in contrast with the case of relatively hotter particles that spread and splash to form a relatively more flat morphology.

Collectively it can be concluded that the titanium oxide APS coatings that can be produced through controlling the deposition parameters, have a surface morphology that can promote non-wetting behaviour and hydrophobicity. In the range of process parameters studied in this work, none of the coatings reached the level of superhydrophobicity (150°) however water contact angles as high as 144° were achieved. This shows that with further modification of deposition parameters, it might be possible to produce superhydrophobic coatings.

Acknowledgement

Preface to Chapter 4.

In the previous chapter, it was demonstrated that atmospheric plasma spray (APS) process parameters can be adjusted to achieve micro-textured TiO_2 coatings that after treatment demonstrated high water repellency. However, this amount of hydrophobicity is not sufficient for anti-icing applications, because to prevent or delay ice formation, a highly hydrophobic or superhydrophobic surface requires high water mobility in addition to high water repellency. The lack of water mobility i.e. sticking of water to the surface is due to the relatively large-scaled and irregular roughness of the surface of the APS coatings which is a result of using micron-sized feedstock powder to generate the coatings. Therefore, suspension plasma spray (SPS) was selected as an alternative. In the SPS process, submicron-sized particles are used in the form of a suspension as feedstock. This enables generating more refined, finely micro-textured and micro-structured surfaces. Therefore, the following chapter is devoted to investigating the capability of the SPS process in generating micro-textured coatings and comparing APS and SPS coatings in terms of their wetting characteristics.

Chapter 4. Developing Hydrophobic and Superhydrophobic TiO$_2$ Coatings by Plasma Spraying[3]

Navid Sharifi, Martin Pugh, Christian Moreau and Ali Dolatabadi

Department of Mechanical and Industrial Engineering, Concordia University

1455 de Maisonneuve Blvd. W, Montreal, Quebec, Canada, H3G 1M8

Abstract

In this work, atmospheric plasma spraying (APS) and suspension plasma spraying (SPS) are employed for developing micro/nano morphologies of superhydrophobic coatings with high water repellence and mobility. Accordingly, multiple coatings were developed with different surface morphologies, then by isolating the effect of surface chemistry using a stearic acid treatment, the importance and influence of the achieved morphologies on wetting behavior of the coatings were investigated. Experimental results show that, although coatings developed by the APS process may reach water contact angles as high as 145°, the water mobility of these coatings is low due to relatively large morphological features resulting from the micron-sized feedstock powder. On the other hand, coatings developed by SPS show superior water repellence (manifested through water contact angles as high as 167°) as well as improved mobility (displayed through water sliding angles as small as 1.3°) due to dual-scale submicron/nano (hierarchical) roughness attributed to the submicron size particles in the feedstock. The dynamic behavior of an impinging water droplet is studied and compared to other existing natural and fabricated superhydrophobic surfaces.

Keywords: superhydrophobic; atmospheric plasma spray; suspension plasma spray; TiO$_2$ coating, wetting; hierarchical surface roughness

---

4.1.   Introduction

The wetting behavior of surfaces is classified as hydrophobic or hydrophilic. A hydrophilic surface tends to be wetted by water whereas a hydrophobic surface has a tendency to repel water. Hydrophilic and hydrophobic surfaces are defined by a surface water contact angle (WCA) of below and above 90° respectively. The wetting behavior of a surface is a function of both its surface chemistry and surface morphology [202]. While surface chemistry is the determining factor when it comes to inherent wetting behavior of an ideally smooth surface, certain surface patterns and morphologies can drastically alter the wettability of a surface.

Schematics demonstrating ideally smooth hydrophilic and hydrophobic surfaces are shown in Figure 4.1 (a) and (b) respectively. The inherent water contact angle (θ_0) of a surface is determined by the balance of interfacial energies between solid, water (liquid) and air (gas) phases and is notably described by Young [42] (Figure 4.1). Accordingly, hydrophobic materials have a low solid/air interfacial energy compared to hydrophilic materials and thus sometimes are referred to as "low surface energy materials". The wetting of a surface is furthermore significantly influenced by the geometrical micro or nano-roughness of the surface [48,203]. As Wenzel [81] and Cassie and Baxter [82] notably explained, the apparent water contact angle of a rough hydrophobic surface (θ_c) is higher than its inherent contact angle as illustrated in Figure 4.1 (c). This is due to the formation of microscopic air pockets between the solid surface and the water droplets. The presence of this air phase increases the water repellence of the surface and facilitates water mobility, which is often manifested through the sliding angle of a surface – the angle to which a surface must be tilted for a water droplet to start to move on it.
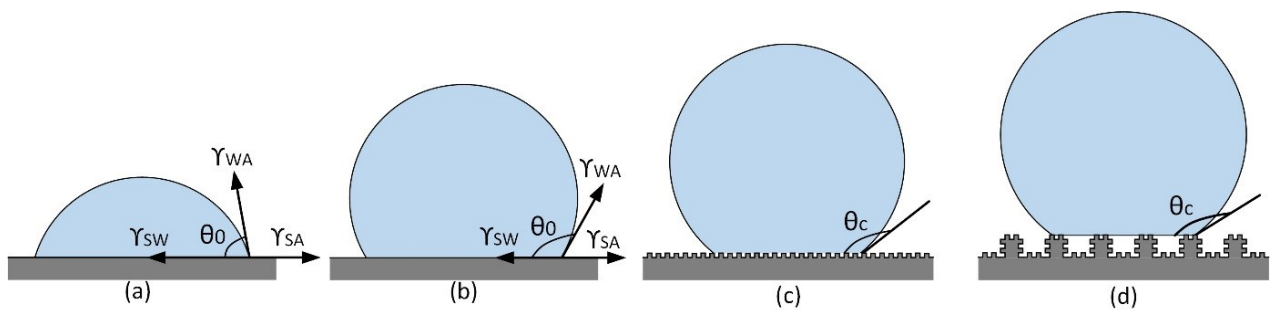
Figure 4.1. Schematic of (a) a smooth hydrophilic, (b) a smooth hydrophobic, (c) single-scale rough hydrophobic and (d) hierarchical rough hydrophobic surface.

Studies show [75] that a dual scale (also known as hierarchical) roughness on the surface can improve the water mobility of a surface further as shown in Figure 4.1 (d). When a surface is

47

highly hydrophobic, it is typically referred to as a superhydrophobic surface. These surfaces are characterised by their extremely high water repellence and non-wettability and in the literature, this is commonly manifested by a water contact angle greater than 150° and a water sliding angle lower than 10° [52].

The concept of structured superhydrophobic surfaces is often associated with the structure of the lotus leaf [90] as a natural superhydrophobic surface with both high water repellence and water mobility [193]. The non-wetting behaviour of a lotus leaf is a result of the combination of a relatively low surface energy material with the hierarchical or dual-scale micro-nano roughness [75] making this type of roughness the most desired morphology for superhydrophobic coatings [92].

The lotus structure inspired superhydrophobic surfaces and have been the subject of intensive research in recent years. Due to their unique wetting behaviour, there are several potential applications for highly hydrophobic and superhydrophobic surfaces including self-cleaning [72], low-friction, drag-reduced [189] and anti-icing surfaces [194]. Several techniques have been developed in recent years to produce bio-mimetic superhydrophobic surfaces [195]. The majority of these techniques combine the use of a low surface energy material and a certain type of surface roughness to achieve low water wettability [98,204]. However, many of these surfaces either lack the desired mechanical durability or have very high production costs [41]. Existing superhydrophobic coatings tend to be either polymer-based, low surface energy materials that have poor mechanical properties or are fabricated using complex or costly techniques such as chemical and electrochemical etching, PVD or laser pulse surface structuring.

Thermal spraying, especially atmospheric plasma spray (APS) and suspension plasma spray (SPS), is a promising method to deposit coatings with structured surfaces to control hydrophobicity. In APS, as a fast and economical process for surface modification [185], coating is the result of the impact, flattening and solidification of melted or partially melted micron-sized (typically larger than 5 μm) particles on the substrate surface [205]. It is important to note that in the APS technique, the use of smaller feedstock particles is limited since these particles do not gain the necessary momentum in the plasma flow and fail to form a coating layer due to their small mass. Suspension plasma spray (SPS) permits the manufacture of thick (from 10 to 300 μm) coatings structured at the sub-micrometer or even nanometer scales [206]. SPS consists of the injection of a continuous stream of suspension (made of a solvent, particles and a dispersant) into

a plasma jet where it is first fragmented into droplets before solvent vaporization and melting of solid particles prior to their impact upon the substrate to form layers of a coating with a minimal thickness of about 10 μm [179]. Both these methods provide cost-efficient and straightforward coating techniques that are applicable to large surfaces such as aerodynamic surfaces of aircraft or exterior parts of a power line. In rare occasions thermal spraying processes have been employed to develop textured hydrophobic and superhydrophobic coatings. For instance, one research by Bidkar et al. [190] and its corresponding patent application [189] focused only on drag reduction properties of such coatings. In another case, Li et al. [185] developed metallic APS coatings that gain superhydrophobicity after being exposed to atmosphere for a period of nearly one month. However, the water mobility of these coatings is not thoroughly explored.

In the present study, the main objective is to investigate the capability of atmospheric plasma spraying and suspension plasma spraying techniques to develop desired roughness and morphologies for high water repelling, high mobility superhydrophobic surfaces. Since the main focus of this research is studying the generated morphologies and their effect on the wetting behavior of the coatings, titanium dioxide as an available, low-cost and chemically inert material is selected as the coating material. The effect of different surface chemistries is removed by treating all the surfaces with a low energy solution of stearic acid, thus enabling us to investigate the effect of surface morphology in terms of static and dynamic wetting behavior of the samples.

4.2. Experimental

For this study two APS coatings and two SPS coatings were developed and their morphology and its respective impact on the wetting behavior of the coatings were studied. The two APS coatings have significantly different deposition conditions leading to two distinctly different morphologies. The SPS coatings were developed using two different precursor suspensions that also resulted in two completely different morphologies.

4.2.1. Materials

For the APS coatings, a commercial Metco 102 titanium dioxide thermal spraying powder (Metco Oerlikon, Fort Saskatchewan, Canada) with a nominal particle size distribution of 11-45 μm was used as the feedstock. For the SPS coatings, the feedstock comprised a sub-micron sized titanium dioxide powder (TKB Trading, Oakland, CA) with an average nominal particle size of 500nm. For the study, two different suspensions of titanium dioxide were prepared in distilled

water and ethanol as solvents respectively. Water was chosen as one of the solvents for the suspension due to near complete dispersion of titanium dioxide in water and ethanol was chosen as it offers a different and distinct suspension compared to water, thus creating a completely altered coating morphology. As dispersing agent, polyacrylic acid (PAA) (Sigma-Aldrich, Oakville, Canada) and polyvinylpyrrolidone (PVP) (Sigma-Aldrich, Oakville, Canada) were used for the water-based (denoted SPS-W) and the ethanol-based (SPS-E) suspensions respectively. The solid content of the suspensions was 10wt% in both cases while the dispersing agent was 5wt% of the solid content. The suspensions were first mechanically stirred for 10 minutes and then sonicated with 65 W power for 10 minutes. The particle size distribution of the suspensions were determined by a Spraytec (Malvern Instruments, UK) unit equipped with a wet dispersion accessory.

An SEM micrograph of the APS feedstock powder is shown in Figure 4.2 (a). The powder consists of particles ranging between approximately 20 to 70 μm in size. The particles are crushed with sharp corners and a variety of random shapes. An SEM micrograph of the SPS feedstock powder is presented in Figure 4.2 (b). This powder consists of particles approximately 500 nm and below.
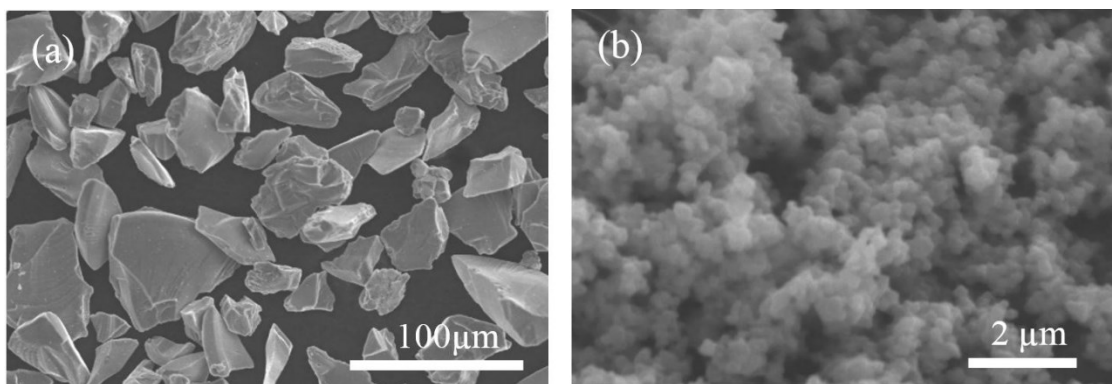
Figure 4.2. SEM micrograph of (a) the APS feedstock TiO_2 powder; and (b): SPS feedstock TiO_2 powder.

The particle size distribution of the water-based suspension (SPS-W) was measured and the result is presented in Figure 4.3. The measured average particle size in terms of Sauter mean diameter (D_{32}) [207] is 504 nm which shows the titanium dioxide particles are reasonably well-dispersed in the solvent due to the fact that TiO_2 is water dispersible.
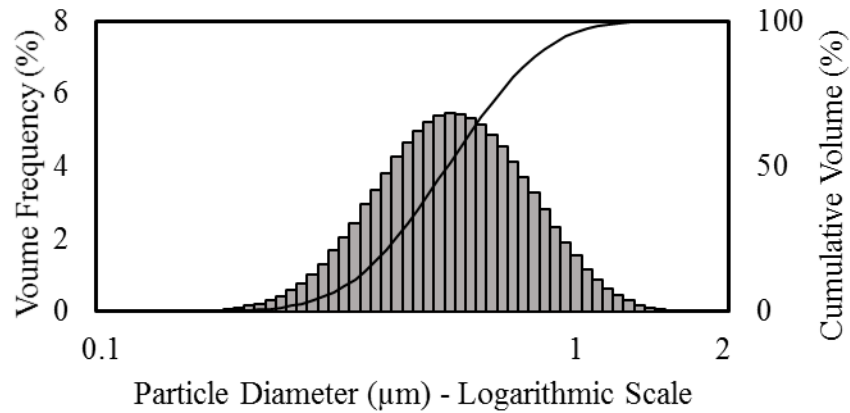
Figure 4.3. Particle size distribution of water-based TiO$_2$ suspension.

Similarly, the particle size distribution of the ethanol-based suspension (SPS-E) is demonstrated in Figure 4.4. In contrast to the water-based suspension, in this case, many of the feedstock particles form remarkably larger aggregates and agglomerates. The Sauter mean diameter of the particles (D32) in this case is 8.1 μm which is one order of magnitude larger than particles in the water-based suspension. It is noteworthy that in Figure 4.4, a second peak of dispersed particles appears at around 1 μm which corresponds to single particles or aggregates with a much smaller number of particles. Although this portion of the particles has a small volume, it consists of far larger number of particles than the large peak on the right side of the diagram.
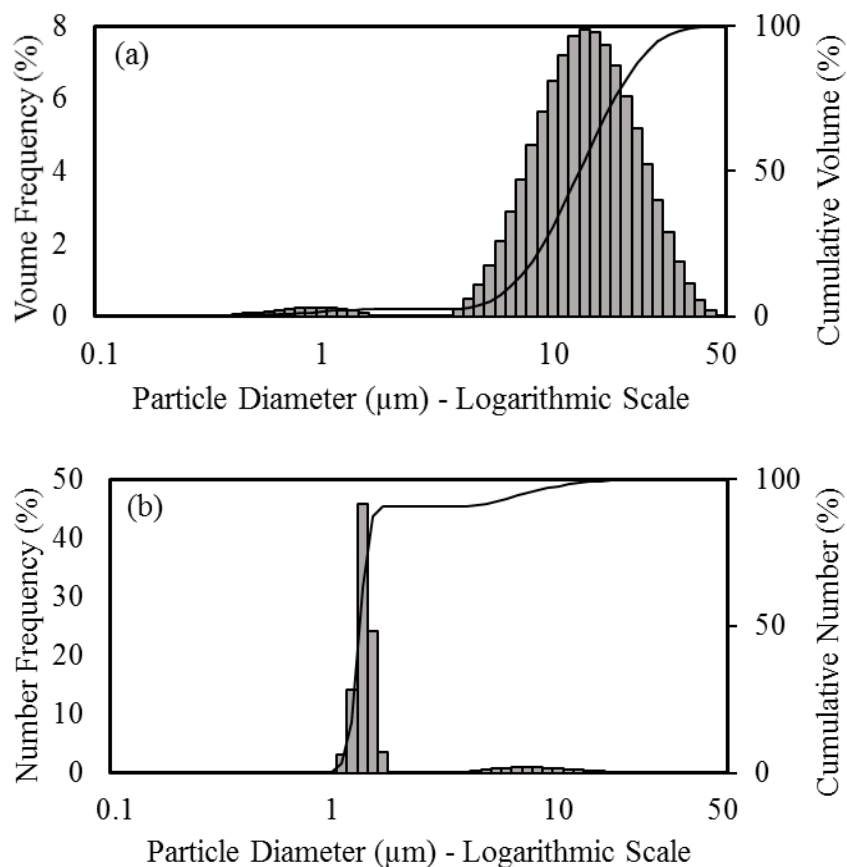
Figure 4.4. Particle size distribution of ethanol-based TiO$_2$ precursor suspension as sprayed; (a) volume frequency, and (b) number frequency of particles.

4.2.2. Sample Preparation

All coating were deposited onto 25 mm × 25 mm × 3 mm stainless steel coupons. Prior to coating, the substrates were grit-blasted using 80 grit Al$_2$O$_3$ particles and then ultrasonically cleaned in acetone to avoid any significant contamination. For all samples, the substrates were preheated to approximately 100°C by the plasma immediately prior to coating. The surface temperature of the coatings was monitored by an A320 ThermoVision infrared camera (FLIR Systems, MA) and was maintained below 200°C for the APS process and below 350°C for SPS using forced air cooling.

Both APS and SPS coating processes were carried out using a 3MB plasma torch (Metco Oerlikon, Westbury, NY). For APS, the feedstock was injected radially into the plasma using a 9MP powder feeder (Metco Oerlikon). For SPS, the feedstock suspension was radially injected into the plasma using a pressure-based feeding unit developed in-house. Pressure tanks were

pressurized using argon. Operating parameters for the two APS (labeled APS1 and APS2) and the two SPS (labeled SPS-W and SPS-E) coatings are presented in Table 4.1.

Table 4.1. Deposition condition and coating parameters.

Parameter	Value			
	APS1	APS2	SPS-W	SPS-E
Argon (primary plasma gas) flow rate [L/min]	40	60	50	
Hydrogen (secondary plasma gas) flow rate [L/min]	6.5	1	5	
Carrier gas (argon) flow rate [L/min]	6		N/A	
Feed Rate [g/min]	20		30	
Plasma Current [A]	500			
Spray Distance [mm]	90		60	
Plasma gun traverse speed [m/s]	1			

A DPV-2000 (Tecnar, St-Bruno, Canada) online diagnosis system was used to monitor the in-flight temperature and velocity of the particles in the APS process at 90 mm from the torch exit.

After coating deposition, all samples were ultrasonically cleaned in acetone. Since the wetting behaviour of such coatings is very sensitive to surface contamination [199], the samples were boiled in deionised water for 10 minutes and then dried with compressed air [200]. Subsequently, the samples were dipped into a 0.5 wt.% solution of stearic acid in 1-propanol and left at room temperature to dry. The stearic acid treatment reduces the surface energy of the coating surface rendering them hydrophobic, eliminates the effect of surface contamination and moreover, ensures that the chemistry of the surface of all coatings is similar, thus isolating the effect of surface roughness and morphology.

4.2.3. Morphology and Structural Characterization

The morphology of the feedstock and coatings (top surface and cross-sectional views) was observed by SEM (Hitachi S-3400N VP). The samples were prepared by standard metallographic methods. Additionally, the morphology of the coatings and various surface roughness parameters were observed by a LEXT OLS4000 confocal laser microscope (Olympus, Toronto, Canada).

Among the various surface roughness parameters, based on the literature [208], the arithmetic average surface roughness (R_a), the root mean square surface roughness (R_q), skewness (R_{sk}) and kurtosis (R_{ku}) were measured and their possible relation with the wettability of the coatings was investigated. The R_a is the most commonly used surface roughness parameter and has been deemed as being related to the water contact angle and thus repellence of a surface [92]. Skewness is a measure of the asymmetry of the surface profile. Kurtosis is a measures of "peakedness" (or alternatively "flatness") of a surface. Skewness and kurtosis have both been used to help predict the water mobility on a surface [209–211]. For the roughness measurements of the samples, five areas of 1×1 mm on different parts of the samples were used.

4.2.4. Wetting Characterization

The imaging for static water contact angle and the water sliding angle measurement of the coatings was carried out using a sessile droplet method at room temperature and humidity. As mentioned previously, the static contact angle is commonly used as a measure of the water repellence of a surface whereas sliding angle is often used to characterise the water mobility of a surface. The static contact angle was measured by putting a 10µL droplet of water on the surface of the samples, capturing an image and then analysing the image to calculate the contact angle. The sliding angle was measured by putting a 10µL droplet of water on a horizontal surface, then tilting the surface until the droplet started to move. The angle to which surface was tilted for the water droplet to move was considered the sliding angle of the surface. The setup for contact angle measurement consisted of a Fastcam SA1 camera (Photron Ltd, Tokyo, Japan), a manual droplet generator and a backlight LED and a stage for the samples with vertical, horizontal and tilting micro-positioners. The image analysis and the measurements were carried out using a code developed by Stalder et al. [212,213] as a plugin to the free image analysis software ImageJ (NIH, MD, USA). The measurements were repeated five times on three different samples with the same deposition process.

This setup was also employed to study the dynamic interaction of an impinging water droplet onto the surface of the coatings. As mobility of a superhydrophobic surface plays a crucial role in many of its potential applications such as anti-icing, it is very important to study different aspects of the dynamic wetting behavior of a superhydrophobic surface in addition to its sliding angle. For this purpose, a 10 µL water droplet, was dropped from various heights onto the surface of the samples. The process of the water droplet interacting with the surface was observed and

recorded through the high speed camera. In the case of relatively high mobility surfaces and depending on the impact velocity of the droplet, it can bounce back and detach from the surface. A very important and common parameter in this regard is the coefficient of restitution of a surface during the impact of a droplet of water. The coefficient of restitution which is the ratio of droplet velocity after and before impact, represents the amount of energy consumed during the interaction of the droplet and the solid surface. In this case, the coefficient of restitution was determined as the ratio between the velocity of the droplet right before impact and right after detaching from the surface. Obviously, a surface with a higher coefficient of restitution has more mobility due to the smaller amount of energy dissipated during the interaction between the solid surface and the water droplet. The coefficient of restitution of the samples was then compared to other commercial and well-known superhydrophobic surfaces including a commercial polymer-based spray product WX2100 (Cytonix Co., MD, USA), a lotus leaf and a nano-grass (denoted NG) surface fabricated by depositing carbon nanotubes on a patterned silicon substrate [214].

4.3. Results and Discussion

4.3.1. APS Process Diagnosis and Selection of Deposition Condition

The temperature and velocity of the in-flight particles measured by the DPV-2000 system for the two APS coatings are shown in Table 4.2. The spray conditions for these two samples were chosen based on a previous study in which the influence of spray condition on particle temperatures and velocities was investigated [196]. These conditions are meant to produce two distinct morphologies resulting from relatively high temperature and low velocity (APS-1) and relatively low temperature and high velocity (APS-2).

Table 4.2. Mean and standard deviation of the temperature and velocity of in-flight particles for the APS coatings.

Sample	Temperature (°C)	Velocity (m/s)
APS-1	2679 ±82	170 ±27
APS-2	2235 ±148	220 ±23

4.3.2. Wetting and Roughness Measurements

The measured values of the static contact angle, sliding angle, arithmetic mean surface roughness (R_a), root mean square surface roughness (R_q), skewness (R_{sk}) and kurtosis (R_{ku}) for the four samples after stearic acid treatment are presented in Table 4.3.

According to Table 4.3, both APS coatings show relatively high contact angle values indicating an elevated water repellence. However, the APS samples lack the desired water mobility as revealed through the observed high sliding angle values. The reasons for such characteristics of the APS coatings are further investigated and discussed in section 4.3.3. On the other hand, both SPS samples show water contact angles above 150° which is the minimum requirement for a superhydrophobic surface. Additionally, the sliding angles of both SPS coatings are smaller than 10° (Table 4.3), which shows these samples have relatively high water mobility. This is particularly true about the SPS-E sample which has very high mobility with a sliding angle of only 1.3°. These results are comparable to those of the state of the art superhydrophobic coatings in the literature [215,216].

Table 4.3. Contact angle, sliding angle, arithmetic surface roughness (R_a), root mean squared surface roughness (R_q) and skewness (R_{sk}) for the APS and SPS samples.

Sample	Contact angle (deg)	Sliding angle (deg)	Roughness, R_a (µm)	Roughness, R_q (µm)	Skewness, R_{sk}	Kurtosis, R_{ku}
APS-1	128 ± 3	> 60	3.7 ± 0.6	4.5 ± 0.5	0.23 ± 0.05	3.2 ± 0.1
APS-2	145 ± 2	> 60	3.8 ± 0.4	4.8 ± 0.5	0.25 ± 0.04	3.0 ± 0.1
SPS-W	156 ± 1	8 ± 1.3	6.2 ± 0.1	7.9 ± 0.1	-0.45 ± 0.04	3.8 ± 0.1
SPS-E	167 ± 1	1.3 ± 0.3	6.7 ± 0.1	8.5 ± 0.1	0.32 ± 0.06	3.9 ± 0.1

Furthermore, both SPS samples have arithmetic roughness (R_a) and root mean square roughness (R_q) values considerably higher than those of the APS samples. The observed increase in the contact angle values with increased roughness is consistent with the Wenzel and Cassie-Baxter wetting models. These models both express that surface roughness has an amplifying effect on water contact angle of a surface. In terms of skewness, both APS surfaces have a positive value. Zero Skewness signifies perfect symmetry about the mean line and the positive skewness value

indicates that both APS surfaces have a disproportionate number of high peaks. On the other hand, the SPS-W surface has a negative skewness value that is almost two times larger in magnitude compared to the APS skewness values. This indicates that the SPS-W sample has a dominant number of valleys compared to the number of peaks. On the other hand, the SPS-E coating has a positive skewness value which is considerably higher than both APS samples. This means that the surface of this coating has a larger number of peaks than valleys. This can contribute to increasing the surface mobility by facilitating the formation of air pockets in the interface between the solid surface and water and reducing the actual contact area between them.

A kurtosis value of 3 signifies a normal (Gaussian) distribution of peaks and a valleys throughout the surface of the sample. According to Table 3, both APS samples have kurtosis values very close to 3. On the other hand, the kurtosis value of the both SPS samples is significantly higher which suggests that these surfaces have comparatively more high peaks and deep vales. This correspondingly demonstrates how surface features contribute to the higher water repellence and mobility of the SPS samples as the water droplets rest on the high peaks and the valleys contribute to further formation of air pockets.

4.3.3. Morphology and Structural Characterization

The top view and the cross-sectional view SEM micrographs of sample APS-1 are shown in Figure 4.5. Due to the high in-flight particle temperature, this coating is formed from a majority of fully molten particles and large splats are visible on the coating top surface. The splats are similarly distinguishable in the cross-sectional view which shows a thicker coating layer compared to APS-2 (Figure 4.6) with a relatively less rough and textured surface. The smaller contact angle of APS-1 compared to APS-2 coatings is attributed to these relatively larger gaps between roughness features.

The top view and the cross-sectional view SEM micrographs of sample APS-2 are shown in Figure 4.6. In this case, due to the lower in-flight particle temperature, this coating is comprised of more partially molten particles than APS-1. Due to the relatively cooler deposition conditions, APS-2 has a smaller coating thickness and a more porous structure. The presence of partially molten particles created a relatively more erratic morphology as shown in Figure 4.6 and consequently resulted in higher contact angle values compared to APS1.
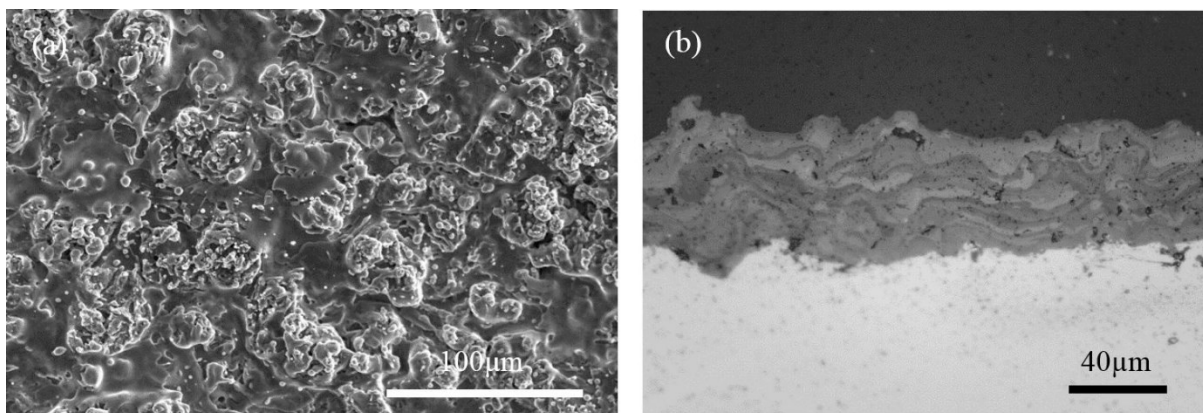
Figure 4.5. SEM micrographs of the APS-1 sample with relatively high particle temperature and low particle velocity; (a) top view, and (b) cross-sectional view.

The APS coatings show relatively high contact angle values, close to superhydrophobic values (150°). However the coatings clearly lack the necessary water mobility as displayed through high sliding angle values. This is due to the relatively large and non-uniform morphological features created by the APS process and its inconsistent pattern. This implies the necessity of using a coating method that provides fine and consistent texture and morphology.
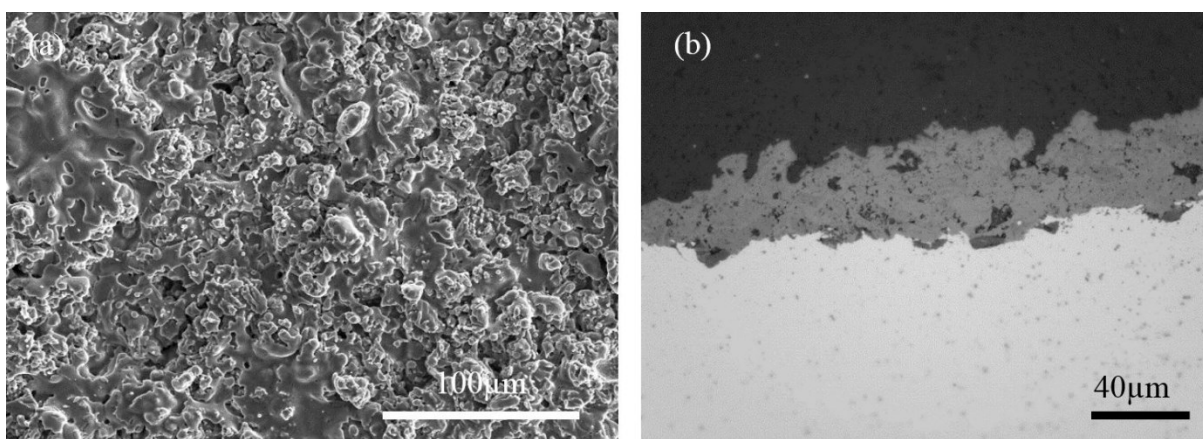
Figure 4.6. SEM micrographs of the APS-2 sample with relatively low particle temperature and high particle velocity; (a) top view, and (b) cross-sectional view.

In suspension plasma spray (SPS) process, the feedstock consists of a suspension of solid particles in a liquid carrier that allows the generation of smaller scaled and refined microstructured coatings. The top view and cross-sectional view SEM micrographs of the SPS-W coating (with TiO_2 suspension in water) are shown in Figure 4.7. Clearly, the coating has a much finer morphology and more consistent pattern compared to the APS samples. This morphology results in an elevated water repellence showcased through the contact angle value of 156° and the desired

water mobility exhibited through a water sliding angle of less than 10°. As visible in the SEM images, the thin coating follows the pattern of the grit-blasted substrate as the roughness features of the substrate are considerably large compared to the thickness of the coatings.
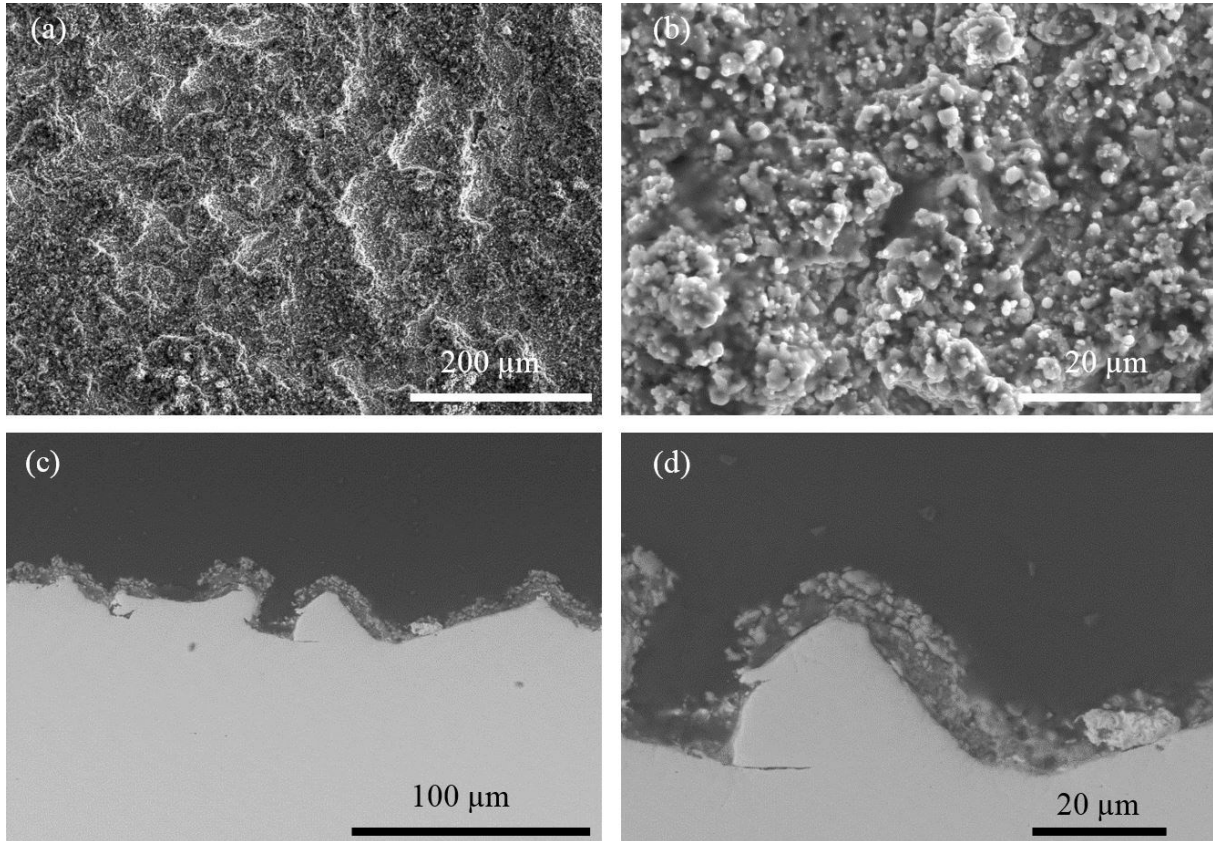
Figure 4.7. SEM micrographs of the SPS-W sample (water-based suspension feedstock); (a) and (b): top view; (c) and (d): cross-sectional view.

The top view and cross-sectional view SEM micrographs of the SPS-E coating (with TiO_2 suspension in ethanol) are shown in Figure 4.8. This coating clearly has a very distinct morphology compared to the SPS-W coating. In this case, as visible in Figure 4.8 (a), protuberances with diameters roughly between 10-20 μm have covered the surface. These protuberances consist of smaller, submicron scale nubs as shown in Figure 4.8 (b). Together these two levels of morphological features create a dual-scale hierarchical roughness on the surface similar to the ideal hierarchical morphology previously discussed in section 4.2. This hierarchical roughness, which is an outcome of the presence of larger aggregates in the precursor suspension of this coating (see Figure 4.4), is the main factor responsible for the improved water repellence and mobility of this coating compared to the other samples in this research. The cross-sectional SEM micrographs

(Figure 4.8 (c) and (d)) show that the SPS-E coating is fairly porous with many roughness features on top. These characteristics contribute to the improved water repellence and mobility of this coating by decreasing the actual contact area between the water droplet surface and the coating as well as by facilitating the formation of micro air pockets. It is noteworthy that the preliminary durability tests show promising result for these coatings. A thorough investigation of water erosion resistance and durability of these coatings in icing condition will be presented in an independent future work.
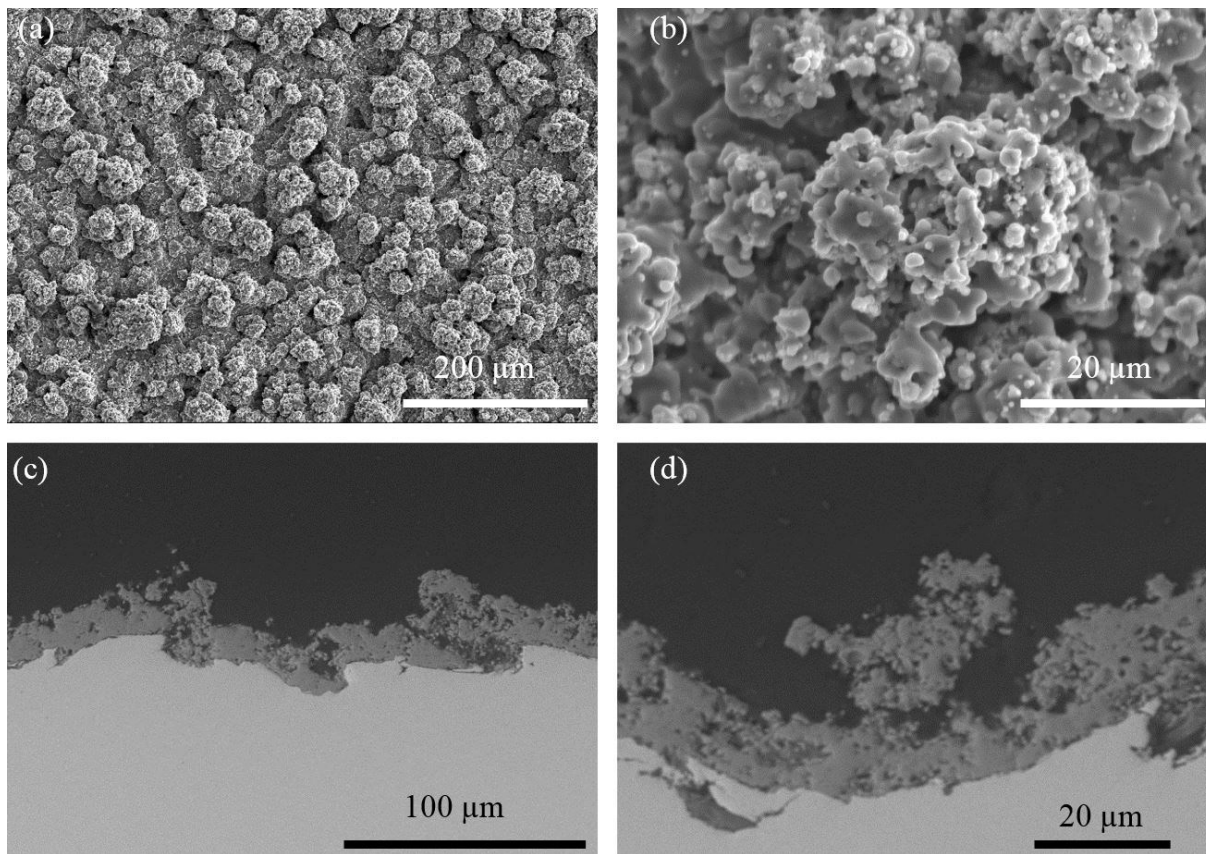
Figure 4.8. SEM micrographs of the SPS-E sample (ethanol-based suspension feedstock); (a) and (b) top view; (c) and (d): cross-sectional view.

4.3.4. Dynamic Wetting Behavior of SPS coatings

The SPS coatings show very interesting results in terms of repellence and mobility. As discussed in previous section, the coefficient of restitution is another important characteristic for evaluating the mobility of superhydrophobic coatings. Figure 4.9 shows images from an experiment that was used to determine the coefficient of restitution for the SPS-E sample.

In Figure 4.9, the different stages of the interaction of a water droplet with a superhydrophobic surface with relatively elevated mobility are demonstrated. These stages include impact, spreading, recoiling, bouncing and detachment. The most important phenomenon observed here is the detachment of the droplet that demonstrates the elevated water mobility of this surface. In the process of the water droplet interacting with the solid surface, the droplet loses part of its energy due to contacting the surface and spreading on it and then recoiling. The energy dissipated through this interaction can be expressed through the coefficient of restitution. Clearly the closer this value is to 1, the better is the water mobility of the surface.
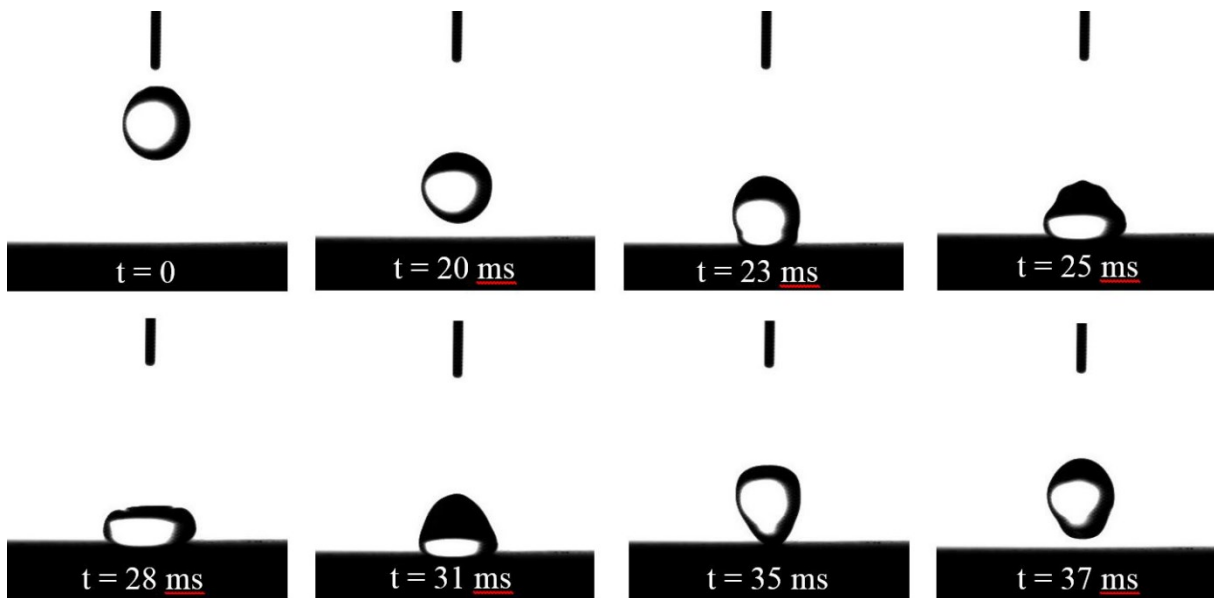
Figure 4.9. Images of an impinging water droplet on the SPS-E coatings. (Elapsed time in millisecond)

The coefficients of restitution for impact velocities of 250 mm/s and 450 mm/s are measured for both SPS samples and are presented in Table 4.4 and compared to three other superhydrophobic surfaces: a commercial polymer-based spray product WX2100, a lotus leaf and a nano-grass (denoted NG) surface fabricated by depositing carbon nanotubes on a patterned silicon substrate [214]. At low impact velocity, both SPS coatings demonstrate a higher coefficient of restitution than the lotus leaf and the commercial WX spray and are comparable to that of the nano-grass. However, at relatively higher impact velocities, the SPS-W coating has a lower coefficient of restitution. This may be attributed to the single scale (submicron) topographical features of this coating and the lack of dual-scale roughness. Conversely, the SPS-E coating that

possesses the hierarchical morphology shows highest value of the coefficient of restitution among all samples. This confirms again the elevated mobility of this sample.

Table 4.4. Coefficients of restitution for: SPS coatings developed in this research, a commercial polymer-based spray coating WX2100, lotus leaf and nano-grass [214].

Surface	Coefficient of Restitution (impact velocity = 250 mm/s)	Coefficient of Restitution (impact velocity = 450 mm/s)
SPS-W	0.82	0.38
SPS-E	0.82	0.48
WX2100 (commercial spray)	0.73	0.48
Lotus leaf [33]	0.75	0.40
Nano-grass [33]	0.83	0.45

4.4. Conclusions

The atmospheric plasma spray (APS) and suspension plasma spray (SPS) techniques were shown to be capable of producing submicron-sized patterned coatings which, after lowering the surface energy, can result in superhydrophobic surfaces with high water repellence. The APS coatings typically lacked high surface mobility due to the random and relatively large surface features resulting from relatively large feedstock particle size. On the other hand, in addition to high water repellence, the SPS coatings demonstrated enhanced water mobility. This wetting behavior was attributed to the characteristic morphology of the SPS coatings. The submicron morphology of the SPS coating resulted from the use of submicron size TiO_2 particles in the form of a suspension as feedstock. Optimum performance was observed with coatings deposited using a TiO_2 suspension in ethanol. In this case a dual-scale hierarchical roughness was formed that provided coatings with significantly improved water mobility.

Using SPS to develop superhydrophobic coatings is a comparatively cost-efficient and straightforward method with the capability to be applied on large surfaces. It is important to note that the superhydrophobic SPS coatings developed in this research are easily applicable to large surfaces in an atmospheric environment without the many complications of complex methods such

as growing the nano-grass and the SPS coating is expected to be far more durable than polymer-based sprays. Moreover, in order to improve the wetting behavior of SPS coatings, it is important to focus on the dual-scale (hierarchical) structure of the coating and using a parametric study to determine the best deposition conditions.

Acknowledgement:

Preface to Chapter 5.

In the previous chapter, it was demonstrated that the suspension plasma spray (SPS) technique is capable of producing micro-textured coating that after treatment to lower their surface energy, show superhydrophobicity. The superhydrophobicity of the SPS TiO_2 coatings is attributed to the hierarchical micro-texture of the coatings. Logically, the next step is to determine the significance of these hierarchical "cauliflower-like" features, how their size, density and uniformity affect the wetting behavior of the coating and how various process parameters of the SPS technique affect the morphology and consequently superhydrophobicity of these coatings. Therefore, the next chapter in this work focuses on an in-depth parametric study of the SPS process and the SPS superhydrophobic coatings.

It is important to note at this point that the SPS TiO_2 coatings that are introduced in the previous chapter and are to be investigated in the following chapter show superhydrophobicity due to the combination of their surface micro-texture and the treatment that lowers their surface energy. Understandably, if a ceramic material similar to TiO_2 in terms of durability was to be found that demonstrates intrinsic hydrophobicity, it would introduce a great potential. Such a material could have been used to generate micro-textured SPS coatings without the need for any further treatment and could show superhydrophobicity due to its hypothetical intrinsic hydrophobicity. As mentioned in Chapter 2, all known engineering metals and ceramics are intrinsically hydrophilic, with the exception of the debateable case of rare-earth oxides. While some researchers claim to have observed indications of intrinsic hydrophobicity in rare-earth oxides, other researchers attribute this to presence of hydrocarbon compounds on the surface. Therefore, in the process of this research efforts have been made to study the validity of such claims and to investigate the potential of rare-earth oxide for developing micro-textured superhydrophobic coatings. The details of these efforts are presented in the Appendix section of this thesis. In short, in these efforts, no evidence was found to support the hypothesis that rare-earth oxides can demonstrate intrinsic hydrophobicity in certain conditions.

Chapter 5. Engineering Surface Texture and Hierarchical Morphology of Suspension Plasma Sprayed TiO$_2$ Coatings to Control Wetting Behavior and Superhydrophobic Properties [4]

Navid Sharifi, Fadhel Ben Ettouil, Christian Moreau, Ali Dolatabadi and Martin Pugh

Department of Mechanical, Industrial and Aerospace Engineering, Concordia University
1455 de Maisonneuve Blvd. W, Montreal, Quebec, Canada, H3G 1M8

Abstract

Beyond its conventional application for developing thermal barrier coatings, suspension plasma spraying (SPS) has shown promise for new applications focusing on surface textured coatings including superhydrophobic coatings. Such coatings have a dual-scale hierarchical morphology or so-called "cauliflower" features on the surface and they demonstrate extreme water repellence and mobility after treatment for lowering their surface energy. Studying and determining suitable process parameters to optimize the wetting properties of these coatings is the focus of this work. Herein, it is demonstrated that by carefully designing and controlling the process parameters, one can generate relatively fine and uniform dual-scale (hierarchical) surface textured coatings that after treatment for lowering their surface energy, show significantly improved water repellence and water mobility with water contact angles as high as 170° and sliding angles as low as 1.3°. It is also demonstrated that both scale levels of surface textures (i.e. micron-scale and nanoscale) are essential for having simultaneously improved water repellence and mobility. Furthermore, it is established that producing finer, more uniformly distributed and packed surface features lead to more consistent and desirable wetting properties. The results show

---

the significant influence of pre-deposition surface roughness, precursor suspension rheology and plasma power on the structure and performance of the developed coatings.

Key words: Suspension plasma spray (SPS), superhydrophobicity, surface texture, surface morphology, parametric study

5.1. Introduction

The plasma spraying technique is an efficient and practical method to generate functional coatings for various applications [166,217–219]. Atmospheric plasma spray (APS) and suspension plasma spray (SPS) have both been largely used for thermal barrier coatings [169], abradable coatings [220] and erosion, corrosion and wear resistant applications [221–223] due to their versatility, deposition rate and scalability. Furthermore, in recent years, new applications have emerged using plasma spraying that are principally focused on generating textured coatings for applications such as superhydrophobic coatings [196,224] and electrochemically active electrodes [225,226]. Due to the novelty of such applications, there is lack of thorough experimental data and published research about them.

Various methods have been used to prepare superhydrophobic coating, including electrodeposition methods [216], vapor deposition [227], lithography [228], laser patterning [229] and sol-gel [200,209]. The vast majority of these works fall into one of two categories: one is using a low surface energy material, the other is using complex methods to tailor the micro-texture of the coatings. The former techniques are typically based on polymeric materials that do not demonstrate mechanical durability and the latter techniques are usually very complex and impractical for industrial applications. In the approach presented in this article we take the middle ground using a technique i.e. SPS which is atmospheric and easily applicable onto large surfaces and we demonstrated that the final micro-texture of the coatings can be controlled by controlling the process parameters in order to obtain desired coating macrotextures.

In general, a main challenge of working with plasma spray processes is the fact that there are numerous process-related and environment-related parameters that affect the structure, properties and characteristics of the final coating [163,230]. Since these processes are carried out in atmospheric conditions, controlling all influential parameters is required to have adequate control over the resulting characteristics and structures. For the APS process, online diagnosis systems such as DPV and Accuraspray (by Tecnar) [231–233] have been developed making it

possible to measure the velocity, temperature and diameter of in-flight particles prior to impact on the substrate. This approach effectively summarizes the effects of process parameter such as plasma power, gas flow and feedstock particle size and provides a comprehensive understanding of the condition of coating formation that greatly facilitates the control and repeatability of the process. However, in the case of the SPS process, since particles are at least an order of magnitude smaller and deposition takes place very close to the plasma jet which is a source of optical noise, online particle diagnostics is challenging and currently under development and investigation. Therefore, to study the effect of process parameters on the suspension plasma spray coatings, it is essential to select a reference set of parameters and then to create a test matrix by changing various parameters one at a time. This allows for investigating the effect of each parameter by isolating the variation of that parameter while constraining the variation of other influential parameters. In the case of parameters that are very difficult to keep constant, such as particle trajectory and substrate temperature, they have been closely monitored to ensure that they remained within a limited range (typically 5% variation).

In recent years, efforts have been made to employ thermal spraying as a relatively fast and efficient surface treatment method for developing coatings with controlled surface wettability. For example Li et al. [185,234] introduced atmospheric plasma sprayed (APS) metallic coatings that demonstrate superhydrophobicity after adsorbing carbon-based components from atmosphere. Guo et al. [186] used vacuum cold spray to deposit a nanostructured coating treated by fluoroalkylsilane that showed highly water-repelling characteristics. Leblanc et al. [189,190] first employed suspension plasma spraying to develop random textured hydrophobic surfaces with reduced drag in interaction with turbulent liquid flow. Chen et al. [192] used flame spraying and a steel mesh as shielding plate to develop cone-like features that improve the wetting behavior of the coating. It is important to note at this point that although some work has been done to study the effect of SPS process parameters [180,235], these investigations has been mainly focused on structural characteristics and properties related to more conventional applications of SPS process such as TBCs.

The main focus of this work is on morphologically textured coatings for roughness-induced superhydrophobic coatings. A thorough parametric study has been carried out to identify the most significant factors that affect the wetting behavior of such coatings and to understand the complex and combined effect of various process parameters as well as morphological features of the

coatings. These features form the base of the extreme water repellence and water mobility that these coatings demonstrate. By designing a test matrix of 24 different test conditions and monitoring and controlling the particle jet trajectory and substrate temperature, samples of textured titanium dioxide coatings have been developed. After treating the samples with stearic acid to isolate and diminish the effect of surface chemistry, all samples have been characterized in terms of wettability and the most interesting ones were selected for further visual and morphological characterization. The objective of this work is to quantify and correlate the effect of process parameters and establish a control over surface texture that consequently leads to a control over wetting properties of the coatings.

5.2.   Materials and Methodology

5.2.1. Coating Development

All samples were manufactured using the suspension plasma spraying (SPS) technique. For preparation of the feedstock suspension, a commercial submicron-sized titanium dioxide powder with average nominal particle diameter of 500 nm (KS-203A/B, TKB Trading, US) was used. The main objective of this work is to study the macrotextures achieved through SPS process and the influential process parameters to control and design the micro-texture to optimize the water repellence and mobility of the coatings. TiO_2 has been selected as the coating material because it is an easily available and inexpensive material with minimal safety concerns and reasonable mechanical and chemical stability. Three different suspensions were prepared to study the effect of suspension composition. In two of the suspensions, ethanol was used as the solvent with 10 wt% solid content of TiO_2 for the first and 20 wt% for the second suspension. For both ethanol-based suspensions, polyvinylpyrrolidone (PVP, Alfa Aesar, US) was added (5 wt% of the solid content) as dispersant to ensure the stability of the suspension and to prevent agglomeration and sedimentation during the spraying process. For the third suspension, deionized distilled water was used as the solvent with 10 wt% solid content. For the water-based suspension, polyacrylic acid (5 wt% of the solid content) was used as the dispersing agent. All three mixtures were mixed by magnetic stirring for 5 minutes and then sonicating for 10 minutes with 50 W of power. This routine was repeated once per each 200 ml of suspension. The particle size distribution of each suspension was obtained using a particle size measurement unit (Spraytec, Malvern, UK) and the

results are presented in Figure 5.1 along with a SEM micrograph of the submicron TiO_2 power. Size distribution characteristics of the three suspensions is presented in Table 5.1.
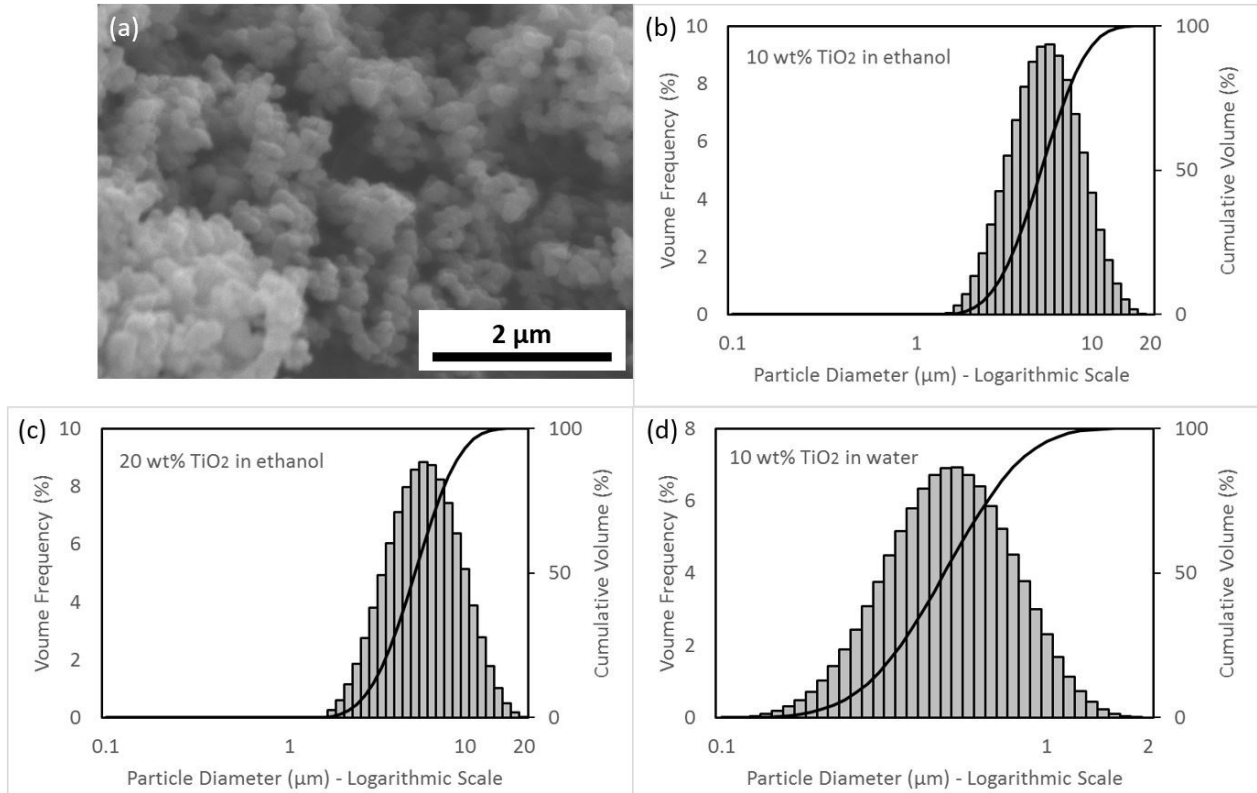
Figure 5.1. (a) SEM micrograph of the feedstock TiO_2 powder; and (b), (c) and (d) particle size distribution of the three suspensions used in this study.

Table 5.1. Size distribution characteristics of the three suspensions used in this work.

Suspension	D_{10} (μm)	D_{50} (μm)	D_{90} (μm)
10 wt% TiO_2 in ethanol	2.9	5.1	8.8
20 wt% TiO_2 in ethanol	3.0	5.4	9.6
10 wt% TiO_2 in water	0.28	0.50	0.86

The coatings were deposited onto flat 304 stainless steel substrates with dimensions of 25 × 25 × 5 mm³. Prior to the deposition, the substrates were grit-blasted by alumina particles and then thoroughly cleaned in acetone followed by isopropyl alcohol. To study the effect of substrate roughness on the morphology and consequently the wettability of the coatings, three different grit sizes were used, namely 24, 80 and 180 grit that using an air pressure of 354 kPa, which produced

a substrate roughness (R_a) of 3.5 µm, 2.5 µm and 1.5 µm, respectively. These three pre-deposition surface roughness values are labeled C (coarse), M (medium) and F (fine).

5.2.2. Test Matrix Design

To deposit the coatings a 3MB plasma torch (Oerlikon Metco, Switzerland) was used. The plasma gas consisted of argon and hydrogen with argon flow rate set on 60 liters per minute and hydrogen flow rate changing to achieve the desired plasma power. The feedstock suspension was stirred during the coating process and was injected radially into the plasma plume as a simple continuous jet with flow rate of 55 grams per minute. Coatings were deposited using 10 consecutive passes of a full spray raster covering the surface of the coupons with a 3 mm overlay distance. To study the effect of various deposition parameters, a test matrix was designed and, overall, eight different combinations of process parameters were used that, combined with three pre-deposition substrate roughness values, produced 24 different samples. The studied parameters include the previously mentioned feedstock suspension compositions, surface roughness prior to deposition, as well as plasma power, plasma torch standoff distance and plasma nozzle diameter. Plasma power was modified by changing the arc current and the amount of hydrogen gas which increases the voltage of the plasma. It is important to note that the reported plasma power here is the input electrical power of the plasma. The thermal efficiency of the process is not measured here but studies on similar working condition typically reported a thermal efficiency of 55-60% [236]. A detailed list of the parameters used to design this test matrix and the corresponding abbreviations are presented in Table 5.2. The test matrix is detailed in Table 5.3.

Table 5.2. Values of variable process parameters and the corresponding abbreviations used in this study.

Variable Parameter	Levels	Abbreviations
Grit-blast	Coarse, Medium, Fine	C, M, F
Suspension solvent	Ethanol, Water	E, W
TiO_2 weight percent	10, 20 (wt%)	10%, 20%
Plasma power	25, 36 kW	LP, HP
Standoff distance	3, 5 (cm)	LSD, HSD
Plasma torch nozzle diameter	5, 8 (mm)	SND, LND

Table 5.3. Test matrix parameters used in this study.

Condition	Solvent	TiO_2 (wt%)	Grit-blast	Plasma power (kW)	Standoff distance (mm)	Plasma nozzle (mm)
10-E-LP	E	10	C, M, F	25	50	8
10-E-HP	E	10	C, M, F	36	50	8
10-E-LSD	E	10	C, M, F	25	30	8
10-E-SND	E	10	C, M, F	25	50	5
10-W-LP	W	10	C, M, F	25	50	8
10-W-HP	W	10	C, M, F	36	50	8
20-E-LP	E	20	C, M, F	25	50	8
20-E-HP	E	20	C, M, F	36	50	8

During the deposition process, the Accuraspray system (Tecnar, Canada) was used to monitor the trajectory of the particle jet to ensure the proper penetration of the particle jet into the plasma plume. Accuraspray is an optical diagnosis unit capable of measuring velocity and temperature of the cloud of particles. The temperature measurements by the Accuraspray system

for SPS process are accompanied by optical noise from plasma due to short spray distance and therefore are not reported in the study. However, the sensor still receives signals from particles that are passing in front of it. Accuraspray software analyzes these signals and identifies the center of the particle jet which slightly deviates from the center of the plasma jet due to axial injection of the particles. In this work, it was confirmed using Accuraspray that the deviation of the center of the particle jet from the center of the plasma plume remained within a range of 6% of the spray distance. This was achieved by slightly adjusting the angle of injection of suspension and without changing plasma gas flow rate. Additionally, to further increase the repeatability of the results and consistency of the comparative study, an infrared camera (A310, FLIR, US) was used to monitor the temperature of the substrate during the deposition process. Two air amplifiers (devices that direct a high volume and high velocity flow of air toward a target) were used during all tests to cool down the substrate and maintain the surface temperature below 600°C in all conditions.

In the suspension injection system, a mass flow meter was used to ensure the constant and steady feeding of the suspension feedstock into the plasma and the density of the suspension was constantly monitored online using a Coriolis flow meter to ensure the quality and characteristics of the suspension were constant during the coating process.

5.2.3. Surface Treatment

After coating, samples were sonicated in deionized distilled water to discard loose solid particles. Afterwards, the samples were thoroughly cleaned in acetone followed by isopropyl alcohol. To make sure the surface of the samples were free of organic contamination from the acetone or isopropyl alcohol, the samples were placed in boiling deionized distilled water as proposed by Gentlemen et al. [199]. In order to reduce the surface energy and also isolate and study the effect of surface roughness on the wetting behavior of the coatings, all samples were dipped into a 0.5 wt% solution of stearic acid in 1-propanol and then dried using compressed dry air [224]. A flat sample treated with stearic acid using the same method yields a contact angle of 97° and sliding does not occur on such surface.

5.2.4. Characterization

To assess the wettability of the different coatings, multiple wetting parameters were measured and compared for all 24 coatings. First of these wetting parameters is static contact angle (CA) which was measured by imaging a 5 µl droplet of high purity deionized distilled water and

analyzing the image using a plugin in the image analysis software ImageJ, developed by Stadler et. al. [212,213]. The second wetting parameter is sliding angle which was measured by placing a droplet of the same size on the surface of the sample, then tilting the sample using a goniometer until the droplet started to move on the surface. The angle at which the droplet starts to move is taken the sliding angle.

The coatings were grouped based on their wetting behavior with respect to the following criteria: for static contact angle, a larger value is better with contact angles higher than 150°considered satisfactory. For sliding angle, a smaller value is better with values smaller than 10° typically considered ideal. Based on these criteria, a third of the samples with the most desirable properties were selected for further analysis as well as a few samples with less desirable wettability which were further analyzed to understand the morphological characteristics that lead to poor performance.

In the next stage of characterization, the top surfaces of the selected samples were examined using a scanning electron microscope (SEM) [S-3400N, Hitachi, Japan]. Micrographs were obtained from the top of all samples at identical magnifications to be able to compare the size, shape and distribution of morphological features and their effect on wettability of the coatings and consequently, the effect of various deposition parameters on the wetting behavior through the variation in corresponding surface morphology. To further study the effect of pre-deposition substrate surface roughness, some selected samples were cut and polished to analyze their cross-sections. These samples were cleaned, then molded in a cold mount resin, ground and polished per standard metallography procedures to prepare cross-section views. These samples were studied using SEM and micrographs of the coatings and coating/substrate interface were taken.

To further investigate roughness features and properties of the coating surfaces, a confocal laser microscope [LEXT OLS4000, Olympus, Japan] was employed. Using the microscope, three 3D maps of the surface of the coatings in 12mm × 2mm areas were obtained in three different spots on the same sample. Each image consists of 96 (24 by 4) single images, digitally stitched together to generate the three-dimensional map of the area which is large enough to be considered an average representation of the surface. Using this image and analytical software, all surface roughness parameters per ISO 25178 were calculated and studied for potential correlation with the wetting behavior of the different coatings. Various surface roughness parameters are presented as some studies [208,209] have shown that topographical characteristics of a surface cannot be

accurately represented using only one surface roughness parameters with one work [92] relating root mean square height of the surface (S_q) to wetting behavior, and others [237] claiming correlation between wettability to skewness (S_{sk}) and kurtosis (S_{ku}) of the surface. Additionally, the surface ratio of the coating surface defined as the ratio of real surface area to the projected surface area was measured and studied. It is noteworthy that since the confocal laser microscopy technique is a line of sight technique, it typically underestimates the value of real surface area but neglecting additional surface area hidden from line of sight. However, since in this work we study the wetting properties of the surface which is affected by interaction of water droplet and the surface, it is expected that the surface ratio, although not a perfect representative but to be an indicator of wetting behavior of the surface. All the aforementioned surface parameters were investigated for a potential correlation with wetting behavior of the coatings. For this purpose the coefficient of correlation was calculated for each surface roughness parameters in respect to the contact angle and sliding angle of the coatings. The parameters with highest relative correlations were selected and used to plot the graphs shown combined effect of surface parameters on wettability of the coatings.

5.3.   Results and Discussion:

In Figure 5.1, the particle size distribution of the three feedstock suspensions is presented. Noting that the average particle size distribution of the TiO$_2$ particles is 500 nm, in the water-based suspension the particles are almost completely dispersed with a nearly perfect Gaussian distribution. However, in the case of both ethanol-based suspensions, a different size range of distribution is observed. This shows that majority of particles are either single or formed small aggregates in the water-based suspension, while a considerable portion of the particles in the ethanol-based suspension formed aggregates with diameters ranging between a few micrometers to a few tens of micrometers. It is noteworthy that the particle size distribution of the two ethanol-based suspensions (10 wt% and 20 wt%) is very similar which shows that in this range, the concentration of TiO$_2$ particles does not considerably affect the size distribution.

5.3.1. Wettability

Table 5.4 presents a summary of wetting tests in terms of water contact angle (WCA), sliding angle (SA). Additionally, the surface roughness measurements results including arithmetical mean height of the surface (S_a), maximum height of the surface (S_z), root mean square

height of the surface (S_q), Skewness of height distribution (S_{sk}), and kurtosis of height distribution (S_{ku}) are presented. From this table, it is observed that all samples have relatively high water contact angle (WCA) values with the majority of samples having a contact angle higher than 150°. However, as previously mentioned, high water contact angles alone cannot guarantee the superhydrophobic behavior of a surface as it only represents the water repellence. To understand the water mobility of a surface, which plays an equally important role in superhydrophobicity, it is necessary to consider the sliding angle values of the surfaces. While some of the samples show sliding angles higher than 10° which is considered the threshold of superhydrophobicity in this article, some other samples show promise with sliding angle values smaller than 10° and in some cases even smaller than 5°. These coatings are the most interesting ones in terms of wettability and surface texture and are examined further. Additionally, the effect of process parameters on wetting behavior of the surface is further analyzed in this article by considering their effect on sliding angle.

Table 5.4. Coating wetting characteristics including: water contact angle (WCA) and sliding angle (SA), and surface roughness measurements including: arithmetical mean height of the surface (S_a), maximum height of the surface (S_z), root mean square height of the surface (S_q), skewness of height distribution (S_{sk}), kurtosis of height distribution (S_{ku}). [mean±SEM]

Condition	Grit-blasting	WCA (°)	SA (°)	S_a (µm)	S_z (µm)	S_q (µm)	S_{sk}	S_{ku}
	C	165±1	11.7±1.7	7.0±0.1	81.0±2.6	8.7±0.2	-0.164 ±0.012	2.9±0.1
10-E-LP	M	162±1	10.3±1.2	5.8±0.1	74.3±2.4	7.3±0.1	-0.479 ±0.049	3.4±0.1
	F	165±1	10.1±0.7	5.7±0.1	62.5±2.3	7.1±0.2	-0.233 ±0.018	3.0±0.1
	C	166±1	4.1±0.5	10.4±0.1	108.8±6.8	13.0±0.2	0.497 ±0.015	3.2±0.1
10-E-HP	M	165±1	3.7±3.7	9.1±0.1	95.8±2.1	11.6±0.2	0.229 ±0.021	3.1±0.1
	F	168±1	1.3±0.3	8.3±0.1	82.1±2.9	10.4±0.1	0.515 ±0.008	3.0±0.1
	C	164±1	16.3±1.1	6.7±0.2	89.5±2.7	10.2±0.2	0.244 ±0.024	3.1±0.1
10-E-LSD	M	155±1	13.3±1.0	5.8±0.2	71.3±4.9	7.3±0.2	0.407 ±0.042	3.2±0.1
	F	165±1	9.8±1.0	5.5±0.1	66.1±2.2	7.0±0.1	0.274 ±0.054	3.3±0.1

10-E-SND	C	165±1	6.2±0.5	10.1±0.1	100.9±1.5	12.6±0.1	0.246 ±0.016	2.9±0.1
	M	159±1	7.2±0.5	7.7±0.1	102.1±15.1	9.6±0.2	0.288 ±0.033	3.6±0.5
	F	163±1	5.3±0.7	8.7±0.2	88.8±2.7	10.8±0.3	0.327 ±0.017	3.0±0.1
10-W-LP	C	137±8	>20	5.1±0.1	71.0±3.3	6.6±0.1	0.566 ±0.041	3.9±0.2
	M	140±5	>20	4.1±0.1	58.7±1.6	5.3±0.1	0.520 ±0.045	4.2±0.2
	F	142±3	>20	3.3±0.1	51.7±3.4	4.2±0.1	0.227 ±0.045	4.0±0.2
10-W-HP	C	154±1	14.2±1.8	6.2±0.1	79.2±1.5	8.5±0.1	0.559 ±0.022	3.8±0.1
	M	152±1	11.1±2.2	4.7±0.2	73.5±3.6	6.2±0.3	0.543 ±0.091	4.5±0.1
	F	159±1	8.4±1.3	5.6±0.2	67.9±3.1	7.4±0.3	0.802 ±0.039	4.0±0.1
20-E-LP	C	165±1	3.8±1.7	8.3±0.1	97.4±7.5	10.2±0.1	0.247 ±0.054	3.0±0.2
	M	169±1	3.4±1.9	8.8±0.2	87.7±2.5	8.4±0.2	0.247 ±0.009	2.8±0.1
	F	170±1	1.4±0.3	8.5±0.1	89.4±3.7	7.8±0.3	0.305 ±0.019	3.0±0.1
20-E-HP	C	157±1	7.1±0.9	10.4±0.3	99.2±2.5	12.9±0.4	0.632 ±0.006	3.0±0.1
	M	155±1	6.3±0.4	9.3±0.2	91.0±4.6	11.6±0.3	0.790 ±0.009	3.2±0.1
	F	160±1	4.0±0.5	9.9±0.2	88.3±1.0	12.3±0.2	0.795 ±0.007	3.1±0.1

Since the surface chemistry is the same for all coatings, the different wetting behaviors are linked to the different coating micro-textures. It is important to study the surfaces with different wetting characteristic to better understand the features and morphological properties that result in such wetting behavior. In Figure 5.3, six of the coatings with distinguishably different wetting behaviors are selected and the SEM micrographs of their surface morphology at two magnifications are presented.

5.3.2. Surface Morphologies

A simple side by side visual comparison of micrographs presented in Figure 5.3, reveals that the morphology of the coatings varies significantly depending on the deposition conditions. In general, using water-based suspension as feedstock [Figure 5.1-(b)] results in a rather mono-scale roughness and the so-called "cauliflower features" with hierarchical morphology are absent. In coatings developed using the water-based suspension (Figure 5.3 (a) and (b)) the primary

surface texture features or so-called cauliflower-like features are not fully formed and clearly distinguishable. In fact, these coatings have only a single scale of roughness instead of the desired hierarchical texture. On the other hand, in ethanol-based coatings, surface micro-texture features with two distinguished size-scales are observed. The smaller scale features are similar to those observed in the water-based process, while the larger scale features (cauliflowers) are unique to the ethanol based coatings. This is partly due to the previously mentioned particle size distribution of the water-based suspension which consists of many fully dispersed solid particles with fewer and smaller aggregates as well as rheological properties of water in comparison to ethanol. The combined effect of suspension characteristics affects the atomization of suspension in the cross-flow interaction with the plasma which significantly influences the coating morphology. Based on the results, there is a considerable difference in the micro-texture of the coatings deposited using water-based and ethanol-based suspensions. This difference can be the result of combination of factors including dispersion of solid particles in the suspension, difference in atomization and the relatively large specific heat capacity and latent heat of vaporization of water in comparison to ethanol. This results in solid particles to be heated less in case of the water-based suspension that produces more unmolten particles. This can be another reason for the coatings deposited through water-based suspension to lack the desired hierarchical texture.
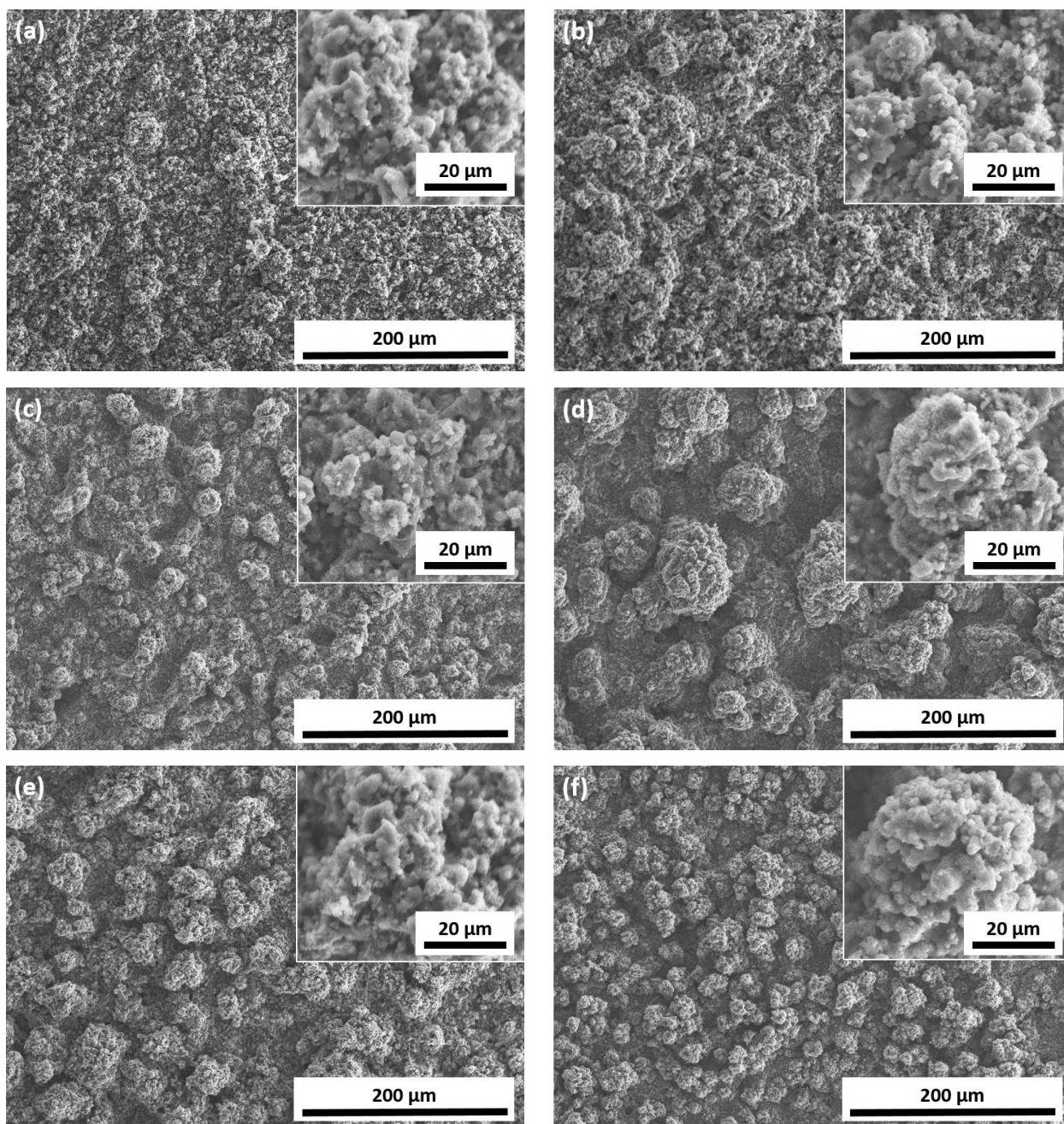
Figure 5.2. SEM micrographs of selected samples deposited though six spraying conditions and representing various surface textures and wetting behaviors. Samples are sorted in order of increasing water repellency and mobility: (a) condition 10-W-LP-M, (b) condition 10-W-HP-M, (c) condition 10-E-LP-M, (d) condition 20-E-HP-M, (e) condition 20-E-LP-M, (f) condition 10-E-HP-F.

As previously mentioned, the SEM micrographs in Figure 5.3 are sorted in order of increasing water repellency and mobility which corresponds to increasing superhydrophobicity

and thus desirability. Close investigation of the micrographs reveal that the improvement in water repellence and mobility can be attributed to two morphological characteristics in these coatings. The first characteristic is the presence of so-called cauliflower-like features on the surface. As seen in the larger magnification inserts in Figure 5.3, at the secondary submicron scale of roughness, all coatings have similar features. It is known that this secondary roughness in a hierarchical morphology has an important role to stabilize the water-solid interface and improve the superhydrophobicity [195]. However, as seen in Figure 5.3 (a) and (b), this submicron roughness alone cannot generate high water repellence and mobility. In fact, the formation and presence of primary roughness features which provides entrapment of air between the solid and water at the interface is necessary to achieve extreme water repellence and mobility. This primary texture is believed to form because of a phenomenon known as the shadow effect in suspension plasma spraying [238,239]. This effect comes into play when initial deposition of particles on the surface creates some bumps that affects the incoming particles' trajectory, causing them to attach to the surface of these bumps and preventing them from attaching to the surrounding regions. This mechanism is the main cause of formation of cauliflower-like features.

The second noteworthy characteristic of the surface texture is uniformity and refinement of the cauliflower-like features. In Figure 5.3 (c) and (d), it is observed that, although these two coatings demonstrate some of the hierarchical features, in the first coating texture, these features are not fully developed and packed while in the second coating texture, the hierarchical features are relatively large and distant. In both cases, when a water droplet is sliding on these surface, if at some points the features are not fully developed or there is a relatively large gap between them, the droplet gets trapped at those points which causes an increase in sliding angle and reduction of mobility. Finally, looking at Figure 5.3 (e) and (f) which are the surface textures that provide the highest mobility, fully developed and packed hierarchical features ultimately result in a surface on which a water droplet easily slides and has extremely high mobility. This is particularly true for the last surface texture which has finer and more uniform features and can provide a sliding angle as low as 1.3°.

5.3.3. Effect of grit-blasting

The effect of grit-blasting with three different grit sizes is shown in Figure 5.4. Accordingly, by moving from coarse to fine grit size, the sliding angle generally decreases. This effect is observed for seven of the original eight deposition conditions. However, for the case of

the water-based suspension at low power, the sliding angle is so large that it is practically impossible to measure the sliding angle consistently and therefore the effect of grit-blasting cannot be correctly determined. In Figure 5.5, SEM micrographs of the cross-section of coatings for 10 wt% TiO_2 ethanol-based suspension deposited at high power respectively on coarse (C), medium (M) and fine (F) grit-blasted coupons are shown. These three coatings have been deposited with the same spray conditions with the only difference being in grit-blasting of the substrates before deposition. By comparing these three SEM micrographs and according to Figure 5.4, it can be concluded that it is the combination of deposition condition and not only the surface grit blasting that determines if hierarchical morphology is developed in the coatings or not. However, for coatings sprayed in other spray conditions, finer grit-blasting results in finer and more uniform surface features that improves both water repellence and mobility and thus is more desirable.

It needs to be noted that investigating the adhesion of the coating to the substrate using conventional bond strength measurement techniques is not practically possible due to the relatively low thickness and high porosity and surface roughness of the coatings. For practical applications such as icing and water erosion the mechanical durability of these coating are to be thoroughly investigated in the future, however, we can report that we have not observed any sign of failure or delamination in the coatings during the process of investigation.
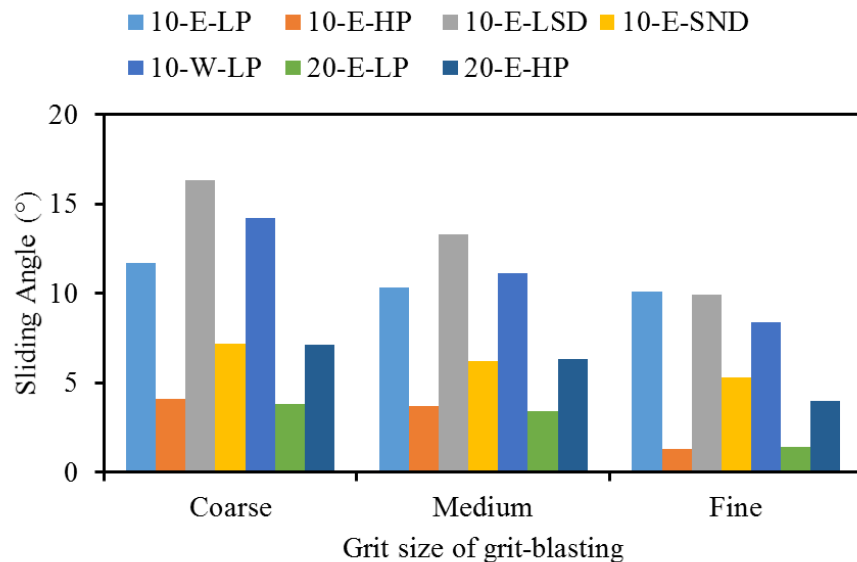
Figure 5.3. Effect of grit size on sliding angle of the coatings.
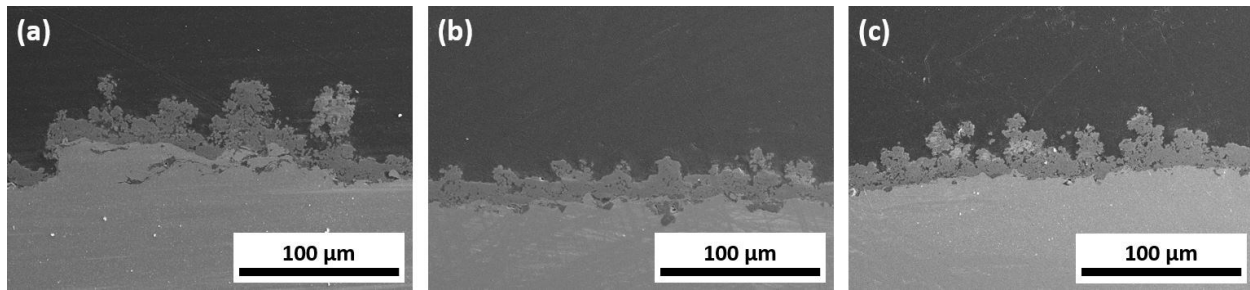
Figure 5.4. SEM micrographs of the cross-section of the coatings deposited at the same process condition with different substrate roughness: (a) 10-E-HP, coarse, (b) 10-E-HP, medium, and (c) 10-E-HP, fine grit-blast.

5.3.4. Effect of suspension solid content and plasma power

The effect of suspension solid content on sliding angle of the coatings is shown in Figure 5.6. In the case of the low power condition, all three coatings show lower sliding angles while increasing the suspension solid content. On the contrary, for high power conditions, increasing the suspension solid content has the reverse effect, reducing the water mobility of the coatings. This apparent contradiction, can be explained by considering the interaction of the suspension feedstock with the plasma plume. It is speculated that, at low power, increasing the solid content of the suspension does not greatly affect the deposition rate as the plasma does not have sufficient power to considerably change the amount of fully molten and deposited particles. In this case, more semi-molten particles cause formation of rougher and more irregular features on the surface that, in turn, improve the mobility of the surface. On the other hand, at high power, the plasma has sufficient power to melt the additional TiO_2 particles and therefore the deposition rate increases. This causes the 20 wt% suspension coating to grow faster which results in larger and more distant morphological features. This is further supported by noticing the relatively larger size of features in Figure 5.3 (d) and by relatively larger thickness of the coating resulted from the 20 wt% suspension deposited in high power condition.

Ethanol-based suspensions
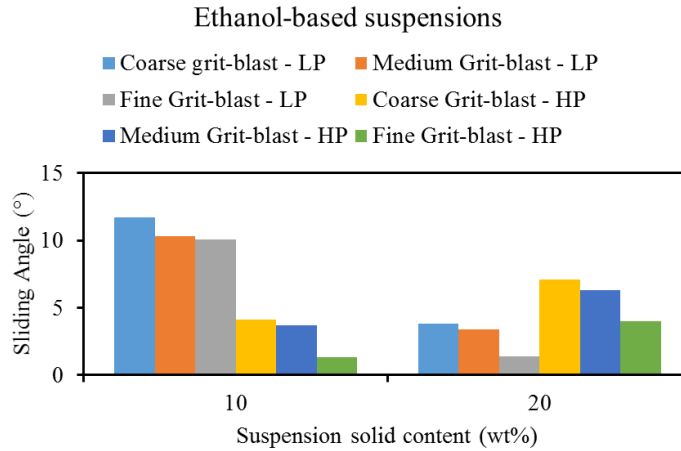
Figure 5.5. Effect of suspension solid content on sliding angle of the coatings.

To compare the deposition rates, the thickness of the coatings deposited using 10 wt% and 20 wt% suspensions for the two power levels 25 kW and 36 kW were measured and the result is reported in Table 5.6. As it can be seen the deposition rate increases more in the case of 25 kW compare to 36 kW which agrees with the discussion made earlier.

Table 5.5. The deposition rate for different powers and suspension solid contents.

Suspension solid content	Coating deposition rate	
	25 kW plasma power	36 kW plasma power
10 wt%	1.8	2.1
20 wt%	3.5	3.6

Figure 5.7 (a) and (b) show the effect of plasma power on the sliding angle for the 10 wt% and 20 wt% ethanol-based suspensions respectively. For the 10 wt% suspension, an increase of the plasma power induces a significant decrease of the sliding angle. The same effect was observed for the water-based suspension since, at low power, these coatings show relatively high (>20°) sliding angles whereas, at high power, these coatings have noticeably lower sliding angle values. However, this effect is reversed for 20 wt% ethanol-based suspension where increasing the plasma power increases the sliding angle. The reason for this behavior as previously mentioned, is believed to be related to a significant increase in deposition rate in the case of the high power deposition of the 20 wt% suspension that results in the formation of relatively large texture features which decrease mobility.

10 wt% Ethanol-based suspension

■ Coarse gritblast   ■ Medium Gritblast   ■ Fine Gritblast

(a)

20 wt% Ethanol-based suspension

■ Coarse gritblast   ■ Medium Gritblast   ■ Fine Gritblast

(b)
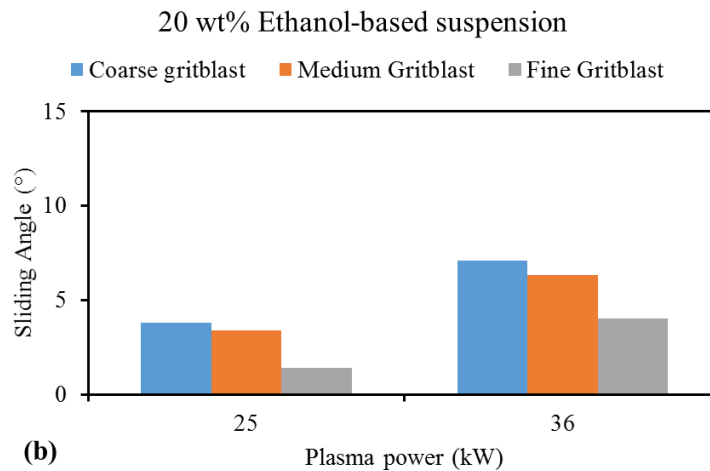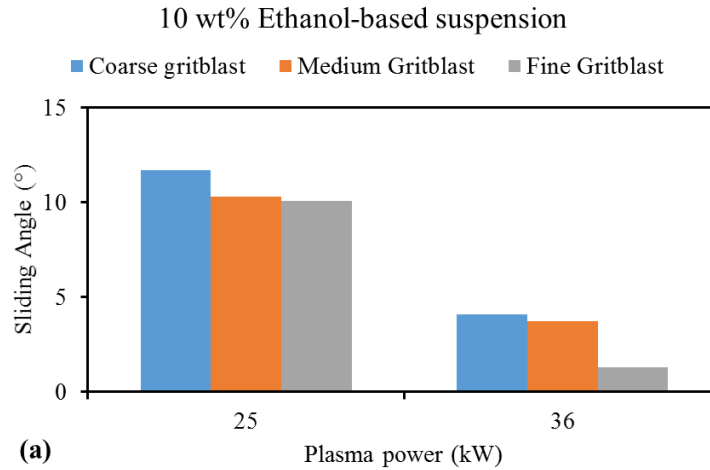
Figure 5.6. Effect of plasma power on sliding angle of the coatings.

5.3.5. Effect of standoff distance

The effect of changing standoff distance on sliding angle is presented in Figure 5.8. It is observed that generally the sliding angle increases when the standoff distance is reduced. In SPS, the standoff distance is relatively small, compared to other thermal spray processes, and the deposition is greatly affected by the turbulent plasma gas flow pattern close to the substrate. In this case, a standoff distance of 3 cm changes the flow pattern significantly and affects the deposition mechanism and formation of hierarchical features preventing the desired surface texture to form correctly and causing the surface mobility to decrease.

10 wt% Ethanol-based suspension
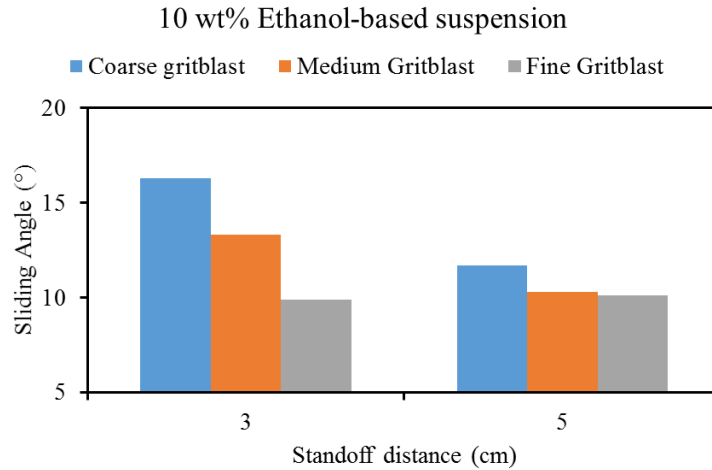
Figure 5.7. Effect of standoff distance on sliding angle of the coatings.

The SPS is complex process that has many influential parameters, and it is difficult to speculate about all observed phenomena. This is particularly true about the influence of spray distance as it is difficult to study the particles' behavior in flight. However, in all mentioned cases, it is observed that sliding angle is relatively large which means that in these coatings the desired features are not fully developed. It is known that the surface roughness has a major role in creating the shadow effect which is the main mechanism responsible for formation of micro-texture features. We can speculate that this effect is more pronounces for 3 cm spray distance because surface roughness influences the flow close to the surface and affects the deposition of the particles. However, as mentioned previously since none of these coatings are among the best performing coatings, we have focused more on more interesting deposition condition.

It is important to note at this point that it has been reported in the literature that [235] spray distance is the only SPS process parameter that influences the phase distribution and ratio of anatase to rutile in SPS TiO_2 coatings. Additionally, typically rutile is the more likely phase to form during plasma spraying of TiO_2 [240] due to high cooling rate. However, in this study, as the coatings are all treated similarly in the stearic acid solution, it is not expected that difference in intrinsic wetting properties of rutile and anatase affect the wetting properties of the coatings. In other words, it is the surface micro-texture and not the phase distribution that is the determining factor in wetting behavior of coating developed in this study.

5.3.6. Effect of plasma gas velocity

Figure 5.9 shows the effect of changing the diameter of the plasma nozzle on the sliding angle of the coatings. By decreasing the diameter of the plasma nozzle and keeping all other parameters the same, the velocity of the plasma gas increases which in turn increases the velocity of the particles and decreases the time that particles travel in the plasma plume. According to the results, increasing the plasma gas velocity through using a smaller plasma nozzle has a positive effect on mobility of the water on the coatings.

10 wt% Ethanol-based suspension

■ Coarse gritblast   ■ Medium Gritblast   ■ Fine Gritblast
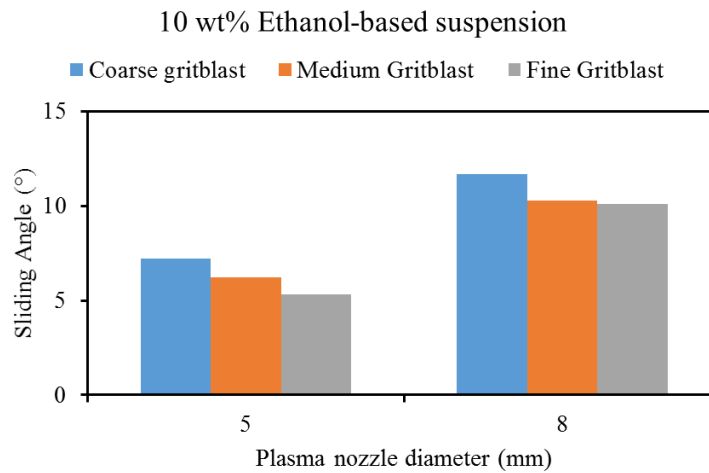
Figure 5.8.Effect of plasma nozzle diameter (and consequently plasma gas velocity) on the sliding angle of the coatings.

5.3.7. Topography

In Table 5.4, multiple surface roughness parameters of the coatings are presented. The first three parameters, arithmetical mean height of the surface (S_a), maximum height of the surface (S_z), root mean square height of the surface (S_q), are all amplitude parameters that relate to the general roughness of a surface. More than one of these parameters is required to represent the actual characteristics of a surface. While all of these parameters show a coefficient of correlation smaller than 0.9 in regards to water contact angle or sliding angle of the samples, they collectively demonstrate an appropriate measure of the roughness of the coatings and it can be concluded that a minimum amplitude of roughness is necessary for these coatings to show reasonable degree of superhydrophobicity.

Skewness (S_{sk}) and kurtosis of height distribution (S_{ku}) are also shown in Table 5.4. Skewness and kurtosis provide additional information about the shape and type of the roughness

on the surface of the coatings. A schematic in Figure 5.10 shows the type of surface features and the corresponding skewness and kurtosis values.
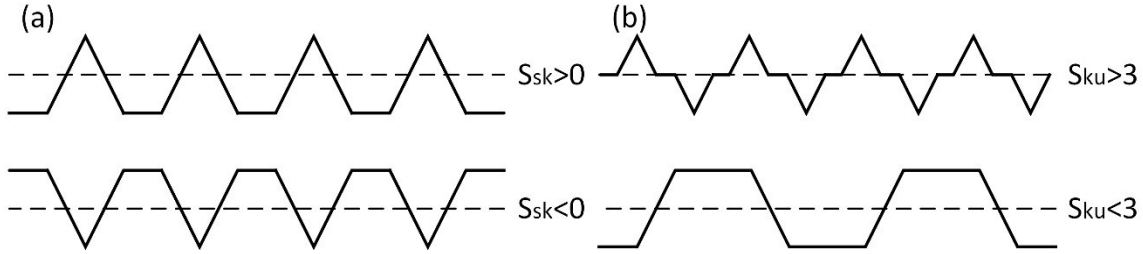
Figure 5.9. Schematic showing the types of surfaces and corresponding skewness and kurtosis values: (a) positive and negative skewness; (b) kurtosis larger and smaller than 3.

According to Table 5.4, the majority of the developed coatings have positive skewness values. In the case of the few negative skewness values, the coatings do not show promising water mobility. This can be explained by the fact that a negatively skewed surface does not allow the formation of large air pockets in the water-solid interface and also results in more solid/liquid interfacial area which reduces the mobility of the surface. In terms of kurtosis, the majority of the coatings have a kurtosis close to 3 which represents their distribution of the peaks and valleys. The coatings that have a relatively large divergence from the normal distribution and their kurtosis value is far from 3 typically do not show significant improvement in water mobility.

A study of correlation coefficient between various surface topographical parameters and surface wettability revealed that the ratio of actual surface area to projected surface area (surface ratio) has the highest correlation coefficient in respect to sliding angle with a value of -0.81 followed by arithmetic mean height with a value of -0.75. Among non-height surface roughness parameters, kurtosis shows the largest correlation with a correlation coefficient of 0.63. Figure 5.11 shows a graph, depicting the variation of the sliding angle of the coatings against the two factors with largest correlation coefficients i.e. the surface ratio and the arithmetic mean height (S_a) of the samples. A second order polynomial is fitted on the data with a coefficient of determination (R^2) of 0.75 and 0.68 respectively.

(a)

$y = 36.512x^2 - 157.95x + 174.09$
$R^2 = 0.7544$

(b)

$y = 0.7539x^2 - 13.904x + 68.49$
$R^2 = 0.6869$
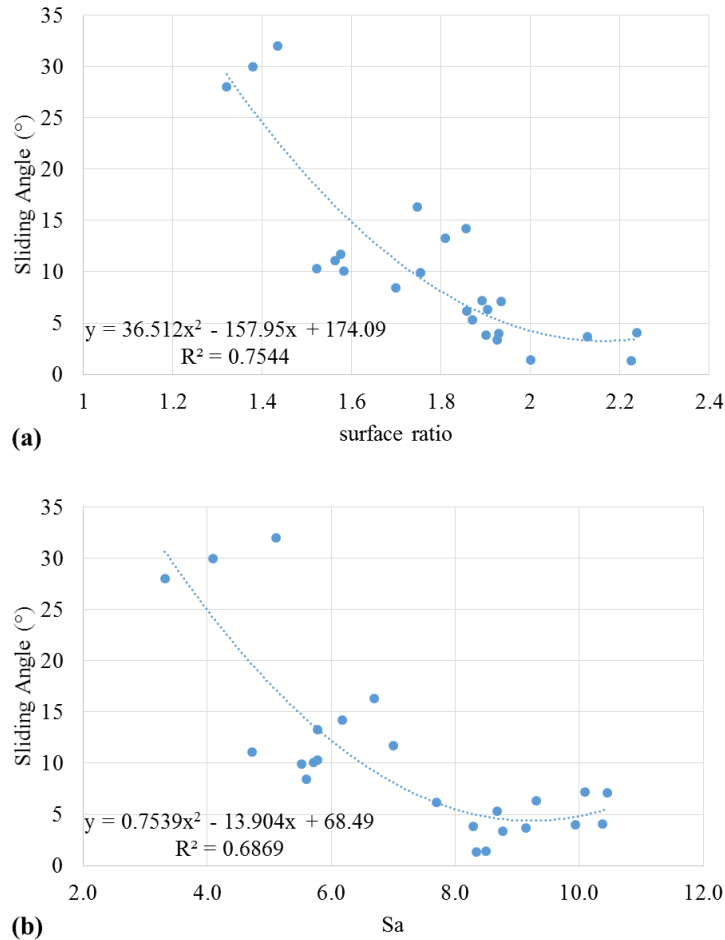
Figure 5.10. Graphs showing the correlation between the sliding angle of the coatings and (a) surface ratio; and (b) arithmetic mean height (R_a) roughness.

In Figure 5.12, two graphs are constructed by plotting the arithmetical mean height of the surface and kurtosis of the coatings surfaces versus the surface ratio of the coatings and the sliding angle value obtained for these coatings is represented by the size of the circles. In these graphs, smaller circles which show coatings with higher water mobility are desirable. As previously mentioned, there is not a single surface roughness parameter that determines or predicts the wetting behavior of a surface. However, looking at a combination of the surface parameters that show the best correlation with the desired wetting behavior (i.e. lower sliding angle and higher mobility), it is possible to identify surface characteristics that seem to indicate improvement in surface wetting behavior. As seen in Figure 5.12 (a) and (b), there are areas (shown by dotted red ovals) in which most coatings with better water mobility are located. In both cases, it is clear from the graphs that larger surface ratios are favorable to achieve higher superhydrophobicity. Furthermore, it can be

concluded that a minimum height in terms of S_a is required to achieve the best result, whereas kurtosis values that deviate too much from normal distribution (i.e. S_{ku}=3 which corresponds to similar number and height of valleys and peaks in the surface topography) are not desirable.

(a)

(b)
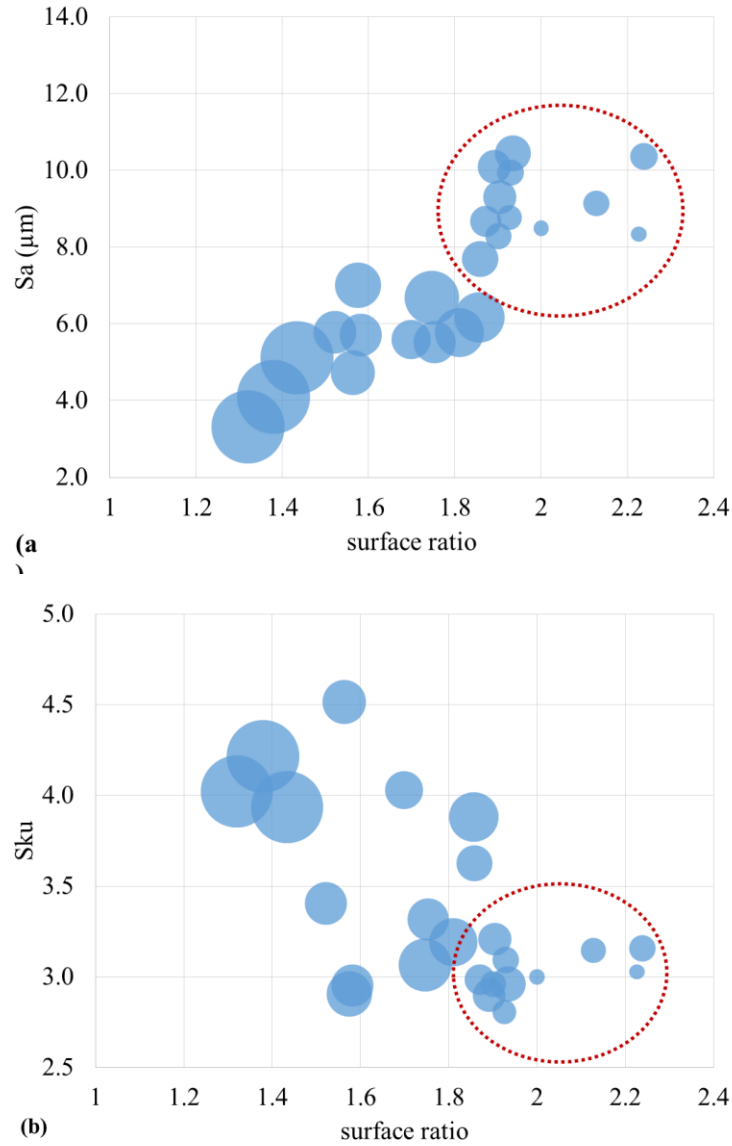
Figure 5.11. (a) Arithmetic mean height of the surface (S_a) plotted against the surface ratio and (b) kurtosis (S_{ku}) of the surface plotted against the surface ratio for all the coatings. The size of the circles is proportional to the value of the sliding angle of each coating, thus the smaller the circle the better the mobility of the coating.

Figure 5.13 schematically demonstrates some of the major conclusions of this study. As shown, finer grit-blasting of the surface prior to deposition results in more refined and more packed 'cauliflower-like' surface features. Such surface micro-texture leads to improved water mobility i.e. small sliding angles. It is important to note that as previously mentioned both primary and secondary roughness features are essential for achieving desired wetting properties in the coatings.
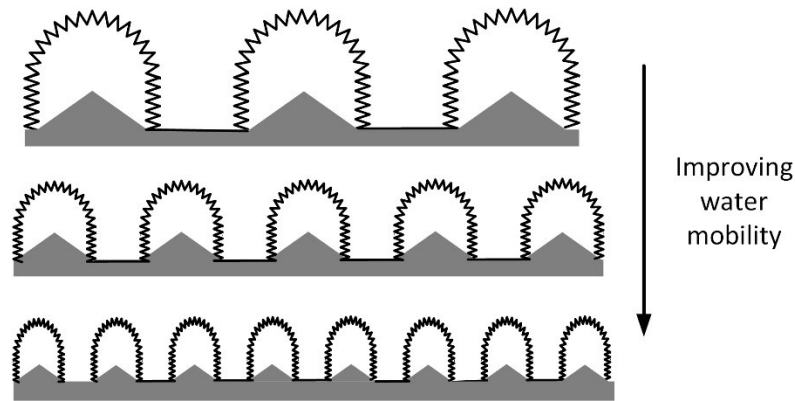
Figure 5.12. A schematic based on findings of this work that demonstrates how refinement of surface texture leads to improvement in water mobility of the surface.

5.4. Summary and Conclusion

The effect of SPS process parameters including substrate roughness, suspension composition and solid content, plasma power, standoff distance and plasma gas velocity on wetting behavior and surface texture of TiO_2 coatings was investigated. It is shown that plasma power, suspension composition and solid content and plasma gas velocity are the most influential parameters while grit-blasting size has a moderate effect. Plasma power improves the surface water mobility for both 10 wt% ethanol-based and water-based suspension coatings, whilst it has an opposite effect on 20 wt% ethanol-based suspension coatings. This is believed to be related to increased deposition efficiency at higher power and higher suspension solid content which results in larger surface features. Water-based suspension is not promising as it generates coatings without the needed hierarchical features. These features are shown to be critical to achieve both high surface water repellence and mobility. In addition to the presence of hierarchical features, the finer and more uniform these features are, the better the wetting behavior of the coatings, making some of them extremely superhydrophobic. Fine grit size during surface preparation has shown to be influential in generating finer and more packed surface textures. The two best coatings in this study

in terms of superhydrophobic performance were achieved using ethanol-based TiO_2 suspension as feedstock deposited onto substrates grit-blasted with the finest grit size and with a plasma gun standoff distance of 50 mm. The best 10 wt% solid content suspension was deposited in high power condition (36 kW) while the best 20 wt% suspension was deposited in low power condition (25 kW). Both these coatings showed extremely high water repellence and mobility manifested by contact angles larger than 165° and sliding angles smaller than 1.5°, respectively. The best coatings developed in this work are comparable to the best results reported in the literature [98,195] in terms of wetting properties.

Acknowledgement

Preface to Chapter 6.

In the previous chapter, the parameters influencing the micro-texture and consequently wettability of SPS TiO$_2$ coatings were studied and the optimized conditions within the operating window of the SPS system for achieving the highest degree of superhydrophobicity were determined. As these coatings are intended to be used for anti-icing applications, the next step is to investigate their performance in icing conditions. Additionally, as one of the main challenges of developing superhydrophobic surfaces for practical applications is the durability of such coatings, it is important to investigate their durability. Therefore, the next chapter is devoted to investigating the icing performance and durability of SPS TiO$_2$ coatings.

Chapter 6. Anti-icing Performance and Durability of Suspension Plasma Sprayed TiO$_2$ Coatings [5]

Navid Sharifi, Ali Dolatabadi, Martin Pugh and Christian Moreau

Department of Mechanical, Industrial and Aerospace Engineering, Concordia University
1455 de Maisonneuve Blvd. W, Montreal, Quebec, Canada, H3G 1M8

Abstract

Superhydrophobic coatings are a potential solution for mitigating the in-flight icing problem for aircraft. However, to develop a superhydrophobic coating which can be practically used for aircraft and that possesses sufficient durability is an ongoing challenge. In this work, superhydrophobic coatings are developed using suspension plasma spraying (SPS) as a flexible, versatile and scalable coating technique. The anti-icing and deicing performances of these SPS coatings are studied in icing wind tunnel experiments. Furthermore, the durability of these SPS coatings is tested in dry particle and cloud-sized water droplet erosion and icing/deicing cyclic tests. The capability of SPS superhydrophobic coatings to reduce ice accretion is comparable to that of commercial superhydrophobic coatings but perform better in deicing tests using heating. Additionally, compared to commercial superhydrophobic coatings, the SPS coatings demonstrate significantly better performance in dry particle and icing/deicing cyclic tests while showing comparable durability in cloud-sized water droplet erosion tests. It is also shown that in case of high intensity water erosion, when the superhydrophobicity of SPS coatings deteriorates, it can be restored using a simple and quick retreatment process due to the robustness of the hierarchical micro-textured TiO$_2$ base coatings.

Key words: Superhydrophobic coating, Suspension plasma spray, Icing, Durability

---

[5] This chapter is to be submitted as an article to the *Journal of Cold Regions Science and Technology*.

6.1. Introduction

In-flight icing poses a major hazard to the safe and efficient operation of aircraft [241]. Ice accretion on various surfaces of aircraft causes an array of issues, including disturbance in aerodynamics, potential damage to external components and interference in the function of its sensors [16,18,242]. As a result, in-flight icing can cause a range of undesired consequences such as flight delays, emergency landings, damaged parts and increased energy consumption to deal with the icing problem [26]. The Federal Aviation Agency (FAA), have reported 319 icing-related accidents during the period of 1998-2007 [30]. Icing is estimated to cost around $96 million annually in terms of injuries and damage in the US only [15]. In addition, ice build-up on wind turbines and power lines due to super-cooled rain droplets can cause major problems [243,244].

In-flight icing occurs due to the presence of super-cooled water droplets i.e. water droplets with a temperature below their freezing point [4,27]. The accumulation of ice as a result of the impact of these droplets on the aircraft surfaces, progressively results in build-up of ice layers that can be as thick as several millimeters [17]. The rate and characteristics of the in-flight ice depend on a number of meteorological parameters. The first parameter is liquid water content (LWC) which is an indicator of the relative humidity in the cloud in terms of grams of water per cubic meter of air. The second parameter is the temperature of the ambient air and water droplets. The third parameter is the average size of water droplets in the cloud (this is expressed as median volumetric diameter-MVD). The typical icing risk conditions are reported in Table 6.1.

Table 6.1. Icing risk conditions [26].

Parameter	Icing risk conditions
Liquid water content (of water in air)	From 0.1 to 3 g/m^3
Temperature	From +4°C to -40°C
Droplet diameter (MVD)	Usually from 1-50 μm but also up to 400 μm

In-flight ice is often categorized into two distinct types [21]. The first type is called glaze or clear ice and typically forms at temperatures close to 0°C when the water droplets do not immediately freeze upon impact but run back and shed on the surface which results in a glassy, transparent, relatively smooth and dense ice. The second type of ice is called rime ice and forms at lower temperatures (typically -10°C and lower) when super-cooled water droplets freeze upon

impact with the substrate, creating a white, irregular ice. Out of these two types, glaze ice is considered to be potentially more dangerous due to its high adhesion and the fact that it can form on various regions of the surface rather than only the point of impact [24].

Various methods have been employed to deal with the icing problem including good weather forecasting, pilot training, optical ice detection systems and computer simulations [22]. Additionally, in-flight anti-icing and deicing systems based on heating or mechanical ice removal have been developed [28,29,31]. This approach can be effective in preventing ice accumulation on the leading edge. However, it is impractical to place heating elements or vibrators below all surfaces that are prone to icing on an aircraft. Therefore, efforts have been focused on using superhydrophobic coatings to prevent or delay ice formation or to reduce ice adhesion, in order to improve the efficiency of thermal and mechanical anti-icing and deicing systems [101,103,245].

Superhydrophobic coatings are surfaces with both high water repellency, manifested through water contact angles of greater than 150°, and high water mobility, manifested through contact angle hysteresis and/or sliding angles lower than 10° [193]. The extreme water repelling characteristic of a superhydrophobic surface is due to the combination of a relatively low surface energy and the presence of a hierarchical micro-texture i.e. a surface texture with both micron-sized and nano-sized roughness [93]. Superhydrophobic surfaces have found potential applications where minimal interaction of a solid surface and a liquid is desired such as anti-icing [246], anti-corrosion [247], drag-reduction [69] and drop-wise condensation [121].

Studies have shown that ice formation can be efficiently delayed or even in certain conditions completely prevented on superhydrophobic surfaces [7,12,62]. This is because super-cooled water droplets do not easily stick on a superhydrophobic surface and mainly bounce off and detach from it before freezing begins. The anti-icing capability of superhydrophobic surfaces, especially in the early stages of ice formation, is demonstrated frequently by comparing the onset of ice nucleation on superhydrophobic and non-superhydrophobic surfaces. However, some such icing experiments have been performed using relatively large and static water droplets [154,248] that do not necessarily represent in-flight icing conditions which involves water micro-droplets impinging on the surface with relatively high velocity.

Furthermore, some studies have claimed that ice adhesion can be significantly reduced on superhydrophobic surfaces due to the formation of air pockets between the solid surface and ice [160,243,249]. However, on the contrary, some other studies have reported an increase in ice

adhesion due to the surface roughness which form a mechanical interlock with the ice [243,250]. These seemingly contradictory observations signify the importance of testing anti-icing performance of each novel superhydrophobic surface in icing conditions simulated in icing wind tunnels to resemble actual in-flight icing conditions.

Another major challenge in developing new superhydrophobic coatings for anti-icing applications is their mechanical durability. Common low-surface-energy materials used to develop superhydrophobic coatings are organic or polymeric materials which typically suffer from poor mechanical durability, especially in terms of erosion resistance. Therefore, considerable efforts have been focused on developing techniques and tests to improve, quantify and compare durability of superhydrophobic coatings [38,251]. Consequently, it is crucial for all new superhydrophobic coatings developed using various surface engineering techniques to be tested for different aspects of mechanical durability such as water erosion, sand erosion and icing/deicing cycles.

Recently suspension plasma spray (SPS) has been employed as a flexible (in terms of variety of materials that can be deposited), versatile and scalable coating techniques to develop superhydrophobic TiO_2 coatings [224]. In addition, the SPS process has been optimized [252] to achieve very high water repellency and mobility. These coatings have shown water contact angles greater than 165°, water sliding angles as low as 1° and water contact angle hysteresis as low as 3°. In this work, the best samples of these SPS coating have been selected and investigated for their icing performance and durability. Results are then compared to commercially available polymer-based superhydrophobic spray-on coatings in order to better demonstrate the characteristics of the SPS superhydrophobic coatings.

6.2. Methodology

In this section, the coating deposition technique is briefly explained (more detailed explanations can be found in previous publications [196,224,252]), followed by two groups of tests designed to evaluate the icing performance and durability of the SPS TiO_2 superhydrophobic coatings.

6.2.1. Coating Fabrication

Coating samples were prepared using suspension plasma spraying of a titanium dioxide suspension feedstock onto 3 × 12 × 120 mm, grinded 304 stainless steel substrates. The feedstock suspension was prepared by mixing 10 wt% of titanium dioxide submicron sized particles (nominal

average particle size 500 µm, TKB Trading, US) into a solvent composed of a mixture of ethanol and ethylene glycol with a weight ratio of 4 to 1. Polyvinylpyrrolidone (PVP) was used as a dispersing agent in the suspension. Prior to deposition, the stainless steel substrates were grit-blasted for cleaning and to increase coating adhesion. A 3MB plasma torch (Oerlikon Metco, Switzerland) was used with a mixture of argon and hydrogen as plasma gas. The total plasma gas flow rate was 60 l/min. The power of the plasma was set to 36 kW by fixing the plasma current to 600 A, and adjusting the hydrogen flow rate so that the plasma power was 60 V. During the deposition, the plasma torch stand-off distance was 5 cm and the suspension feed rate was 55 g/min. The robot that was used to move the plasma torch had a lateral speed of 1 m/s and a raster pattern with an overlap distance of 3 mm was used for deposition. After coating, the samples were cleaned with compressed dry air, decontaminated in boiling water and then isopropyl alcohol and finally treated with a solution of stearic acid in 1-propanol. A more detailed description of the development of these superhydrophobic titanium dioxide coatings and optimization of the process to achieve the high water repellency and mobility can be found in the authors' previous articles [252]. The SPS TiO_2 superhydrophobic samples are denoted as "SPS" throughout this paper.

For comparison purposes, two commercial superhydrophobic products, NeverWet® (Rust-Oleum, Canada) and Ultra-Ever Dry® (Ultratech International, USA) were used. These samples are denoted as "NW" and "UED" respectively throughout this article. Coatings were prepared on substrates similar to those used for preparation of SPS coatings and according to the manufacturer instructions. These additional samples were tested in the same conditions as SPS coatings to compare durability and performance.

6.2.2. Icing Tests

Two groups of tests were used to evaluate the different superhydrophobic coatings. The first group of tests were designed to evaluate the icing performance of the samples and included ice accretion and heated deicing tests. The second group of tests were designed to evaluate the durability of the coatings. They included dry particle erosion, cloud-sized droplet erosion, high intensity water erosion and icing/deicing cyclic tests. All icing tests and droplet erosion and icing/deicing cyclic durability tests were carried out using a closed loop icing wind tunnel at Concordia University. A schematic of the icing wind tunnel is shown in Figure 6.1. The test section of the wind tunnel has a square-shaped cross section with a width of 10 cm. The air velocity in the test section can reach a maximum of 45 m/s and the temperature of the air in the test section

can be reduced to a minimum of -20°C with an air velocity of approximately 10 m/s. It is important to note that the minimum operating temperature of the wind tunnel increases with increasing air velocity due to the decreased residence time of air in the chiller. The liquid water content in the test section can be varied between 0.2-1 g/m^3.
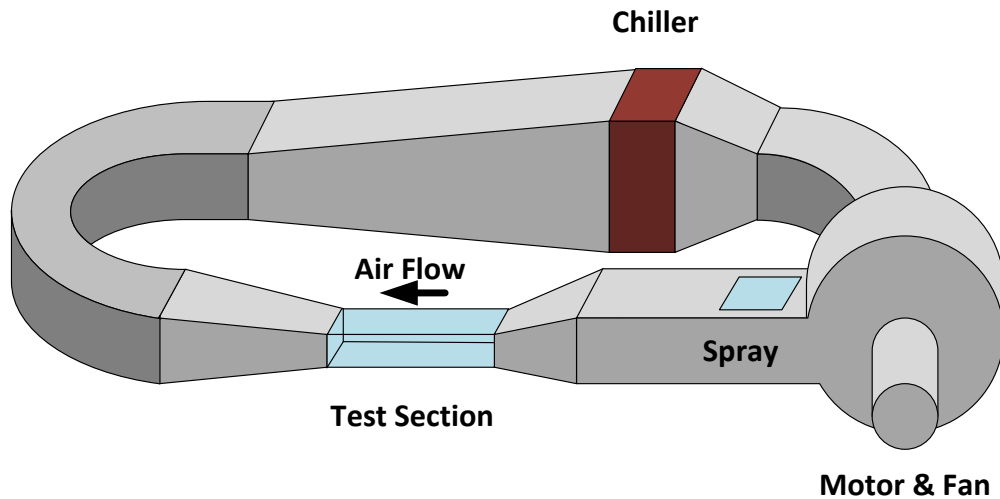
Figure 6.1. Schematic of the icing wind tunnel.

The water droplets were injected into the air stream using an air atomizing spray nozzle placed after the fan. The size distribution and spray pattern can be adjusted using the air flow and water flow controllers. The spray of droplets in the test section was characterized using a phase Doppler particle analyzer (PDPA), and in all the tests performed, the spray had an LWC of 0.5 g/m^3 with a median volume diameter (MVD) of 30 μm [253]. For the spray, cold distilled water was used. For icing tests the water was maintained below 4°C to ensure super-cooled water droplets reach the test section. The placement of the spray nozzle at 1.14 m upstream ensured that the water droplets in the test section had approximately the same velocity and temperature as the air stream. Furthermore, the air stream velocity was measured using a Pitot tube probe and compared to the velocity of particles measure by PDPA to ensure that they were within 5% difference of each other.

A schematic of the sample holder that was used in the icing wind tunnel for icing and water droplet impact tests is shown in Figure 6.2. The flexible heater shown in this schematic was used in the heated deicing tests. The details of these tests are discussed in the following sections.
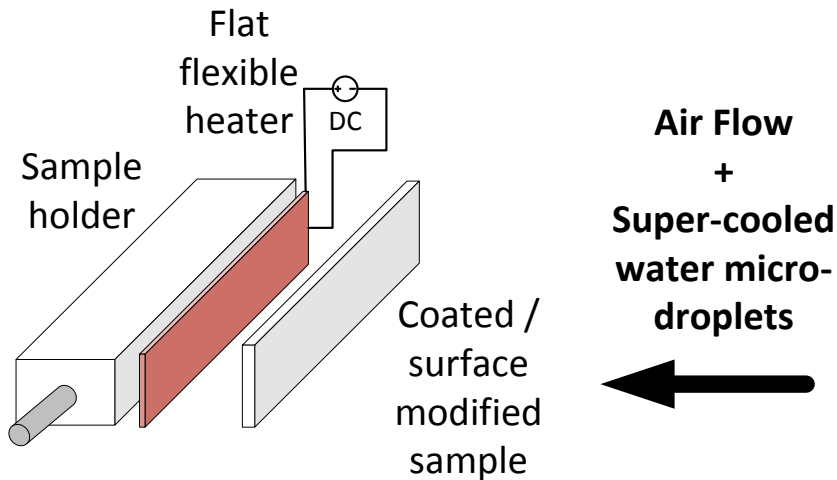
Figure 6.2. Schematic of the sample holder used in the wind tunnel for icing and water droplet impact tests.

6.2.2.1.   *Ice Accretion Test*

Multiple sets of operating conditions were designed to represent various in-flight icing scenarios within the capabilities of the testing equipment. In all these conditions, the liquid water content (LWC) and median volume diameter (MVD) were 0.5 g/m³ and 30 μm, respectively which correspond to the icing risk conditions presented in Table 6.1. In the case of air stream velocity, two values were selected, one being the maximum capacity of the wind tunnel i.e. 45 m/s and the other one corresponding to a motor frequency of half of maximum power which gave 25 m/s. It is important to note that by increasing the air stream velocity, the water input was adjusted to ensure that the LWC value remained constant for all tests. In terms of temperature, two temperatures were selected, one slightly below the freezing temperature of water i.e. -3±1°C which typically results in formation of clear ice. The other temperature was -10±1°C which was the maximum cooling capacity of the chiller at an air velocity of 45 m/s and typically causes the formation of rime ice. Except at the stagnation point/region, the impact of super-cooled water droplets on aerodynamic surfaces of aircraft is not perpendicular, therefore, samples were tested with both 90° and 45° angle of impacts to better represent the various surfaces of an aircraft. In order to better assess the delay in ice formation, the duration of each ice accretion test was 1 minute. The coupons were carefully weighed before and after each test to determine the weight of ice formed during the test. Each test was repeated 9 times for each sample.

Table 6.2. The wind tunnel operating condition.

Variable	Value(s)
Air stream velocity (m/s)	23 and 45
Air stream temperature (°C)	-3 and -10
Angle of impact [AoI] (°)	45 and 90
LWC (g/m^3)	0.5
MVD of water droplets (µm)	30

6.2.2.2.   *Heated Deicing Tests*

To evaluate the potential contribution of superhydrophobic coatings to the deicing process using heating, a flexible flat heating element was placed under the coupons (Figure 6.2). Then each sample was exposed to the harshest icing condition given in Table 6.2 for 1 minute. Then the spray was stopped while the rest of the operating parameters were kept constant. Then the sample was turned 45° so that the surface of the sample was at a diagonal with respect to the direction of the air stream before heating began. This step was necessary because if the sample was left perpendicular to the air direction, after heating the ice that is in direct contact with the substrate would melt, causing a gap between the remainder of the ice and the substrate surface which resulted in the layer of ice remaining intact. The heater under the sample was turned on with 24 W electrical power. The time necessary for complete ice removal was measured as the deicing time. It is important to note that in some cases, complete ice removal meant that the ice was completely melted, and in some cases after melting the layer close to the substrate surface, the remainder of ice would fly away from the test coupon. Both these conditions were accepted as the ultimate condition of ice removal.

For any icing condition, if enough heat input is given to the substrate, it is possible to maintain its surface free of ice. Consequently, another test was designed to measure the heat input required to maintain an ice-free surface. In this test, similar to the deicing test, a heater was positioned under the samples and they were fixed in the wind tunnel with the water spray closed. The heater was turned on and enough time was given for the temperature profile to reach steady state. The steady state was ensured by placing a small thermocouple under the samples, between

the heater and the samples. When this thermocouple showed a constant temperature i.e. steady state condition was achieved, the spray was started. If ice started to form on the surface of the sample, the test was stopped, the sample was deiced, dried and the test was repeated with a heat input 1 W higher than the previous run. If no ice had formed on the sample, the same process was repeated with a 1 W decrease in heating. Using a trial and error method, the minimum electrical power required to maintain an ice-free surface was measured and reported for each coating as well as for an uncoated sample.

6.2.3. Durability Tests

Four different tests were used to evaluate the durability of the superhydrophobic coating including dry particle erosion, cloud-sized water droplet erosion, high intensity water erosion and icing/deicing cyclic tests. These tests were designed to measure the deterioration of superhydrophobic behavior of the coatings after being exposed to erosive and destructive factors. The superhydrophobicity of samples was evaluated based on measurement of static contact angle (CA), contact angle hysteresis (CAH) and sliding angle (SA) of water on the surface. These wetting characteristics were each measured using an in-house setup, using a camera, a tilting surface which could be tilted with the precision of 1° and an automatic droplet dispenser. The CA and SA were measured using a 10 µL droplet of distilled and deionized water. For measuring advancing and receding contact angles (ACA and RCA respectively), an inflating/deflating droplet technique was used with the size of the droplet changing between 5 and 10 µL. The CAH was calculated as the difference between ACA and RCA values. An open source plug-in [212,213] to the image analysis software ImageJ was used to analyze the images and determine the contact angles.

6.2.3.1. *Dry Particles Erosion Test*

For evaluating the resistance of superhydrophobic coatings to solid particle erosion, a technique which is frequently used in literature [38,251,254–256] was employed. In this test, a fixed amount of abrasive particles, in this case 5 g of aluminum oxide particles (particle size of 125 µm) was poured onto the surface of the coatings from a fixed distance of 30 cm. The samples were placed at a 45° angle with respect to falling particles to ensure that particles move away from the point of impact. Erosion occurs due to the impact of falling particles accelerated only due to gravity. Afterwards, the surface of the samples was cleaned using compressed air and CA, CAH and SA of the samples were measured. This cycle was repeated 5 times for each sample.

6.2.3.2.   Cloud-Sized Water Droplet Erosion Test

To evaluate the resistance of coatings to water droplet impact, similar to what happens in flight conditions, the samples were exposed to a spray of cloud-sized droplets inside the wind tunnel. This test was performed at room temperature with an air stream velocity of 45 m/s and a droplet MVD of 150 μm with a perpendicular angle of impact for a duration of 5 minutes for each cycle. It must be noted that the 150 μm droplet size used in this test is considerably higher than the cloud droplet size (typically MVD = 1-50 μm). This droplet size was selected to reduce test times since it would take a long time for 50 μm droplets to cause noticeable deterioration. After each cycle, the samples were removed from the test section, dried using compressed air and CA, CAH and SA of the coatings were measured and reported.

6.2.3.3.   High Intensity Water Erosion Test

A high intensity water erosion rig with a rotating disk was used for this test. This rig was originally designed for testing erosion resistant coatings according to ASTM G73 standard [221,257]. The resulting erosion aggressiveness is far more severe than water erosion conditions encountered in flight conditions. Indeed, water erosion rate is directly proportional to the mass and velocity of impacting water droplets [258]. In this work, the water erosion rig was used at its least intense setting with water droplets with an average diameter of 260 μm and impact velocity of 200 m/s. For an aircraft flying though clouds, which typically happens after takeoff and before landing, the speed is between 80-120 m/s and the droplet size in clouds is typically 5 – 50 μm [5]. Therefore, the kinetic energy of water droplets upon impact is at approximately three orders of magnitude higher in this test compared to in-flight conditions. However, it must be noted that an aircraft sometimes needs to fly though rain droplets which are larger than cloud-sized droplets but their impact on the surfaces of aircraft occurs with smaller velocities. Therefore, it is reasonable to assume that the type of erosion occurring during this high intensity water erosion test can be of the similar magnitude to the erosion from raindrops due to similar impact energy. Additionally, this test can be seen as an accelerated indicator of durability of superhydrophobic surfaces exposed to water droplet erosion. The minimum duration of the test with repeatable and consistent conditions was 5 seconds but the test was repeated for durations of 10, 20, 60, 300 and 12000 seconds as long as the coatings survived. After exposing the samples to this test, the samples were visually

inspected and the wetting behavior of the samples was tested. Finally, micrographs of the eroded regions were prepared using SEM to study the wear damage.

6.2.3.4.   Icing/Deicing Cyclic Test

To evaluate the durability of the coatings exposed to repetitive icing/deicing cycles, only the harshest icing condition i.e. highest air velocity and 90° angle of impact at -10°C was selected. The samples were exposed to this condition for a duration of 1 min, removed from the test section and then heated using a heat gun until the ice was fully molten. The samples were then dried using compressed air, and the SCA, CAH and SA of the samples were measured. This cycle was repeated multiple times for each sample. The total number of icing/deicing cycles was selected individually for each sample based on the observed changes in their corresponding wetting properties. It is important to note that the 1 minute duration of the test was selected due to the fact that any longer duration for each run was not expected to have a significant effect because as soon as a complete layer of ice forms on the surface, the impinging droplets will impact on the ice layer rather than the actual surface of the samples.

6.3.   Results and Discussion

After measuring the "as prepared" wetting behavior, SEM micrographs of the SPS and commercial spray-on coatings were recorded (Figure 6.3). The difference between the surface micro-texture of the SPS coating in comparison to the commercial polymeric coatings is clearly seen. While the commercial coatings have a single scale surface roughness and mainly rely on their surface chemistry to deliver the superhydrophobic behavior, the SPS coating has a distinct hierarchical surface micro-texture which, in combination with the surface treatment for lowering the surface energy, results in superhydrophobic behavior of this type of coating. It has been demonstrated [224,252] that SPS coatings without the hierarchical micro-texture do not demonstrate the same extreme water repelling behavior as hierarchical coatings.
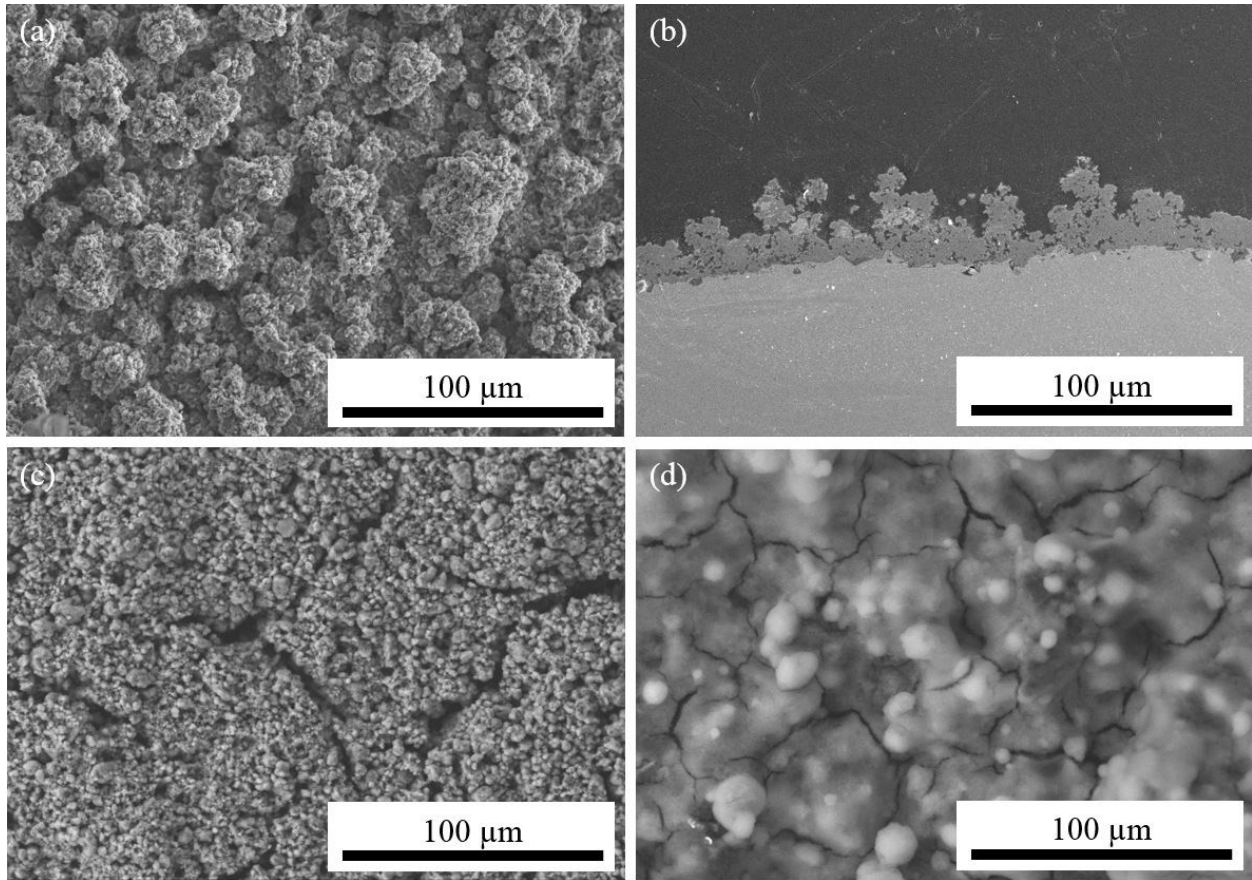
Figure 6.3. SEM micrographs of: (a) top and (b) cross-section of SPS coating; (c) UlterEver Dry coating; and (d) NeverWet coating.

6.3.1. Icing Tests

6.3.1.1. *Ice Accretion Test*

To evaluate the icing performance of the SPS superhydrophobic coatings in various conditions, a total of eight sets of icing parameters were selected as explained in the experimental section. For each set of icing conditions, the experiment was carried out nine times and the average value for ice accretion in terms of mass of ice is reported. The results for each case are compared to the results for an uncoated substrate. The ice accretion test results, reported in Table 6.3 show that the SPS superhydrophobic coating decreases the amount of accumulated ice in all tested icing conditions by providing delay in the ice formation. The reduction of ice accretion ranges from 13 to 62 percent depending on the conditions. The highest decrease is observed for 23 m/s (lower) air velocity, -3°C (higher) temperature and an angle of impact of 45° which corresponds to glaze ice formation. This is expected as in temperatures closer to the freezing point, there is less chance of

water droplets freezing immediately upon impact and the 45° angle of impact facilitates the removal of droplets by the oncoming air flow (similar to the majority of aerodynamic surfaces of aircrafts).

In general, according to Table 6.3, the effect of a superhydrophobic coating on decreasing ice accretion is more pronounced at -3°C when glaze ice typically forms compared to -10°C when rime ice typically forms. This is because droplets with a relatively higher temperature stay liquid for a longer time and there is more chance of them being removed by the air stream due to the superhydrophobic behavior of the coating. This is potentially a benefit since as was mentioned in the introduction, glaze ice is typically considered to be more hazardous compared to rime ice.

Furthermore, according to Table 6.3, the decrease in ice accretion is larger for all cases when impact occurred at 45° compared to 90°. This is expected as the tilted surface allows more efficient removal of water droplets by the air stream and reduces freezing on the surface. At this point it should be noted that aircraft surfaces are normally curved and normal impact occurs around the stagnation point. Therefore the 90° angle of impact can be considered the worst-case scenario. It is reasonable to expect a more efficient decrease in icing for an aerodynamic shape such as an airfoil [253].

Table 6.3. Ice accretion test results. For all conditions, LWC = 0.5 g/m^3, MVD = 30 μm and test duration was 60 s. [St. Dev. = standard deviation; Est. Unc. = estimated uncertainty calculated using the root of the sum of the squares RSS]

Condition	Air Stream Velocity (m/s)	Air Stream Temperature (°C)	Angle of impact (°)	Type of ice	Ice accretion on uncoated sample (g) [± St. Dev.]	Ice accretion on SPS sample (g) [±St. Dev.]	Icing decrease (%) [±Est. Unc.]
1	23	-3	45	Glaze	0.98 ±0.02	0.37 ±0.04	62 ±5
2	23	-3	90	Glaze	0.96 ±0.02	0.49 ±0.02	49 ±3
3	23	-10	45	Rime	1.12 ±0.02	0.51 ±0.02	54 ±3
4	23	-10	90	Rime	1.3 ±0.02	0.87 ±0.03	33 ±4
5	45	-3	45	Glaze	0.97 ±0.02	0.43 ±0.03	55 ±4
6	45	-3	90	Glaze	1.11 ±0.03	0.54 ±0.02	51 ±4
7	45	-10	45	Rime	1.49 ±0.02	0.84 ±0.02	43 ±3
8	45	-10	90	Rime	1.83 ±0.04	1.58 ±0.04	13 ±9

The effect of air stream velocity is more complex than the previous two parameters. Since doubling the air stream velocity value while keeping all other parameters constant means that the number of droplets coming towards the surface has also doubled; one might expect to observe a significant increase in ice accretion. However, this is not the case according to Table 6.3. For both uncoated and coated samples, the increase in the mass of ice for doubling the air velocity is relatively small and in a couple of cases this increase is negligible. To explain this observation, it is necessary to consider the aerodynamic characteristics of the test section and the samples. Since the samples in this test are all flat, in the case of 90° angle of impact, a strong stagnation region in the air flow is created. In both 45° and 90° angle of impact conditions, all droplets coming towards the surface of the samples do not necessarily impact on the surface and a number of them, especially the smaller droplets, are deviated by the air flow going around the sample. Increasing the velocity of the air stream can amplify this phenomenon which can explain why the ice accretion is not significantly increased by doubling the air stream velocity.

To compare the effect of the SPS superhydrophobic coating on decreasing icing with commercial superhydrophobic coatings, samples of the two commercial coatings were prepared and tested in two icing conditions (Conditions 1 and 8 in Table 6.3). The results are compared with the uncoated sample in Figure 6.4. This figure shows that, in these two icing conditions, all three superhydrophobic coatings decrease the ice accretion. The SPS coating shows slightly better performance in Condition 1 whereas, in Condition 8 the inverse is observed but the difference between the three coatings is smaller.
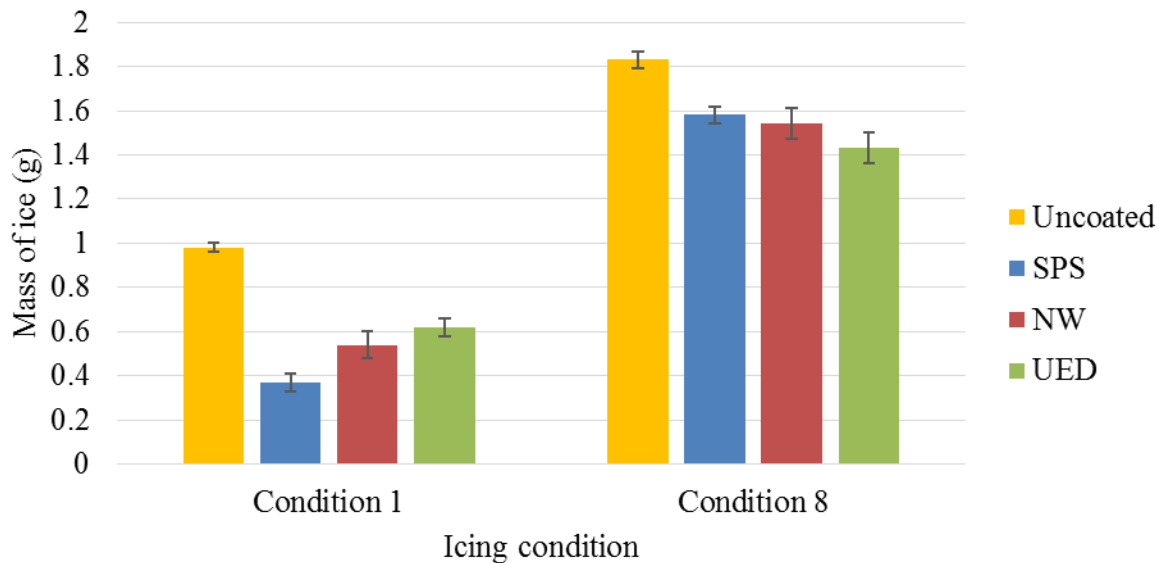
Figure 6.4. Ice accretion test comparison for uncoated sample versus the SPS, and the two commercial (NW and UED) coatings. (The error bars represent standard deviation)

6.3.1.2. *Heated Deicing Tests*

To study the effect of superhydrophobic coating on deicing time using heating, the three superhydrophobic coatings were put in icing Condition 8 for one minute. Afterwards, the water spray was stopped, and the sample was tilted to a 45° angle relative to the air stream. The electrical heating element underneath the sample was then turn on to a power of 24 W. The time for the samples to become completely ice-free was measured and is reported in Table 6.4. For all three superhydrophobic coatings, the deicing time was significantly shorter than that of the uncoated sample. One important observation is that for the three superhydrophobic surfaces, the ice-free surface was achieved due to detachment of the ice at some point after heating started, but for the uncoated sample, the ice-free surface was achieved by melting all the ice on the surface.

Furthermore, the SPS superhydrophobic coating demonstrated the shortest deicing time compared to the other two commercial coatings. This can be attributed to the fact that the commercial coating are several hundreds of micrometers thick layers of polymer that act as a thermal insulator, delaying the heating of the interface of ice and sample. The SPS coating on the other hand is only 10-20 μm thick and TiO_2 has a thermal conductivity considerably larger than most polymers, and therefore, the thin SPS coating is not a significant barrier to heating the interface and therefore deicing is faster for it.

Table 6.4. Deicing time of each sample for 24 W heating power. [St. Dev. = standard deviation; Est. Unc. = estimated uncertainty calculated using the root of the sum of the squares RSS]

Sample	Deicing time (s) [± St. Dev.]	Improvement (%) [± Est. Unc.]
Uncoated	173 ± 8	--
SPS	34 ± 4	80 ± 5
NW	58 ± 3	66 ± 5
UED	47 ± 3	73 ± 5

To further study the effect of a superhydrophobic surface on deicing, another experiment was designed to determine the minimum electrical power required to maintain an ice-free surface for various samples. This experiment was performed in 23 m/s air stream velocity and -3°C air temperature with two 45° and 90° angle of impact (Conditions 1 and 2 in Table 6.3 respectively). The results are reported in Table 6.5. For all three superhydrophobic coatings, less electrical heat input was required to maintain an ice-free surface compared to the uncoated sample. It is noteworthy that the SPS coating in both conditions requires the least amount of heat to maintain an ice-free surface. As discussed above, this can be attributed to the thickness of the coatings and the fact that the relatively thicker polymeric coatings act as a thermal barrier, requiring more power to increase the surface temperature to a level sufficient for preventing ice formation.

Table 6.5. Minimum electrical power required to maintain an ice-free surface at two angles of impact (AoI).

Sample	AoI = 90°		AoI = 45°	
	Power (W)	Improvement (%)	Power (W)	Improvement (%)
Uncoated	36	--	24	--
SPS	30	17	16	33
NW	33	8	20	17
UED	33	8	21	13

It is important to note at this point that overall, we can see that superhydrophobic coatings can contribute to mitigating the icing by reducing ice accretion, reducing the deicing time and reducing the heat required to maintain an ice-free surface. The performance of the SPS coating in decreasing ice accretion is similar to the commercial spray superhydrophobic coatings. However, the SPS coating has lower deicing time and requires less heat input to maintain an ice-free surface compared to both commercial polymeric superhydrophobic coatings. This difference is mainly due to the thickness of the polymeric coatings which causes them to act as a barrier to the heating from underneath the surface of the samples. Now that it has been established that the SPS coating performs positively in mitigating the icing and improving deicing, in the next sections its durability and mechanical performance are studied and compared to the commercial superhydrophobic coatings.

6.3.2. Durability Tests

6.3.2.1. Dry Particle Erosion Test

The first set of durability tests were designed to evaluate the dry particle erosion resistance of the superhydrophobic coatings. The change in wetting characteristics of the coatings after multiple iterations of the dry particle erosion test is shown in Figure 6.5.

According to Figure 6.5, the SPS coating shows significantly better durability in this test. The CA of the SPS coating does not change significantly even after five repetitions of this test. Furthermore, the SPS coating still shows a reasonable water mobility after five iterations of the

test with a SA of below 10° and a CAH of below 20°. This is in contrast with both commercial coatings that quickly deteriorate and lose their superhydrophobic behavior after a few iterations of the test. Indeed, as shown in Figure 6.5, the CA of both commercial coatings drops to below 150° after two iterations. More importantly, both commercial coatings lose their water mobility (having CAH of more than 60°) and a water droplet pins on their surface i.e. no sliding occurs, after only one iteration.
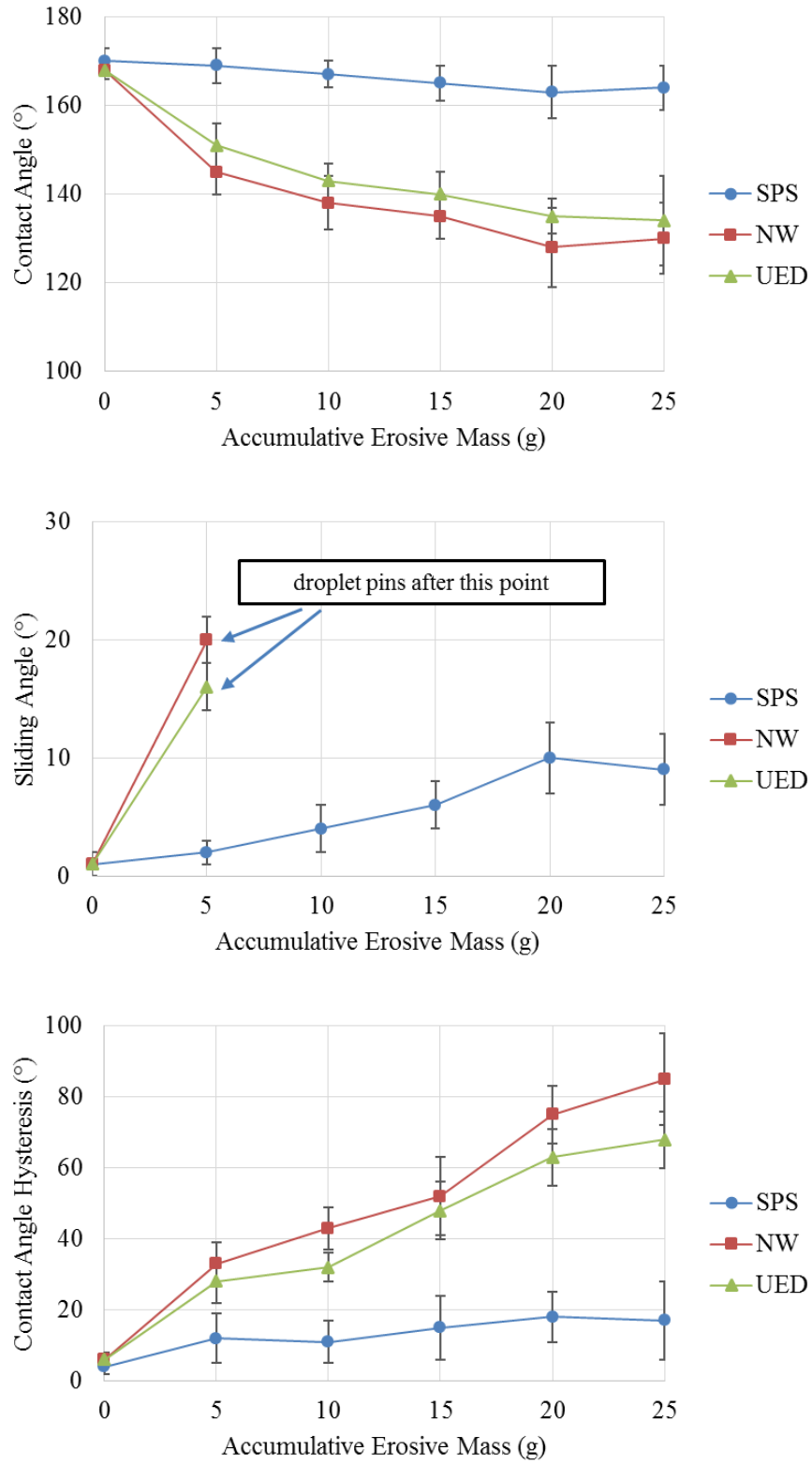
Figure 6.5. Change in CA, CAH and SA of different coating per accumulated mass of erosive particles [error bars represent standard deviation].

The significant difference between the SPS coating and the commercial polymer coatings in terms of dry particle erosion is due to the relatively soft nature of the polymeric coatings. This allows for the erosive particles to not only remove material from the surface of the coating and damage the coating microtexture, but also for especially smaller particles, to penetrate the coating and adhere to the surface. This penetration and embedding of small alumina particles in the polymeric coatings was observed using optical microscopy. These microscopic particles result in a rapid deterioration of superhydrophobic characteristic of the polymeric coatings. On the other hand, the SPS coating, made of TiO_2, is significantly harder and more resistant to penetration of abrasive particles. Thus, most abrasive particles are removed easily by the compressed air.

6.3.2.2.   *Cloud-Sized Water Droplet Erosion Test*

In the next step of durability testing, the water droplet erosion resistance of the superhydrophobic coatings was evaluated. It worth noting that these droplets are five times larger in diameter than the droplets used in the icing test (i.e. MVD = 30μm). This droplet size is considerable larger than the water droplets that impact on the surfaces of the aircraft while passing through clouds in icing conditions. However, they can reasonably represent larger rain droplets that impact onto the aircraft surface in lower altitudes. As mentioned before, these droplets were characterized using the PDPA laser system which revealed their velocity to be close to 45 m/s just before the impact on the substrate. This velocity is roughly half of the velocity of a passenger aircraft when it passes through the clouds.

The change in CA, SA and CAH of the coatings after multiple iterations of the cloud-sized water droplet erosion test is shown in Figure 6.6. It is clear that out of the three samples, the UED commercial coating is more resistant to water droplet erosion. The change in wetting characteristics of the SPS coating is very close to the NW commercial coating. The deterioration in superhydrophobic properties of the SPS coating occurs mainly due to gradual removal of the thin stearic acid layer from the surface which will be discussed further in the following paragraph. This stearic acid is extremely thin and transparent and therefore it is very difficult to give an exact value for its thickness.
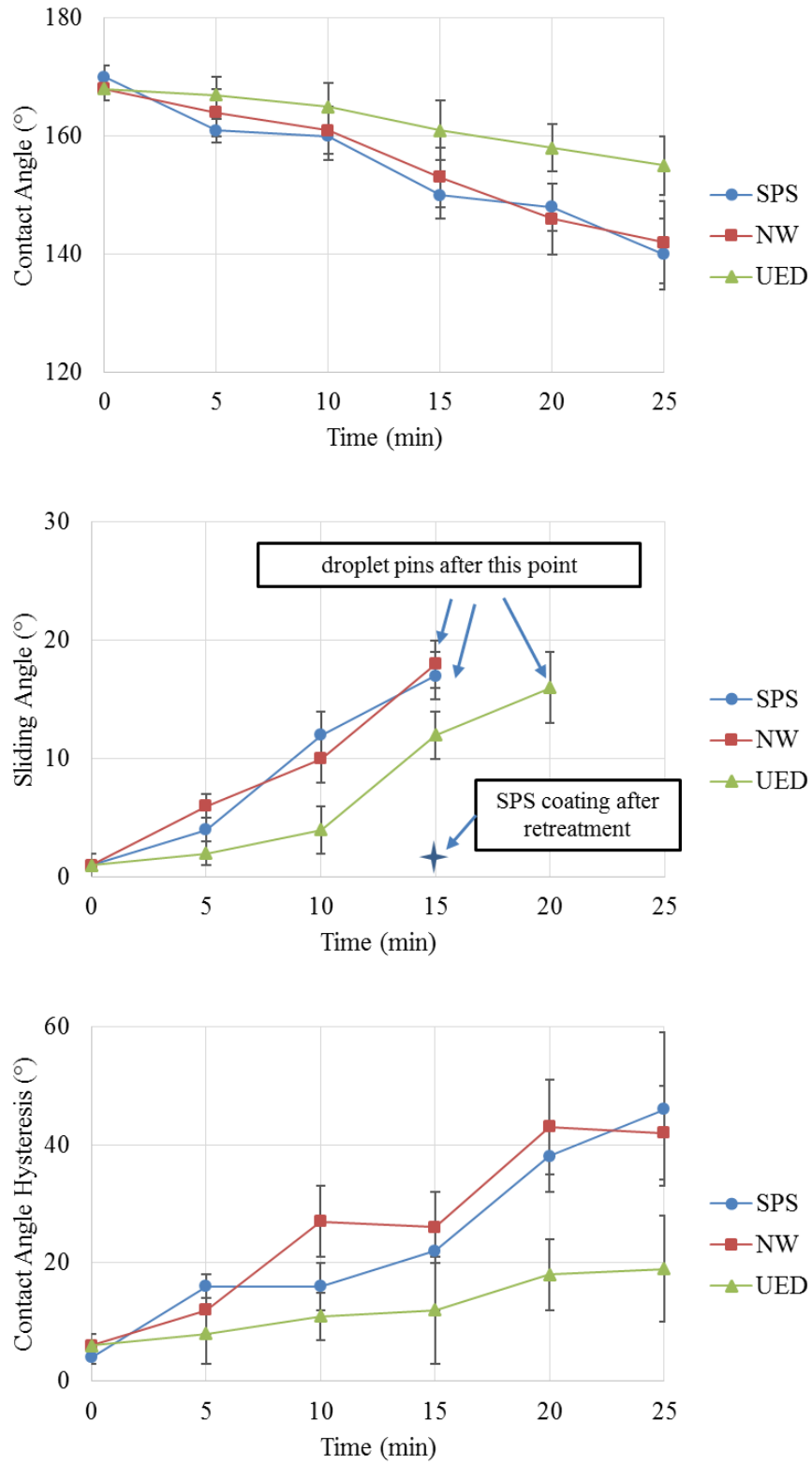
Figure 6.6. Change in CA, CAH and SA of different coatings per exposure time to 150 µm cloud-sized water droplet impacts at 45 m/s [error bars represent standard deviation].

There are two important points to consider regarding the cloud-sized water droplet erosion results. First, attempts to increase the thickness of the stearic acid treatment and consequently improving its durability can cause negative side effect since a relatively thick layer of stearic acid covers some of the hierarchical features of the coating micro-texture and results in reduced contact angle and water mobility of the coating. Second, an advantage of the SPS coating compared to the commercial coatings is that after the superhydrophobicity of the SPS coating has been reduced due to water erosion, a simple and quick retreatment by stearic acid solution immediately recovers the CA, SA and CAH to their initial values as demonstrated in Figure 6.6 This was experimentally demonstrated. This is in contrast to the commercial polymeric coatings where after the coatings are damaged, the surface needs to be cleaned of the remaining coating and then the coated again. This advantage is because while the stearic acid layer is removed by cloud-sized droplet erosion, the bulk of the TiO_2 base coating remains intact with its hierarchical micro-texture remaining unaffected by the water droplet erosion. On the contrary, when the wetting behavior of the commercial superhydrophobic coatings deteriorate, it is due to damage to the bulk of the coating.

6.3.2.3.   *High Intensity Water Erosion Test*

To verify that the bulk of the SPS coating is more resistant to water droplet erosion, a high intensity water erosion test was designed and performed on all coatings. As detailed in Methodology section, this test was performed using a test setup specifically designed to test water erosion resistant coatings. Noting that even the mildest setting of this specific test was too erosive for the superhydrophobic coatings, this least intensive condition with MVD = 260 μm droplet size and 200 m/s droplet impact velocity was used.

The results of high intensity water erosion are demonstrated in Figure 6.7. It is also noteworthy that the shortest duration of test possible while having consistent and repeatable impact results was 5 seconds. As demonstrated in Figure 6.7, both commercial spray-on coatings failed completely even for this 5 second test i.e. the coatings were completely removed at the line of impact and the surface of the substrates were completely visible. The SPS coating lost its superhydrophobicity with its CA dropping to below 120°, no sliding and CAH increasing to larger than 40° after the 5 second test. However, no considerable loss of coating mass was observed for the SPS coating after 5, 10 and 20 seconds of testing and the first considerable loss of mass which was approximately 3% occurred after 60 seconds of testing. After each step of this test, the SPS

samples were retreated with stearic acid solution and their CA, SA and CAH was re-measured. It was observed that for the samples exposed to the erosion test up to 60 second, the superhydrophobic characteristics would completely recover after retreatment by stearic acid solution. The SPS samples that were exposed to the erosion test for longer than 60 seconds did not recover their original wetting values after retreatment and the coatings would show reduced water mobility. This was due to physical removal of coating material and damage to the hierarchical micro-texture of the coatings.

SEM micrographs of the surface of the coating after 120, 300 and 600 seconds is demonstrated in Figure 6.7 (b), (c) and (d) consecutively. It can be seen in Figure 6.7 (b) that the cauliflower-like features of the coating are mainly removed in the initial stages of the coating erosion. Although at this point only around 20% of the mass of the coating has been removed, since the hierarchical micro-texture of the surface is lost, the coating cannot regain superhydrophobicity even after retreatment.
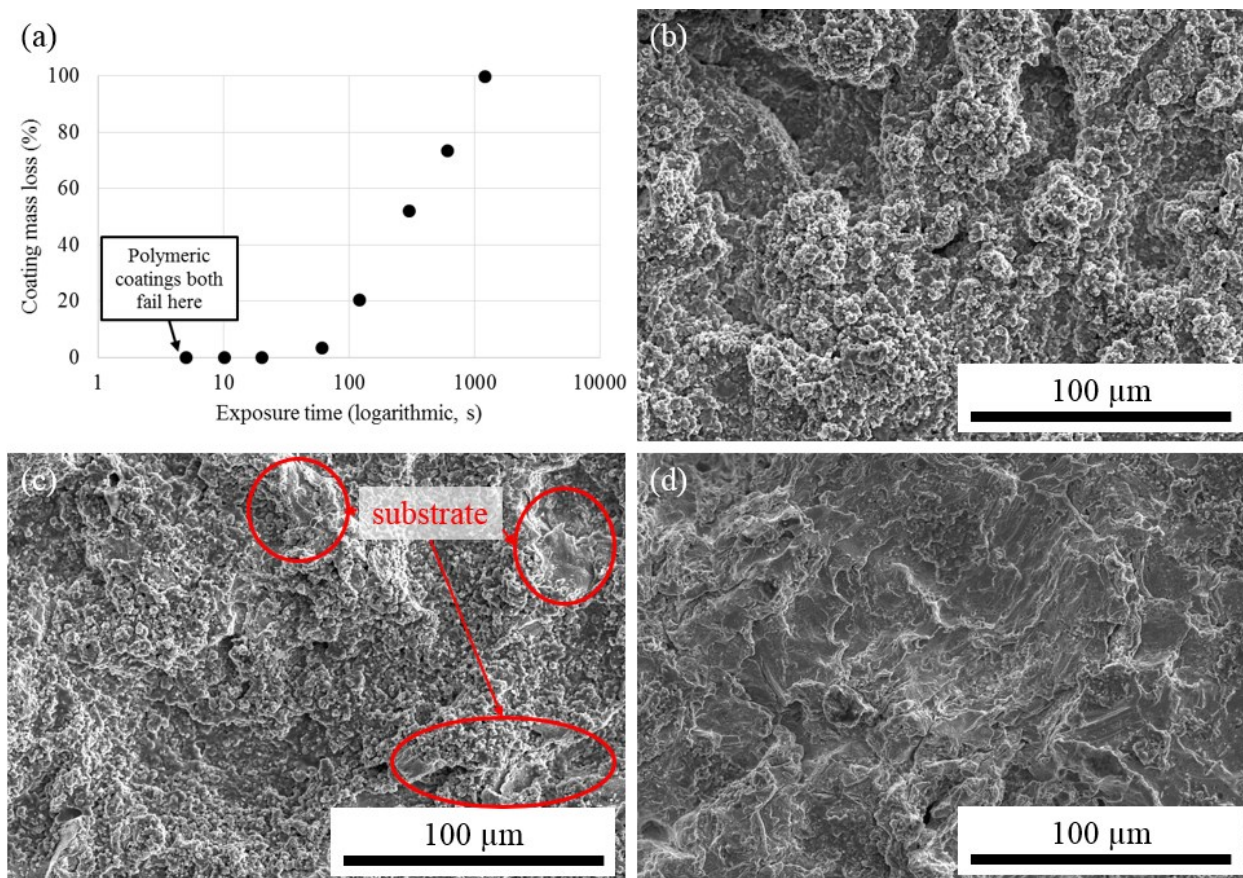
Figure 6.7. (a) Percent of coating material removed versus time in high intensity water erosion test. (b), (c) and (d) SEM micrographs of SPS coating after 120, 300 and 600 seconds, respectively.

In Figure 6.7 (c) it is observed that the bulk of the SPS coating is gradually removed and in some regions the steel substrate is visible after 300 seconds and more. In Figure 6.7 (d), mainly the substrate is visible and only small fractions of the coating material can be observed at some spots. As mentioned before the SPS coating remains almost completely intact after 20 seconds with the hierarchical micro-texture preserved and it loses only 3% of its mass after 60 seconds. On the other hand, complete failure of both commercial spray coatings occurs faster than the shortest testing duration which is 5 seconds. It can be concluded that the bulk of the SPS coating is at least an order of magnitude more resistance to water erosion in this test than the commercial superhydrophobic spray coatings.

6.3.2.4.   Icing/Deicing Cyclic Test

The last test was designed to evaluate the durability of the superhydrophobic coatings to repeated cycles of icing and deicing. As detailed in methodology section, this test involved forming ice on the surface of the coatings in the wind tunnel for the duration of one minute, then deicing and drying using a heat gun. This cycle was carried out in groups of ten repetitions after which the wetting characteristics of the coating were re-evaluated. Changes in the wetting characteristics of the coatings after exposure to multiple cycles of icing/deicing are demonstrated in Figure 6.8. It was observed that the superhydrophobic characteristics of the polymeric commercial coatings deteriorate quite rapidly after being exposed to multiple icing and deicing cycles. In fact, both NW and UED coatings show a quick drop in CA value and a sharp increase in SA and CA hysteresis after 10 icing/deicing cycles.

In contrast, the SPS superhydrophobic coating shows almost no significant deterioration of properties after 50 icing/deicing cycles. The main contributor to this significantly different behavior can be the fact that as water droplets freeze on the surface of the polymeric coatings, the change of volume of the ice causes damage to the surface of the relatively soft polymeric coatings. On the other hand, the SPS TiO_2 coating's micro-texture remains unaffected due to the higher hardness and stiffness of TiO_2.
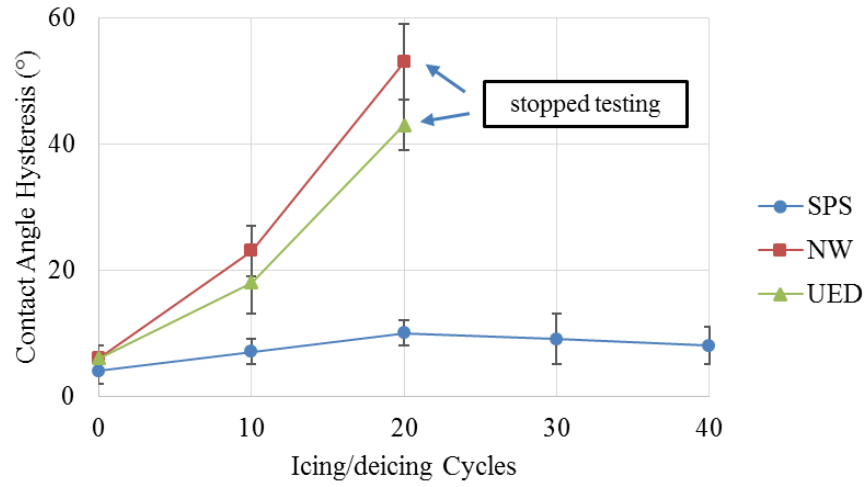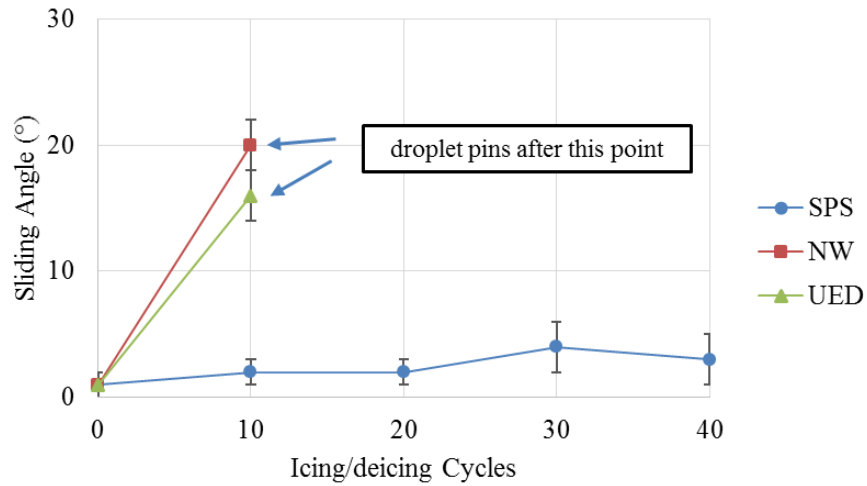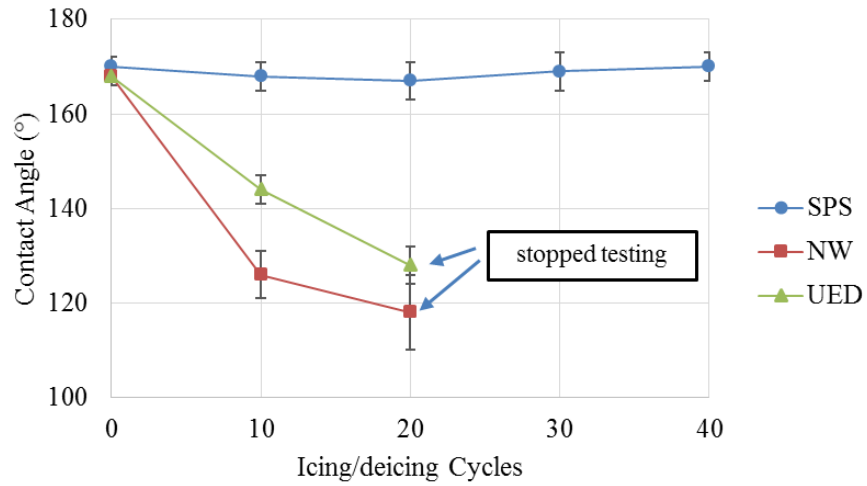
Figure 6.8. Change in SA and CAH of samples after multiple icing/deicing cycles [error bars represent standard deviation].

It was observed in the durability tests that the SPS coating is considerably more resistant to dry particle erosion and cyclic icing/deicing in comparison to both commercial superhydrophobic coatings. While in both of these tests the SPS coating preserves its superhydrophobic properties, the commercial coatings lose their properties and become sticky. Regarding the water erosion cloud-sized droplet test, it was demonstrated that the SPS coating performs similar to the NW commercial coatings while the UED commercial coating showed somewhat more resistance. However, it was demonstrated that the SPS coating has an advantage in terms of reparability. This is because the hierarchical micro-texture of the SPS TiO_2 remains intact and is at least an order of magnitude more erosion resistant compared to the bulk of the commercial coatings when tested in high intensity erosion resistance tests. As long as the hierarchical micro-textured TiO_2 is preserved, the coating can be simply re-treated with the stearic acid solution to regain its superhydrophobicity. This is in contrast to the commercial polymeric coating that if damaged, need to be completely removed, cleaned and recoated.

6.4. Summary and Conclusions

In this work, a superhydrophobic coating was prepared by suspension plasma spraying (SPS) of a TiO2 feedstock suspension onto grit-blasted substrates to generate a hierarchically micro-textured surface. The coating was then treated with a solution of stearic acid to lower its surface energy which resulted in superhydrophobic behavior with a contact angle (CA) as high as 170°, a sliding angle (SA) of 1° and a contact angle hysteresis of 4°. This coating was tested to evaluate its potential performance in mitigating in-flight icing under simulated icing conditions in a wind tunnel. The results are then compared to two different commercial, polymer-based superhydrophobic spray coatings. Additionally, since durability and especially erosion resistance are a major challenge in preparing superhydrophobic coatings for practical applications and more specifically anti-icing for aircraft; these coatings are tested for their erosion resistance and cyclic icing/deicing durability.

Regarding the icing tests, it is found that the SPS coatings has a positive effect in decreasing the ice accretion and its performance in this case is similar to the performance of commercial superhydrophobic coating. However, in terms of facilitating heated deicing using an electrical heater placed under the samples, the SPS coating decreases both the deicing time and the electrical power required to maintain an ice-free surface more than the commercial coatings. This is mainly

attributed to the fact that the commercial polymeric coatings are relatively thick and act as a barrier to heat transfer as opposed to the relatively thin SPS coating which significantly reduces this effect.

Regarding the durability tests, the SPS superhydrophobic coating demonstrated significantly better resistance to dry particle erosion compared to the two commercial coatings. This is due to the fact that the commercial polymer coatings are relatively soft and permit the sharp microscopic abrasive particles to penetrate into and adhere to the surface, causing a rapid deterioration of superhydrophobic behavior. On the other hand, the SPS coating is significantly more resistant to penetration and damage by abrasive particles due to the harder and stiffer TiO_2 ceramic. Furthermore, the SPS coatings also show significantly more durability after being exposed to multiple icing/deicing cycles. This considerable difference is once more attributed to the softer nature of polymer coatings compared to the harder and stiffer SPS TiO_2 coatings.

In terms of cloud-sized water droplet erosion, the SPS coating shows a behavior similar to one of the commercial coatings, the NeverWet (NW), while the other commercial coating, UltraEver Dry (UED) demonstrates slightly better resistance to water droplet erosion. However, it is very important to note that the SPS superhydrophobic coating present a potentially beneficial feature compared to both commercial coatings due to the fact that the hierarchical micro-texture and the bulk of the SPS coating remain intact after being exposed to extended water droplet erosion. This permits a quick and easy recovery of superhydrophobicity of the SPS coating using a simple retreatment with the stearic acid solution. This is in contrast to the commercial polymeric coating which, if damaged, requires complete removal, cleaning and recoating to be used again. The durability of the hierarchical micro-texture of the SPS TiO_2 is demonstrated through a high intensity water erosion test. In this test, the SPS coating was shown to be at least one order of magnitude more durable in intensive water erosion. The collection of the results and conclusions presented here suggest that the SPS superhydrophobic coatings could be a very efficient and rather durable candidate to be used for anti-icing protection on aircraft.

Acknowledgement

Chapter 7. Conclusions, Contributions and Recommendations

7.1. Summary and Conclusions

The main objective of this work was to develop a scalable and durable superhydrophobic coating using thermal spray process that could be used as an anti-icing application for aircraft and to mitigate the in-flight icing problem. The methodology of the research was based on the fact that a combination of a hierarchical micro-texture and a low surface energy is required to achieve superhydrophobicity. Thermal spray processes were selected as they operate in atmospheric conditions, are scalable and can be applied onto large surfaces, and are capable of depositing almost all engineering ceramics and metals.

Initially, the atmospheric plasma spray technique (APS) was used to deposit TiO_2 micro-textured coatings. The coatings were later treated by a stearic acid solution to lower their surface energy and making them hydrophobic. While all APS coatings demonstrated relatively high water repellency after treatment, all coatings showed low water mobility. Furthermore, it was demonstrated that relatively low deposition temperature (but still high enough to melt the particles) and relatively higher particle velocity contributed to increasing the hydrophobicity of the coatings. Despite relatively high water repellency, i.e. water contact angles as high as 141°, a water droplet would pin on their surface with limited water mobility. This was attributed to the relatively large and random roughness features resulted from the use of relatively large (typically between 10-100 μm in diameter) feedstock powder in the APS technique which caused coarse surface micro-texture. This surface was not efficient enough to create a superhydrophobic surface after treatment for lowering the surface energy. Consequently, in order to achieve finer micro-textures, the suspension plasma spray (SPS) technique was selected as an alternative.

The SPS coatings generated from both water-based and ethanol-based suspension feedstocks demonstrated significantly higher water mobility and consequently superhydrophobicity compared to the APS coatings. However, the coating generated using the

ethanol based suspension demonstrated even higher water repellence and mobility manifested through water contact angles higher than 165° and water sliding angle lower than 2°. SEM investigations revealed that the use ethanol-based suspension resulted in a coating that has two scales of surface roughness; a primary micron-sized and a secondary submicron-sized roughness. This hierarchical surface micro-texture was found to be the main reason for the high superhydrophobicity of this coating. Additionally, the water repelling behavior of the SPS coatings were compared to that of the lotus leaf as a natural superhydrophobic surface and a nano-grass superhydrophobic coating developed by researchers. The SPS coatings showed high water mobility in terms of having coefficient of restitutions comparable to that of the lotus leaf and the nano-grass coating.

Subsequently, a matrix of experiments was designed to study the effect of various parameters on morphology and superhydrophobicity of the SPS TiO_2 coatings. It was demonstrated that by carefully designing and controlling the process parameters, one can generate relatively fine and uniform dual-scale (hierarchical) surface textured coatings that after treatment for lowering their surface energy, show significantly improved water repellence and water mobility with water contact angles as high as 170° and sliding angles as low as 1.3°. Additionally it was shown that both scale levels of surface textures (i.e. micron-scale and nanoscale) are essential for having simultaneously improved water repellence and mobility.

Subsequently, the anti-icing and deicing performances and the durability of the superhydrophobic SPS coatings were studied and the results were then compared to two commercially available superhydrophobic polymeric spray coatings. Regarding the icing tests, it was found that the SPS coating decreases the ice accretion between 13 to 62 percent depending on the icing conditions. Moreover, in terms of facilitating heated deicing, the SPS coating decreases both the deicing time and the electrical power required to maintain an ice-free surface more compared to the commercially available spray-on coatings. This is mainly attributed to the fact that the commercial polymeric coating are relatively thick layers that act as a barrier to heat transfer as opposed to the relatively thin SPS coating which significantly reduce this effect.

Regarding the durability of the coating, the SPS superhydrophobic coating demonstrated significantly better resistance to dry particle erosion compared to the two commercial coatings. Furthermore, the SPS coatings also show significantly more durability after being exposed to multiple icing/deicing cycles. This considerable difference is once more attributed to the softer

nature of polymer coatings compared to the harder and stiffer SPS TiO$_2$ coatings. In terms of cloud-sized water droplet erosion, the SPS coating shows a behavior similar to one of the commercial coatings, the NeverWet (NW), while the other commercial coating, UltraEver Dry (UED) demonstrates slightly better resistance to cloud-sized water droplet erosion. However, it is very important to note that the SPS superhydrophobic coating presents a potentially beneficial feature compared to both commercial coatings due to the fact that the hierarchical micro-texture and the bulk of the SPS coating remains intact after being exposed to extended water droplet erosion. This permits a quick and easy recovery of superhydrophobicity of the SPS coating using a simple retreatment with the stearic acid solution. The durability of the hierarchical micro-texture of the SPS TiO$_2$ is demonstrated though a high intensity water erosion test. In this test the SPS coating is shown to be at least one order of magnitude more durable in intensive water erosion.

The collection of the results and conclusions presented here suggest that the SPS superhydrophobic coatings could be a very efficient and more durable candidate to be used for anti-icing protection on aircraft as commercial alternative coating solutions.

7.2. Contributions

The main contributions of this research can be summarized as follows.

- Hierarchically micro-textured TiO$_2$ coatings were developed using a suspension plasma spray (SPS) technique that, after treatment for lowering their surface energy, demonstrate superhydrophobicity with contact angles as high as 170°, sliding angles as low as 1° and contact angle hysteresis as low as 4°.

- A parametric study was used to optimize process parameters for controlling and engineering coating micro-texture and it was determined that having a finer pre-deposition surface roughness accompanied by optimized deposition conditions can result in uniform, fine and packed surface micro-texture features and consequently better water repellency and mobility.

- The developed SPS TiO$_2$ superhydrophobic coatings showed remarkable capability in reducing ice accretion, especially in the case of glaze ice which is considered the more dangerous type of ice. These coatings also required significantly reduced heating time and heat input to maintain an ice-free surface.

- The coatings showed significantly better resistance to dry particle erosion compared to commercial, polymer-based, superhydrophobic spray coatings.
- The coatings showed significantly better durability after being exposed to numerous icing/deicing cycles compared to commercial, polymer-based, superhydrophobic spray coatings.

7.3. Recommendations for future work

To build on the contributions and conclusions of this work for further improvement and potentially implementation of the superhydrophobic SPS coating for application in aircraft the following suggestions are presented.

- The significance of pre-deposition surface preparation was revealed in this work. Further study of various surface preparation techniques, especially techniques that enable more control and regularity is recommended. Based on the findings of this work, there may be a benefit in having a more uniform and controlled micro-texture on the substrate that permits accurate engineering of the location, uniformity and packing of surface micro-texture features which may lead to even better hierarchically textured superhydrophobic coatings.
- Although the stearic acid treatment already demonstrates desirable characteristics, its durability can still be improved, especially its resistance against cloud-sized droplet erosion. It is important that any alternative to this stearic acid treatment needs to be a very thin layer, as this is the key factor for the coating's significant resistance to dry particle erosion and icing/deicing cycles. As was demonstrated, a significantly thicker and softer alternative has potential drawback in this regards.
- All the coatings studied in this work were deposited on flat substrates. However for most potential applications in aircraft, the target surfaces are curved. It is important to optimize these coatings for curved surfaces as the surface curvature can potentially influence the micro-texture and characteristics of the SPS coatings significantly.
- There is an additional drawback of using flat samples in icing and deicing experiments as well. Flat samples disturb the aerodynamics of the test chamber of the wind tunnel and do not necessarily best represent the shape of an airfoil. Also,

in the case of an airfoil in icing conditions, the leading edge, which is the point of stagnating air flow, plays an important role in initiation and formation of ice. Therefore, it is highly recommended to study the performance of the superhydrophobic SPS coatings in both icing and deicing scenarios using an airfoil shape, or maybe even for more simplicity, cylindrical samples.

- The durability of SPS superhydrophobic coatings needs to be further studied in outdoor environment, exposure to UV and other potentially degrading factors.

References

[1]   Authority, Civil Aviation. "Aircraft icing handbook." Safety Education and Publishing Unit: New Zealand (2000): 2.

[2]   W.A. Cooper, W.R. Sand, M.K. Politovich, D.L. Veal, Effects of icing on performance of a research airplane, J. Aircr. 21 (1984) 708–715.

[3]   S. Green, A Study of U.S. Inflight Icing Accidents and Incidents, 1978 to 2002, in: 44th AIAA Aerosp. Sci. Meet. Exhib., American Institute of Aeronautics and Astronautics, (2006).

[4]   M.K. Politovich, Aircraft Icing Caused by Large Supercooled Droplets, J. Appl. Meteorol. 28 (1989) 856–868.

[5]   M.K. Politovich, Predicting In-Flight Aircraft Icing Intensity, J. Aircr. 40 (2003) 639–644.

[6]   P. Schultz, M.K. Politovich, Toward the Improvement of Aircraft-Icing Forecasts for the Continental United States, Weather Forecast. 7 (1992) 491–500.

[7]   P. Tourkine, M. Le Merrer, D. Quéré, Delayed freezing on water repellent materials, Langmuir. 25 (2009) 7214–7216.

[8]   T. Bharathidasan, S.V. Kumar, M.S. Bobji, R.P.S. Chakradhar, B.J. Basu, Effect of wettability and surface roughness on ice-adhesion strength of hydrophilic, hydrophobic and superhydrophobic surfaces, Appl. Surf. Sci. 314 (2014) 241–250.

[9]   E. Celia, T. Darmanin, E. Taffin de Givenchy, S. Amigoni, F.F.F. Guittard, Recent advances in designing superhydrophobic surfaces, J. Colloid Interface Sci. 402 (2013) 1–18.

[10]   Y.Y. Yan, N. Gao, W. Barthlott, Mimicking natural superhydrophobic surfaces and grasping the wetting process: a review on recent progress in preparing superhydrophobic surfaces., Adv. Colloid Interface Sci. 169 (2011) 80–105.

[11]   S.H. Kim, Fabrication of Superhydrophobic Surfaces, J. Adhes. Sci. Technol. 22 (2008) 235–250.

[12]   P. Zhang, F.Y. Lv, A review of the recent advances in superhydrophobic surfaces and the emerging energy-related applications, Energy. 82 (2015) 1068–1087.

[13] R. Rasmussen, C. Wade, A. Ramsay, D. Fleming, T. Lisi, R.K. Moore, et al., New ground deicing hazard associated with freezing drizzle ingestion by jet engines, J. Aircr. 43 (2006) 1448–1457.

[14] P. Appiah-Kubi, U.S Inflight Icing Accidents and Incidents, 2006 to 2010., The University of Tennessee, Knoxville, (2011).

[15] J. Hallett, G. Isaac, M. Politovich, D. Marcotte, A. Reehorst, C. Ryerson, Alliance Icing Research Study II (AIRS II) Science Plan, (2003).

[16] M. Bragg, G.M. Gregorek, J.D. Lee, Airfoil Aerodynamics in Icing Conditions, J. Aircr. 23 (1985) 76–81.

[17] A. Reehorst, J. Chung, M. Potapczuk, Y. Choo, Study of Icing Effects on Performance and Controllability of an Accident Aircraft, J. Aircr. 37 (2000).

[18] M.K. Politovich, Response of a research aircraft to icing and evaluation of severity indices, J. Aircr. 33 (1996) 291–297.

[19] J.C.T. Martin, The Adverse Aerodynamic Effects of Inflight Icing on Airplane Operation, Transp. Canada Aviat. Saf. Lett. 1 (2007) 17–22.

[20] Hazardous Weather Phenomena Airframe Icing, Bureau of Metheorology, Austrailian Government (2013).

[21] M.K. Politovich, Predicting Glaze or Rime Ice Growth on Airfoils, J. Aircr. 37 (2000) 117–122.

[22] Federal Aviation Administration (FAA), Pilot Guide: Flight in Icing Condition, U.S. Department of Transportation (2015).

[23] B. Robichaud, J. Mullock, The Weather of Atlantic Canada and Eastern Quebec Graphic Area Forecast 34, (2000).

[24] T. Cebeci, F. Kafyeke, Aircraft Icing, Annu. Rev. Fluid Mech. 35 (2003) 11–21.

[25] N. Czernkovich, Understanding in-flight icing, in: Transp. Canada Aviat. Saf. Semin., Citeseer, 2004: pp. 1–21.

[26] G. Mingione, M. Barocco, E. Denti, F.G. Bindi, Flight in Icing Condition, Tech. Rep., 1997.

[27]   S.G. Cober, G.A. Isaac, J.W. Strapp, Characterizations of Aircraft Icing Environments that Include Supercooled Large Drops, J. Appl. Meteorol. 40 (2001) 1984–2002.

[28]   M.B. Bragg, T. Basar, W.R. Perkins, M.S. Selig, P.G. Voulgaris, J.W. Melody, et al., Smart Icing Systems for Aircraft Icing Safety, AIAA Pap. 813 (2002).

[29]   A. Lampton, J. Valasek, Prediction of icing effects on the lateral/directional stability and control of light airplanes, Aerosp. Sci. Technol. 23 (2012) 305–311.

[30]   F. Caliskan, C. Hajiyev, A review of in-flight detection and identification of aircraft icing and reconfigurable control, Prog. Aerosp. Sci. 60 (2013) 12–34.

[31]   G.A. Isaac, S.G. Cober, J.W. Strapp, A.V. Korolev, A. Tremblay, D.L. Marcotte, Recent Canadian Research on Aircraft In-Flight Icing, Can. Aeronaut. Sp. J. 47 (2001) 213–221.

[32]   L. Cao, A.K. Jones, V.K. Sikka, J. Wu, D. Gao, Anti-Icing Superhydrophobic Coatings, Langmuir. 25 (2009) 12444–12448.

[33]   O. Parent, A. Ilinca, Anti-icing and de-icing techniques for wind turbines: Critical review, Cold Reg. Sci. Technol. 65 (2011) 88–96.

[34]   M. Mohammadi, D. De Pauw, M. Tembely, A. Dolatabadi, Droplet impact and solidification on hydrophilic and superhydrophobic substrates in icing conditions, in: 43rd Fluid Dyn. Conf., (2013): pp. 1–5.

[35]   S.A. Kulinich, M. Farzaneh, Ice adhesion on super-hydrophobic surfaces, Appl. Surf. Sci. 255 (2009) 8153–8157.

[36]   S.A. Kulinich, S. Farhadi, K. Nose, X.W. Du, Superhydrophobic surfaces: Are they really ice-repellent?, Langmuir. 27 (2011) 25–29.

[37]   S. Jung, M. Dorrestijn, D. Raps, A. Das, C.M. Megaridis, D. Poulikakos, Are superhydrophobic surfaces best for icephobicity?, Langmuir. 27 (2011) 3059–3066.

[38]   A. Milionis, E. Loth, I.S. Bayer, Recent advances in the mechanical durability of superhydrophobic materials, Adv. Colloid Interface Sci. 229 (2016) 57–79.

[39]   S. Wang, K. Liu, X. Yao, L. Jiang, Bioinspired surfaces with superwettability: New insight on theory, design, and applications, Chem. Rev. 115 (2015) 8230–8293.

[40] L. Yin, L. Zhu, Q. Wang, J. Ding, Q. Chen, Superhydrophobicity of natural and artificial surfaces under controlled condensation conditions, ACS Appl. Mater. Interfaces. 3 (2011) 1254–1260.

[41] X.-M. Li, D. Reinhoudt, M. Crego-Calama, What do we need for a superhydrophobic surface? A review on the recent progress in the preparation of superhydrophobic surfaces, Chem. Soc. Rev. 36 (2007) 1350–1368.

[42] T. Young, An Essay on the Cohesion of Fluids, Philos. Trans. R. Soc. London. 95 (1805) 65–87.

[43] R. Tadmor, Line energy and the relation between advancing, receding, and Young contact angles, Langmuir. 20 (2004) 7659–7664.

[44] E. Chibowski, K. Terpilowski, Surface free energy of sulfur-Revisited. I. Yellow and orange samples solidified against glass surface, J. Colloid Interface Sci. 319 (2008) 505–513.

[45] Y.T. Cheng, D.E. Rodak, Is the lotus leaf superhydrophobic?, Appl. Phys. Lett. 86 (2005) 1–3.

[46] C.W. Extrand, Criteria for ultralyophobic surfaces, Langmuir. 20 (2004) 5013–5018.

[47] D. Quéré, Non-sticking drops, Reports Prog. Phys. 68 (2005) 2495–2532.

[48] W. Chen, A.Y. Fadeev, M.C. Hsieh, D. Öner, J. Youngblood, T.J. McCarthy, Ultrahydrophobic and Ultralyophobic Surfaces: Some Comments and Examples, Langmuir. 15 (1999) 3395–3399.

[49] A. Accardo, F. Gentile, F. Mecarini, F. De Angelis, M. Burghammer, E. Di Fabrizio, et al., Ultrahydrophobic PMMA micro- and nano-textured surfaces fabricated by optical lithography and plasma etching for X-ray diffraction studies, Microelectron. Eng. 88 (2011) 1660–1663.

[50] M. Callies, D. Quéré, On water repellency, Soft Matter. 1 (2005) 55.

[51] S. Anand, A.T. Paxson, R. Dhiman, J.D. Smith, K.K. Varanasi, Enhanced Condensation on Lubricant- Impregnated Nanotextured Surfaces, ACS Nano. 6 (2012) 10122–10129.

[52] S. Wang, L. Jiang, Definition of Superhydrophobic States, Adv. Mater. 19 (2007) 3423–3424.

[53] P.J. Graham, M.M. Farhangi, A. Dolatabadi, Dynamics of droplet coalescence in response to increasing hydrophobicity, Phys. Fluids. 24 (2012).

[54] D. Richard, C. Clanet, D. Quéré, Surface phenomena: Contact time of a bouncing drop, Nature. 417 (2002) 811–811.

[55] J.C. Bird, R. Dhiman, H.M. Kwon, K.K. Varanasi, Reducing the contact time of a bouncing drop, Nature. 503 (2013) 385–388.

[56] K.H. Hunt, F.R.E. Crossley, Coefficient of Restitution Interpreted as Damping in Vibroimpact, J. Appl. Mech. 42 (1975) 440.

[57] D. Richard, D. Quéré, Bouncing water drops, Europhys. Lett. 50 (2000) 769–775.

[58] X. Li, X. Ma, Z. Lan, Dynamic behavior of the water droplet impact on a textured hydrophobic/superhydrophobic surface: The effect of the remaining liquid film arising on the pillars' tops on the contact time, Langmuir. 26 (2010) 4831–4838.

[59] Y.C. Jung, B. Bhushan, Y.C. Jung, B. Bhushan, Dynamic Effects of Bouncing Water Droplets on Superhydrophobic Surfaces Dynamic Effects of Bouncing Water Droplets on Superhydrophobic, (2008) 6262–6269.

[60] Z. Wang, C. Lopez, A. Hirsa, N. Koratkar, Impact dynamics and rebound of water droplets on superhydrophobic carbon nanotube arrays, Appl. Phys. Lett. 91 (2007) 2005–2008.

[61] Y.H. Yeong, J. Burton, E. Loth, I.S. Bayer, Drop Impact and Rebound Dynamics on an Inclined Superhydrophobic Surface, Langmuir. 30 (2014) 12027–12038.

[62] G. Fang, A. Amirfazli, Understanding the anti-icing behavior of superhydrophobic surfaces, Surf. Innov. 2 (2014) 94–102.

[63] C. Volat, M. Farzaneh, A. Leblond, De-icing / Anti-icing Techniques for Power Lines: Current Methods and Future Direction, 11 Th Int. Work. Atmos. Icing Struct. (2005).

[64] S. Farhadi, M. Farzaneh, S.A.A. Kulinich, Anti-icing performance of superhydrophobic surfaces, Appl. Surf. Sci. 257 (2011) 6264–6269.

[65] R. Blossey, Self-cleaning surfaces — virtual realities, Nat. Mater. 2 (2003) 301–306.

[66] R. Fürstner, W. Barthlott, C. Neinhuis, P. Walzel, Wetting and self-cleaning properties of

artificial superhydrophobic surfaces, Langmuir. 21 (2005) 956–961.

[67]   B. Bhushan, Y.C. Jung, K. Koch, Self-cleaning efficiency of artificial superhydrophobic surfaces, Langmuir. 25 (2009) 3240–3248.

[68]   R.J. Daniello, N.E. Waterhouse, J.P. Rothstein, Drag reduction in turbulent flows over superhydrophobic surfaces, Phys. Fluids. 21 (2009).

[69]   C. Lee, C.J. Kim, Underwater restoration and retention of gases on superhydrophobic surfaces for drag reduction, Phys. Rev. Lett. 106 (2011) 1–4.

[70]   G. McHale, M.I. Newton, N.J. Shirtcliffe, Immersed superhydrophobic surfaces: Gas exchange, slip and drag reduction properties, Soft Matter. 6 (2010) 714–719.

[71]   N. Wang, D. Xiong, Y. Deng, Y. Shi, K. Wang, Mechanically robust superhydrophobic steel surface with anti-icing, UV-durability, and corrosion resistance properties, ACS Appl. Mater. Interfaces. 7 (2015) 6260–6272.

[72]   S.S. Latthe, P. Sudhagar, A. Devadoss, A.M. Kumar, S. Liu, C. Terashima, et al., A mechanically bendable superhydrophobic steel surface with self-cleaning and corrosion-resistant properties, J. Mater. Chem. A. 3 (2015) 14263–14271.

[73]   X. Chen, J. Yuan, J. Huang, K. Ren, Y. Liu, S. Lu, et al., Large-scale fabrication of superhydrophobic polyurethane/nano-Al2O3 coatings by suspension flame spraying for anti-corrosion applications, Appl. Surf. Sci. 311 (2014) 864–869.

[74]   B. Bhushan, Y.C. Jung, K. Koch, Micro-, nano- and hierarchical structures for superhydrophobicity, self-cleaning and low adhesion., Philos. Trans. A. Math. Phys. Eng. Sci. 367 (2009) 1631–1672.

[75]   W. Barthlott, C. Neinhuis, Purity of the sacred lotus, or escape from contamination in biological surfaces, Planta. 202 (1997) 1–8.

[76]   T. Darmanin, F. Guittard, Superhydrophobic and superoleophobic properties in nature, Mater. Today. 18 (2015) 273–285.

[77]   Z. Guo, W. Liu, Biomimic from the superhydrophobic plant leaves in nature: Binary structure and unitary structure, Plant Sci. 172 (2007) 1103–1112.

[78]   K. Koch, B. Bhushan, W. Barthlott, Diversity of structure, morphology and wetting of plant

surfaces, Soft Matter. 4 (2008) 1943.

[79] Y. Zheng, X. Gao, L. Jiang, Directional adhesion of superhydrophobic butterfly wings, Soft Matter. 3 (2007) 178–182.

[80] M. Nosonovsky, B. Bhushan, Multiscale Dissipative Mechanisms and Hierarchical Surfaces, Springer (2008).

[81] R.N. Wenzel, Resistance of solid surfaces to wetting by water., J. Ind. Eng. Chem. (Washington, D. C.). 28 (1936) 988–994.

[82] A.B.D. Cassie, S. Baxter, B.D. Cassie, Wettability of porous surfaces, Trans. Faraday Soc. 40 (1944) 546–551.

[83] M. Nosonovsky, B. Bhushan, Patterned Nonadhesive surfaces: Superhydrophobicity and wetting regime transitions, Langmuir. 24 (2008) 1525–1533.

[84] P. Roach, N.J. Shirtcliffe, M.I. Newton, Progess in superhydrophobic surface development, Soft Matter. 4 (2008) 224.

[85] L. Barbieri, E. Wagner, P. Hoffmann, Water wetting transition parameters of perfluorinated substrates with periodically distributed flat-top microscale obstacles, Langmuir. 23 (2007) 1723–1734.

[86] Y.C. Jung, B. Bhushan, Wetting behaviour during evaporation and condensation of water microdroplets on superhydrophobic patterned surfaces, J. Microsc. 229 (2008) 127–140.

[87] B. Bhushan, Y. Chae Jung, Wetting study of patterned surfaces for superhydrophobicity, Ultramicroscopy. 107 (2007) 1033–1041.

[88] B. Bhushan, M. Nosonovsky, Y.C. Jung, Towards optimization of patterned superhydrophobic surfaces, J. R. Soc. Interface. 4 (2007) 643–648.

[89] Y.C. Jung, B. Bhushan, Wetting transition of water droplets on superhydrophobic patterned surfaces, Scr. Mater. 57 (2007) 1057–1060.

[90] S.S. Latthe, C. Terashima, K. Nakata, A. Fujishima, Superhydrophobic Surfaces Developed by Mimicking Hierarchical Surface Morphology of Lotus Leaf, Molecules. 19 (2014).

[91] D. Öner, T.J. McCarthy, Ultrahydrophobic surfaces. Effects of topography length scales on

wettability, Langmuir. 16 (2000) 7777–7782.

[92] C. Yang, U. Tartaglino, B.N.J. Persson, Influence of Surface Roughness on Superhydrophobicity, Phys. Rev. Lett. 97 (2006) 116103.

[93] J.B. Boreyko, C.H. Baker, C.R. Poley, C.H. Chen, Wetting and dewetting transitions on hierarchical superhydrophobic surfaces, Langmuir. 27 (2011) 7502–7509.

[94] K. Koch, B. Bhushan, W. Barthlott, Multifunctional surface structures of plants: An inspiration for biomimetics, Prog. Mater. Sci. 54 (2009) 137–178.

[95] K. Koch, B. Bhushan, Y.C. Jung, W. Barthlott, Fabrication of artificial Lotus leaves and significance of hierarchical structure for superhydrophobicity and low adhesion, Soft Matter. 5 (2009) 1386.

[96] B. Bhushan, Y.C. Jung, Wetting, adhesion and friction of superhydrophobic and hydrophilic leaves and fabricated micro/nanopatterned surfaces, J. Phys. Condens. Matter. 20 (2008) 225010–24.

[97] M. Ma, R.M. Hill, Superhydrophobic surfaces, Curr. Opin. Colloid Interface Sci. 11 (2006) 193–202.

[98] Z. Guo, W. Liu, B.L. Su, Superhydrophobic surfaces: From natural to biomimetic to functional, J. Colloid Interface Sci. 353 (2011) 335–355.

[99] T.M. Schutzius, S. Jung, T. Maitra, P. Eberle, C. Antonini, C. Stamatopoulos, et al., Physics of icing and rational design of surfaces with extraordinary icephobicity, Langmuir. 31 (2015) 4807–4821.

[100] P. Guo, Y. Zheng, M. Wen, C. Song, Y. Lin, L. Jiang, Icephobic/anti-icing properties of micro/nanostructured surfaces, Adv. Mater. 24 (2012) 2642–2648.

[101] Y. Wang, J. Xue, Q. Wang, Q. Chen, J. Ding, Verification of icephobic/anti-icing properties of a superhydrophobic surface, ACS Appl. Mater. Interfaces. 5 (2013) 3370–3381.

[102] M. Ruan, W. Li, B. Wang, B. Deng, F. Ma, Z. Yu, Preparation and anti-icing behavior of superhydrophobic surfaces on aluminum alloy substrates, Langmuir. 29 (2013) 8482–8491.

[103] L.B. Boinovich, A.M. Emelyanenko, Anti-icing potential of superhydrophobic coatings, Mendeleev Commun. 23 (2013) 3–10.

[104] Z. Sun, T. Liao, K. Liu, L. Jiang, J.H. Kim, S.X. Dou, Fly-eye inspired superhydrophobic anti-fogging inorganic nanostructures, Small. 10 (2014) 3001–3006.

[105] Z.C. Yuekun Lai, Yuxin Tang, Jiaojiao Gong, Dangguo Gong, Lifeng Chi, Changjian Lin, Transparent superhydrophobic/superhydrophilic TiO$_2$- based coatings for self-cleaning and anti- fogging, J. Mater. Chem. 22 (2012) 7420–7426.

[106] P. Varshney, S. Mohapatra, A. Kumar, Fabrication of Mechanically Stable Superhydrophobic Aluminium Surface with Excellent Self-Cleaning and Anti-Fogging Properties, Biomimetics. 2 (2017) 2.

[107] Y.T. Cheng, D.E. Rodak, Y. Chen, Y. Zhang, L. Shi, J. Li, et al., Transparent superhydrophobic/superhydrophilic coatings for self-cleaning and anti-fogging, Appl. Phys. Lett. 101 (2012) 33701.

[108] P. Varshney, J. Lomga, P.K. Gupta, S.S. Mohapatra, A. Kumar, Durable and regenerable superhydrophobic coatings for aluminium surfaces with excellent self-cleaning and anti-fogging properties, Tribol. Int. 119 (2018) 38–44.

[109] T. Son, E. Yang, E. Yu, K.H. Oh, M.W. Moon, H.Y. Kim, Effects of surface nanostructures on self-cleaning and anti-fogging characteristics of transparent glass, J. Mech. Sci. Technol. 31 (2017) 5407–5414.

[110] H. Liu, S. Szunerits, W. Xu, R. Boukherroub, Preparation of superhydrophobic coatings on zinc as effective corrosion barriers, ACS Appl. Mater. Interfaces. 1 (2009) 1150–1153.

[111] A.V. Rao, S.S. Latthe, S.A. Mahadik, C. Kappenstein, Mechanically stable and corrosion resistant superhydrophobic sol-gel coatings on copper substrate, Appl. Surf. Sci. 257 (2011) 5772–5776.

[112] F. Zhang, L. Zhao, H. Chen, S. Xu, D.G. Evans, X. Duan, Corrosion resistance of superhydrophobic layered double hydroxide films on aluminum, Angew. Chemie - Int. Ed. 47 (2008) 2466–2469.

[113] Z. Wang, Y. Su, Q. Li, Y. Liu, Z. She, F. Chen, et al., Researching a highly anti-corrosion superhydrophobic film fabricated on AZ91D magnesium alloy and its anti-bacteria adhesion effect, Mater. Charact. 99 (2015) 200–209.

[114] L. Feng, Z. Zhang, Z. Mai, Y. Ma, B. Liu, L. Jiang, et al., A super-hydrophobic and super-oleophilic coating mesh film for the separation of oil and water, Angew. Chemie - Int. Ed. 43 (2004) 2012–2014.

[115] C. Wang, T. Yao, J. Wu, C. Ma, Z. Fan, Z. Wang, et al., Facile Approach in Fabricating Superhydrophobic and Superoleophilic Surface for Water and Oil Mixture Separation, Appl. Mater. Interfaces. 1 (2009) 2613–2617.

[116] A. Li, H.-X. Sun, D.-Z. Tan, W.-J. Fan, S.-H. Wen, X.-J. Qing, et al., Superhydrophobic conjugated microporous polymers for separation and adsorption, Energy Environ. Sci. 4 (2011) 2062.

[117] T. Min, J. Kim, Effects of hydrophobic surface on skin-friction drag, Phys. Fluids. 16 (2004) L55–L58.

[118] Y.C. Jung, B. Bhushan, Mechanically durable carbon nanotube - Composite hierarchical structures with superhydrophobicity, self-cleaning, and low-drag, ACS Nano. 3 (2009) 4155–4163.

[119] C.H. Choi, U. Ulmanella, J. Kim, C.M. Ho, C.J. Kim, Effective slip and friction reduction in nanograted superhydrophobic microchannels, Phys. Fluids. 18 (2006).

[120] J.B. Boreyko, C.H. Chen, Self-propelled dropwise condensate on superhydrophobic surfaces, Phys. Rev. Lett. 103 (2009).

[121] C. Chen, Q. Cai, C. Tsai, C.-L. Chen, G. Xiong, Y. Yu, et al., Dropwise condensation on superhydrophobic surfaces with two-tier roughness, Appl. Phys. Lett. 90 (2007) 1–4.

[122] N. Miljkovic, R. Enright, E.N. Wang, Effect of droplet morphology on growth dynamics and heat transfer during condensation on superhydrophobic nanostructured surfaces, ACS Nano. 6 (2012) 1776–1785.

[123] T. Sun, H. Tan, D. Han, Q. Fu, L. Jiang, No platelet can adhere-largely improved blood compatibility on nanostructured superhydrophobic surfaces, Small. 1 (2005) 959–963.

[124] A.C. Lima, J.F. Mano, Micro/nano-structured superhydrophobic surfaces in the biomedical field: part II: applications overview., Nanomedicine (Lond). 10 (2015) 271–97.

[125] L. Zhai, M.C. Berg, F.Ç. Cebeci, Y. Kim, J.M. Milwid, M.F. Rubner, et al., Patterned

superhydrophobic surfaces: Toward a synthetic mimic of the namib desert beetle, Nano Lett. 6 (2006) 1213–1217.

[126] V. Mortazavi, M.M. Khonsari, On the degradation of superhydrophobic surfaces: A review, Wear. 372–373 (2017) 145–157.

[127] M.J. Kreder, J. Alvarenga, P. Kim, J. Aizenberg, Design of anti-icing surfaces: smooth, textured or slippery?, Nat. Rev. Mater. 1 (2016) 15003.

[128] R.S. Lima, B.R. Marple, Thermal spray coatings engineered from nanostructured ceramic agglomerated powders for structural, thermal barrier and biomedical applications: A review, J. Therm. Spray Technol. 16 (2007) 40–63.

[129] J.Y. Shiu, C.W. Kuo, P. Chen, C.Y. Mou, Fabrication of Tunable Superhydrophobic Surfaces by Nanosphere Lithography, Chem. Mater. 16 (2004) 561–564.

[130] A. Pozzato, S.D. Zilio, G. Fois, D. Vendramin, G. Mistura, M. Belotti, et al., Superhydrophobic surfaces fabricated by nanoimprint lithography, Microelectron. Eng. 83 (2006) 884–888.

[131] B. Qian, Z. Shen, Fabrication of superhydrophobic surfaces by dislocation-selective chemical etching on aluminum, copper, and zinc substrates, Langmuir. 21 (2005) 9007–9009.

[132] Y. Xiu, L. Zhu, D.W. Hess, C.P. Wong, Hierarchical silicon etched structures for controlled hydrophobicity/ superhydrophobicity, Nano Lett. 7 (2007) 3388–3393.

[133] A. Hozumi, O. Takai, Preparation of ultra water-repellent films by microwave plasma-enhanced CVD, Thin Solid Films. 303 (1997) 222–225.

[134] C.R. Crick, I.P. Parkin, CVD of copper and copper oxide thin films via the in situ reduction of copper(ii) nitrate—a route to conformal superhydrophobic coatings, J. Mater. Chem. 21 (2011) 14712.

[135] L. Wang, S. Guo, X. Hu, S. Dong, Facile electrochemical approach to fabricate hierarchical flowerlike gold microstructures: Electrodeposited superhydrophobic surface, Electrochem. Commun. 10 (2008) 95–99.

[136] M. Manca, A. Cannavale, L. De Marco, A.S. Aricò, R. Cingolani, G. Gigli, Durable

superhydrophobic and antireflective surfaces by trimethylsilanized silica nanoparticles-based sol-gel processing, Langmuir. 25 (2009) 6357–6362.

[137] Y. Li, F. Liu, J. Sun, A facile layer-by-layer deposition process for the fabrication of highly transparent superhydrophobic coatings, Chem. Commun. (2009) 2730.

[138] X. Song, J. Zhai, Y. Wang, L. Jiang, Fabrication of superhydrophobic surfaces by self-assembly and their water-adhesion properties, J. Phys. Chem. B. 109 (2005) 4048–4052.

[139] T. Baldacchini, J.E. Carey, M. Zhou, E. Mazur, Superhydrophobic surfaces prepared by microstructuring of silicon using a femtosecond laser, Langmuir. 22 (2006) 4917–4919.

[140] B. Wu, M. Zhou, J. Li, X. Ye, G. Li, L. Cai, Superhydrophobic surfaces fabricated by microstructuring of stainless steel using a femtosecond laser, Appl. Surf. Sci. 256 (2009) 61–66.

[141] E. Fadeeva, V.K. Truong, M. Stiesch, B.N. Chichkov, R.J. Crawford, J. Wang, et al., Bacterial retention on superhydrophobic titanium surfaces fabricated by femtosecond laser ablation, Langmuir. 27 (2011) 3012–3019.

[142] I.-K. Oh, K. Kim, Z. Lee, K.Y. Ko, C.-W. Lee, S.J. Lee, et al., Hydrophobicity of Rare Earth Oxides Grown by Atomic Layer Deposition, Chem. Mater. 27 (2014) 148–156.

[143] S. Zenkin, Š. Kos, J. Musil, Hydrophobicity of thin films of compounds of low-electronegativity metals, J. Am. Ceram. Soc. 2717 (2014) 2713–2717.

[144] F. Pedraza, S.A. Mahadik, B. Bouchaud, Synthesis of ceria based superhydrophobic coating on Ni20Cr substrate via cathodic electrodeposition, Phys. Chem. Chem. Phys. 17 (2015) 31750–31757.

[145] E. Külah, L. Marot, R. Steiner, A. Romanyuk, T.A. Jung, A. Wäckerlin, et al., Surface chemistry of rare-earth oxide surfaces at ambient conditions: reactions with water and hydrocarbons, Sci. Rep. 7 (2017) 43369.

[146] R. Lundy, C. Byrne, J. Bogan, K. Nolan, M.N. Collins, E. Dalton, et al., Exploring the Role of Adsorption and Surface State on the Hydrophobicity of Rare Earth Oxides, ACS Appl. Mater. Interfaces. 9 (2017) 13751–13760.

[147] N.J. Lawrence, K. Jiang, C.L. Cheung, Formation of a porous cerium oxide membrane by

anodization., Chem. Commun. (Camb). 47 (2011) 2703–2705.

[148] L. Martínez, E. Román, J.L. de Segovia, S. Poupard, J. Creus, F. Pedraza, Surface study of cerium oxide based coatings obtained by cathodic electrodeposition on zinc, Appl. Surf. Sci. 257 (2011) 6202–6207.

[149] G. Azimi, R. Dhiman, H.-M. Kwon, A.T. Paxson, K.K. Varanasi, Hydrophobicity of rare-earth oxide ceramics, Nat. Mater. 12 (2013) 315–20.

[150] D.J. Preston, N. Miljkovic, J. Sack, R. Enright, J. Queeney, E.N. Wang, Effect of Hydrocarbon Adsorption on the Wettability of Rare Earth Oxide Ceramics, Appl. Phys. Lett. 105 (2014) 11601.

[151] S. Khan, G. Azimi, B. Yildiz, K.K. Varanasi, Role of surface oxygen-to-metal ratio on the wettability of rare-earth oxides, Appl. Phys. Lett. 106 (2015) 61601.

[152] L. Mishchenko, B. Hatton, V. Bahadur, J.A. Taylor, T. Krupenkin, J. Aizenberg, Design of ice-free nanostructured surfaces based on repulsion of impacting water droplets, ACS Nano. 4 (2010) 7699–7707.

[153] H. Wang, G. He, Q. Tian, Effects of nano-fluorocarbon coating on icing, Appl. Surf. Sci. 258 (2012) 7219–7224.

[154] R. Liao, Z. Zuo, C. Guo, Y. Yuan, A. Zhuang, Fabrication of superhydrophobic surface on aluminum by continuous chemical etching and its anti-icing property, Appl. Surf. Sci. 317 (2014) 701–709.

[155] F. Arianpour, M. Farzaneh, S.A. Kulinich, Hydrophobic and ice-retarding properties of doped silicone rubber coatings, Appl. Surf. Sci. 265 (2013) 546–552.

[156] X. Li, Y. Zhao, H. Li, X. Yuan, Preparation and icephobic properties of polymethyltrifluoropropylsiloxane-polyacrylate block copolymers, Appl. Surf. Sci. 316 (2014) 222–231.

[157] L. Zhu, J. Xue, Y. Wang, Q. Chen, J. Ding, Q. Wang, Ice-phobic coatings based on silicon-oil-infused polydimethylsiloxane, ACS Appl. Mater. Interfaces. 5 (2013) 4053–4062.

[158] H. Sojoudi, G.H. McKinley, K.K. Gleason, Linker-free grafting of fluorinated polymeric cross-linked network bilayers for durable reduction of ice adhesion, Mater. Horiz. 2 (2015)

91–99.

[159] M. Susoff, K. Siegmann, C. Pfaffenroth, M. Hirayama, Evaluation of icephobic coatings - Screening of different coatings and influence of roughness, Appl. Surf. Sci. 282 (2013) 870–879.

[160] K.K. Varanasi, T. Deng, J.D. Smith, M. Hsu, N. Bhate, Frost formation and ice adhesion on superhydrophobic surfaces, Appl. Phys. Lett. 97 (2010) 234102.

[161] S. Yang, Q. Xia, L. Zhu, J. Xue, Q. Wang, Q.M. Chen, Research on the icephobic properties of fluoropolymer-based materials, Appl. Surf. Sci. 257 (2011) 4956–4962.

[162] T. Wang, Y. Zheng, A.R.O. Raji, Y. Li, W.K.A. Sikkema, J.M. Tour, Passive Anti-Icing and Active Deicing Films, ACS Appl. Mater. Interfaces. 8 (2016) 14169–14173.

[163] P. Fauchais, M. Vardelle, A. Vardelle, L. Bianchi, Plasma spray: Study of the coating generation, Ceram. Int. 22 (1996) 295–303.

[164] J.R. Davis, Handbook pf Thermal Spray Technology, ASM International, (2004).

[165] P. Fauchais, Understanding plasma spraying, J. Phys. D. Appl. Phys. 37 (2004) R86–R108.

[166] P.L. Fauchais, J.V.R. Heberlein, M.I. Boulos, Thermal Spray Fundamentals, (2014).

[167] H. Herman, S. Sampath, R. McCune, Thermal spray: Current status and future trends, MRS Bull. 25 (2000) 17–25.

[168] A. Feuerstein, J. Knapp, T. Taylor, A. Ashary, A. Bolcavage, N. Hitchman, Technical and economical aspects of current thermal barrier coating systems for gas turbine engines by thermal spray and EBPVD: A review, J. Therm. Spray Technol. 17 (2008) 199–213.

[169] W. Beele, G. Marijnissen, A. van Lieshout, The evolution of thermal barrier coatings — status and upcoming solutions for today's key issues, Surf. Coatings Technol. 120–121 (1999) 61–67.

[170] P. Fauchais, M. Vardelle, S. Goutier, Latest Researches Advances of Plasma Spraying: From Splat to Coating Formation, J. Therm. Spray Technol. 25 (2016) 1534–1553.

[171] A. Vardelle, C. Moreau, N.J. Themelis, C. Chazelas, A Perspective on Plasma Spray Technology, Plasma Chem. Plasma Process. 35 (2014) 491–509.

[172] A. Vardelle, C. Moreau, J. Akedo, H. Ashrafizadeh, C.C. Berndt, J.O. Berghaus, et al., The 2016 Thermal Spray Roadmap, J. Therm. Spray Technol. 25 (2016) 1376–1440.

[173] P. Fauchais, G. Montavon, Latest developments in suspension and liquid precursor thermal spraying, in: J. Therm. Spray Technol., 2010: pp. 226–239.

[174] P. Sokołowski, S. Kozerski, L. Pawłowski, A. Ambroziak, The key process parameters influencing formation of columnar microstructure in suspension plasma sprayed zirconia coatings, Surf. Coatings Technol. 260 (2014) 97–106.

[175] P. Fauchais, R. Etchart-Salas, C. Delbos, M. Tognonvi, V. Rat, J.F. Coudert, et al., Suspension and solution plasma spraying of finely structured layers: potential application to SOFCs, J. Phys. D. Appl. Phys. 40 (2007) 2394–2406.

[176] P. Fauchais, R. Etchart-Salas, V. Rat, J.F. Coudert, N. Caron, K. Wittmann-Ténèze, Parameters controlling liquid plasma spraying: Solutions, sols, or suspensions, J. Therm. Spray Technol. 17 (2008) 31–59.

[177] C.-J. Li, G.-J. Yang, C.-X. Li, Development of the particle interface bonding in thermal spray coatings for expanding high performance applications, Int. Therm. Spray Conf. Expo. - Air, Land, Water Hum. Body Therm. Spray Sci. Appl. ITSC 2012. (2012) 47–57.

[178] N. Curry, K. VanEvery, T. Snyder, J. Susnjar, S. Bjorklund, Performance Testing of Suspension Plasma Sprayed Thermal Barrier Coatings Produced with Varied Suspension Parameters, Coatings. 5 (2015) 338–356.

[179] F. Ben Ettouil, A. Denoirjean, A. Grimaud, G. Montavon, P. Fauchais, Sub-micrometer-sized Y-PSZ thermal barrier coatings manufactured by suspension plasma spraying: process, structure and some functional properties, 3rd Int. Work. Adv. Ceram. (2008).

[180] K. VanEvery, M.J.M. Krane, R.W. Trice, Parametric study of suspension plasma spray processing parameters on coating microstructures manufactured from nanoscale yttria-stabilized zirconia, Surf. Coatings Technol. 206 (2012) 2464–2473.

[181] M. Harju, E. Levänen, T. Mäntylä, Wetting behaviour of plasma sprayed oxide coatings, Appl. Surf. Sci. 252 (2006) 8514–8520.

[182] H. Teisala, M. Tuominen, M. Aromaa, J.M. Mäkelä, M. Stepien, J.J. Saarinen, et al.,

Development of superhydrophobic coating on paperboard surface using the Liquid Flame Spray, Surf. Coatings Technol. 205 (2010) 436–445.

[183] V. Eigenbrod, C. Hensch, H. Pulker, Superhydrophobic Coatings for Technical Applications, Vak. Forsch. Und Prax. 23 (2011) 24–27.

[184] C. Zhang, R.Q. Guo, Y. Yang, Y. Wu, L. Liu, Influence of the size of spraying powders on the microstructure and corrosion resistance of Fe-based amorphous coating, Electrochim. Acta. 56 (2011) 6380–6388.

[185] Z. Li, Y. Zheng, J. Zhao, L. Cui, Wettability of atmospheric plasma sprayed Fe, Ni, Cr and their mixture coatings, J. Therm. Spray Technol. 21 (2012) 255–262.

[186] C.-J. Li, Preparation and Characterization of Super-Hydrophobic Surface Through Particle Deposition by Vacuum Cold Spray, in: Int. Therm. Spray Conf. Expo., ASM, (2012).

[187] M.M. Gentleman, J.A. Ruud, M.L. Blohm, M. Manoharan, Wetting resistant materials and articles made therewith, U.S. Patent No. 7,897,271. (2013).

[188] Y. Cai, T.W. Coyle, G. Azimi, J. Mostaghimi, Superhydrophobic Ceramic Coatings by Solution Precursor Plasma Spray, Sci. Rep. 6 (2016) 24670.

[189] L.S. Leblanc, J.A. Ruud, K.P. Mcevoy, A.J. Kulkarni, Methods of coating a surface and articles with coated surface, U.S. Patent Application No. 13/723,301 (2014).

[190] R. a. Bidkar, L. Leblanc, A.J. Kulkarni, V. Bahadur, S.L. Ceccio, M. Perlin, Skin-friction drag reduction in the turbulent regime using random-textured hydrophobic surfaces, Phys. Fluids. 26 (2014) 85108.

[191] H. Koivuluoto, C. Stenroos, M. Kylmälahti, M. Apostol, J. Kiilakoski, P. Vuoristo, Anti-icing Behavior of Thermally Sprayed Polymer Coatings, J. Therm. Spray Technol. (2016).

[192] X. Chen, Y. Gong, D. Li, H. Li, Robust and easy-repairable superhydrophobic surfaces with multiple length-scale topography constructed by thermal spray route, Colloids Surfaces A Physicochem. Eng. Asp. 492 (2016) 19–25.

[193] A. Lafuma, D. Quéré, Superhydrophobic states, Nat. Mater. 2 (2003) 457–460.

[194] K. Liu, X. Yao, L. Jiang, Recent developments in bio-inspired special wettability, Chem. Soc. Rev. 39 (2010) 3240–3255.

[195] B. Bhushan, Y.C. Jung, Natural and biomimetic artificial surfaces for superhydrophobicity, self-cleaning, low adhesion, and drag reduction, Prog. Mater. Sci. 56 (2011) 1–108.

[196] N. Sharifi, F. Ben Ettouil, M. Mousavi, M. Pugh, C. Moreau, A. Dolatabadi, Superhydrophoibcity and Water Repelling Characteristics of Thermally Sprayed Coatings, in: Int. Therm. Spray Conf. Expo., ASM, (2013).

[197] R. Wang, K. Hashimoto, A. Fujishima, M. Chikuni, E. Kojima, A. Kitamura, et al., Light-induced amphiphilic surfaces, Nature. 388 (1997) 431.

[198] U. Diebold, The surface science of titanium dioxide, Surf. Sci. Rep. 48 (2003) 53–229.

[199] M.M. Gentleman, J.A. Ruud, Role of Hydroxyls in Oxide Wettability, Langmuir. 26 (2010) 1408–1411.

[200] C.-H. Xue, S.-T. Jia, H.-Z. Chen, M. Wang, Superhydrophobic cotton fabrics prepared by sol–gel coating of TiO_2 and surface hydrophobization, Sci. Technol. Adv. Mater. 9 (2008) 35001–5.

[201] B. CHEN, L.I. Chang-Jiu, T. GUO, Y.A.O. Jian-Tao, Y. Guan-Jun, L.I. Cheng-Xin, Mimic Lotus Surface with Super-Hydrophobicity Prepared through Surface-Molten Particle Deposition by flame spraying Assisted with Modification, National Lecture Conference Proceedings. 96 (2012) 57–58.

[202] C. Dorrer, J. Rühe, Some thoughts on superhydrophobic wetting, Soft Matter. 5 (2009) 51.

[203] R.E. Johnson, R.H. Dettre, Contact Angle Hysteresis. III. Study of an Idealized Heterogeneous Surface, J. Phys. Chem. 68 (1964) 1744–1750.

[204] A.B. Gurav, S.S. Latthe, R.S. Vhatkar, J.G. Lee, D.Y. Kim, J.J. Park, et al., Superhydrophobic surface decorated with vertical ZnO nanorods modified by stearic acid, Ceram. Int. 40 (2014) 7151–7160.

[205] A. Haddadi, F. Nardou, A. Grimaud, P. Fauchais, Generation of the first layers of a zirconia plasma sprayed coating: Correlation between splat layering and spraying parameters, in: ASM International, Materials Park, OH (United States), United States, (1995).

[206] R. Vaßen, H. Kaßner, A. Stuke, F. Hauler, D. Hathiramani, D. Stöver, Advanced thermal spray technologies for applications in energy systems, Surf. Coatings Technol. 202 (2008)

4432–4437.

[207] J. Sauter, Determining size of drops in fuel mixture of internal combustion engines, (1926).

[208] M. Miwa, A. Nakajima, A. Fujishima, K. Hashimoto, T. Watanabe, Effects of the Surface Roughness on Sliding Angles of Water Droplets on Superhydrophobic Surfaces, Langmuir. 16 (2000) 5754–5760.

[209] X. Zhang, M. Järn, J. Peltonen, V. Pore, T. Vuorinen, E. Levänen, et al., Analysis of roughness parameters to specify superhydrophobic antireflective boehmite films made by the sol-gel process, J. Eur. Ceram. Soc. 28 (2008) 2177–2181.

[210] B. Bhushan, Y.C. Jung, Micro- and nanoscale characterization of hydrophobic and hydrophilic leaf surfaces, Nanotechnology. 17 (2006) 2758–2772.

[211] N.D. Boscher, V. Vaché, P. Carminati, P. Grysan, P. Choquet, A simple and scalable approach towards the preparation of superhydrophobic surfaces – importance of the surface roughness skewness, J. Mater. Chem. A. 2 (2014) 5744.

[212] A.F. Stalder, G. Kulik, D. Sage, L. Barbieri, P. Hoffmann, A snake-based approach to accurate determination of both contact points and contact angles, Colloids Surfaces A Physicochem. Eng. Asp. 286 (2006) 92–103.

[213] A.F. Stalder, T. Melchior, M. Müller, D. Sage, T. Blu, M. Unser, Low-bond axisymmetric drop shape analysis for surface tension and contact angle measurements of sessile drops, Colloids Surfaces A Physicochem. Eng. Asp. 364 (2010) 72–81.

[214] L. Chen, Z. Xiao, P.C.H. Chan, Y.-K. Lee, Z. Li, A comparative study of droplet impact dynamics on a dual-scaled superhydrophobic surface and lotus leaf, Appl. Surf. Sci. 257 (2011) 8857–8863.

[215] D.-Y. Kim, J.-G. Lee, B.N. Joshi, S.S. Latthe, S.S. Al-Deyab, S.S. Yoon, Self-cleaning superhydrophobic films by supersonic-spraying polytetrafluoroethylene–titania nanoparticles, J. Mater. Chem. A. 3 (2015) 3975–3983.

[216] H. Yoon, H. Kim, S.S. Latthe, M. Kim, S. Al-Deyab, S.S. Yoon, A highly transparent self-cleaning superhydrophobic surface by organosilane-coated alumina particles deposited via electrospraying, J. Mater. Chem. A. 3 (2015) 11403–11410.

[217] R.C. Tucker, P.S.T. Inc, Thermal Spray Coatings, Handb. Surf. Eng. (1993) 1446–1471.

[218] J.R. Davis, Handbook pf Thermal Spray Technology, ASM International, (2004).

[219] L. Pawlowski, The Science and Engineering of Thermal Spray Coatings, 2008.

[220] H.I. Faraoun, T. Grosdidier, J.L. Seichepine, D. Goran, H. Aourag, C. Coddet, et al., Improvement of thermally sprayed abradable coating by microstructure control, Surf. Coatings Technol. 201 (2006) 2303–2312.

[221] M.S. Mahdipoor, F. Tarasi, C. Moreau, A. Dolatabadi, M. Medraj, HVOF sprayed coatings of nano-agglomerated tungsten-carbide/cobalt powders for water droplet erosion application, Wear. 330–331 (2015) 338–347.

[222] D.U. Toma, W. Brandl, G. Marginean, Wear and corrosion behaviour of thermally sprayed cermet coatings.pdf, Surf. Coatings Technol. 138 (2001) 149–158.

[223] M. Mohanty, R.W. Smith, M. De Bonte, J.P. Celis, E. Lugscheider, Sliding wear behavior of thermally sprayed 75/25 Cr3C2/NiCr wear resistant coatings, Wear. 198 (1996) 251–266. doi:10.1016/0043-1648(96)06983-9.

[224] N. Sharifi, M. Pugh, C. Moreau, A. Dolatabadi, Developing hydrophobic and superhydrophobic TiO_2 coatings by plasma spraying, Surf. Coatings Technol. (2016).

[225] M. Aghasibeig, A. Dolatabadi, R. Wuthrich, C. Moreau, Three-dimensional electrode coatings for hydrogen production manufactured by combined atmospheric and suspension plasma spray, Surf. Coatings Technol. 291 (2016) 348–355.

[226] M. Aghasibeig, C. Moreau, A. Dolatabadi, R. Wuthrich, Fabrication of nickel electrode coatings by combination of atmospheric and suspension plasma spray processes, Surf. Coatings Technol. 285 (2016) 68–76.

[227] C. Peng, S. Xing, Z. Yuan, J. Xiao, C. Wang, J. Zeng, Preparation and anti-icing of superhydrophobic PVDF coating on a wind turbine blade, Appl. Surf. Sci. 259 (2012) 764–768.

[228] J. Durret, N. Frolet, C. Gourgon, Hydrophobicity and anti-icing performances of nanoimprinted and roughened fluoropolymers films under overcooled temperature, Microelectron. Eng. 155 (2016) 1–6.

[229] G. Azimi, H.-M. Kwon, K.K. Varanasi, Superhydrophobic surfaces by laser ablation of rare-earth oxide ceramics, MRS Commun. 4 (2014) 1–5.

[230] P. Fauchais, M. Fukumoto, A. Vardelle, M. Vardelle, Knowledge Concerning Splat Formation: An Invited Review, J. Therm. Spray Technol. 13 (2004) 337–360.

[231] C. Moreau, P. Gougeon, M. Lamontagne, V. Lacasse, G. Vaudreuil, P. Cielo, On-line control of the plasma spraying process by monitoring the temperature, velocity, and trajectory of in-flight particles, ASM International, Materials Park, OH (United States), (1994).

[232] C. Moreau, Towards a better control of thermal spray processes, National Research Council Canada, Industrial Materials Institute, (1997).

[233] G. Mauer, R. Vaßen, D. Stöver, Comparison and applications of DPV-2000 and accuraspray-g3 diagnostic systems, J. Therm. Spray Technol. 16 (2007) 414–424.

[234] Z. Li, Y. Zheng, L. Cui, Preparation of metallic coatings with reversibly switchable wettability based on plasma spraying technology, J. Coatings Technol. Res. 9 (2012) 579–587.

[235] R. Jaworski, L. Pawlowski, F. Roudet, S. Kozerski, A. Le Maguer, Influence of suspension plasma spraying process parameters on TiO 2 coatings microstructure, J. Therm. Spray Technol. 17 (2008) 73–81.

[236] E. Moreau, C. Chazelas, G. Mariaux, A. Vardelle, Modeling the Restrike Mode Operation of a DC Plasma Spray Torch, J. Therm. Spray Technol. 15 (2006) 524–530.

[237] J.I. Rosales-Leal, M.A. Rodríguez-Valverde, G. Mazzaglia, P.J. Ramón-Torregrosa, L. Díaz-Rodríguez, O. García-Martínez, et al., Effect of roughness, wettability and morphology of engineered titanium surfaces on osteoblast-like cell adhesion, Colloids Surfaces A Physicochem. Eng. Asp. 365 (2010) 222–229.

[238] K. Vanevery, M.J.M. Krane, R.W. Trice, H. Wang, W. Porter, M. Besser, et al., Column formation in suspension plasma-sprayed coatings and resultant thermal properties, J. Therm. Spray Technol. 20 (2011) 817–828.

[239] P. Sokolowski, L. Pawlowski, D. Dietrich, T. Lampke, D. Jech, Advanced Microscopic

Study of Suspension Plasma-Sprayed Zirconia Coatings with Different Microstructures, J. Therm. Spray Technol. 25 (2016) 94–104.

[240] F.-L. Toma, G. Bertrand, D. Klein, C. Coddet, C. Meunier, Nanostructured photocatalytic titania coatings formed by suspension plasma spraying, J. Therm. Spray Technol. 15 (2006) 587–592.

[241] W.J. Baars, R.O. Stearman, C.E. Tinney, A review on the impact of icing on aircraft stability and control., J. Aeroelasticity 2 (2010) 35–52.

[242] C. Antonini, M. Innocenti, T. Horn, M. Marengo, A. Amirfazli, Understanding the effect of superhydrophobic coatings on energy reduction in anti-icing systems, Cold Reg. Sci. Technol. 67 (2011) 58–67.

[243] E.J.Y. Ling, V. Uong, J.S. Renault-Crispo, A.M. Kietzig, P. Servio, Reducing Ice Adhesion on Nonsmooth Metallic Surfaces: Wettability and Topography Effects, ACS Appl. Mater. Interfaces. 8 (2016) 8789–8800.

[244] S. Bengaluru Subramanyam, V. Kondrashov, J. Rühe, K.K. Varanasi, Low Ice Adhesion on Nano-Textured Superhydrophobic Surfaces under Supersaturated Conditions, ACS Appl. Mater. Interfaces. 8 (2016) 12583–12587.

[245] D.K. Sarkar, M. Farzaneh, Superhydrophobic Coatings with Reduced Ice Adhesion, J. Adhes. Sci. Technol. 23 (2009) 1215–1237.

[246] G. Momen, R. Jafari, M. Farzaneh, Ice repellency behaviour of superhydrophobic surfaces: Effects of atmospheric icing conditions and surface roughness, Appl. Surf. Sci. 349 (2015) 211–218.

[247] S. Zheng, C. Li, Q. Fu, W. Hu, T. Xiang, Q. Wang, et al., Development of stable superhydrophobic coatings on aluminum surface for corrosion-resistant, self-cleaning, and anti-icing applications, Mater. Des. 93 (2016) 261–270.

[248] Z.J. Wang, D.J. Kwon, K. Lawrence DeVries, J.M. Park, Frost formation and anti-icing performance of a hydrophobic coating on aluminum, Exp. Therm. Fluid Sci. 60 (2015) 132–137.

[249] C. Laforte, A. Beisswenger, Icephobic Material Centrifuge Adhesion Test, Proc. Int. Work.

Atmos. Icing Struct. (IWAIS XI). (2005) 1–5.

[250] J. Chen, J. Liu, M. He, K. Li, D. Cui, Q. Zhang, et al., Superhydrophobic surfaces cannot reduce ice adhesion, Appl. Phys. Lett. 101 (2012) 111603.

[251] I. Malavasi, I. Bernagozzi, C. Antonini, M. Marengo, Assessing durability of superhydrophobic surfaces, Surf. Innov. 3 (2014) 49–60.

[252] N. Sharifi, F. Ben Ettouil, C. Moreau, A. Dolatabadi, M. Pugh, Engineering surface texture and hierarchical morphology of suspension plasma sprayed TiO 2 coatings to control wetting behavior and superhydrophobic properties, Surf. Coatings Technol. 329 (2017) 139–148.

[253] D. De Pauw, A. Dolatabadi, Effect of Superhydrophobic Coating on the Anti-Icing and Deicing of an Airfoil, J. Aircr. 54 (2017) 490–499.

[254] L. Xu, D. Zhu, X. Lu, Q. Lu, Transparent, thermally and mechanically stable superhydrophobic coating prepared by an electrochemical template strategy, J. Mat. Chem. A. 2015;3(7):3801-7..

[255] X. Deng, L. Mammen, Y. Zhao, P. Lellig, K. Müllen, C. Li, et al., Transparent, thermally stable and mechanically robust superhydrophobic surfaces made from porous silica capsules, Adv. Mater. 23 (2011) 2962–2965.

[256] X. Deng, L. Mammen, H.-J. Butt, D. Vollmer, Candle Soot as a Template for a Transparent Robust Superamphiphobic Coating, Science (80-.). 335 (2012) 67 LP-70.

[257] A. Standard, G73, 2010, Standard test method for liquid impingement erosion using rotating apparatus, (2010).

[258] M.S. Mahdipoor, D. Kevorkov, P. Jedrzejowski, M. Medraj, Water droplet erosion mechanism of nearly fully-lamellar gamma TiAl alloy, Mater. Des. 89 (2016) 1095–1106.

Appendix: Studying the Wetting Behavior of Rare-Earth Oxides

Introduction

It was discussed in literature review of Chapter 2, that the only known materials with intrinsic hydrophobicity i.e. the static contact angle of a smooth sample of these materials is larger than 90°, are hydrocarbon and polymeric materials. An exception to this is the arguable case of rare-earth oxides. In some recent publications [142–144], some or all of the rare-earth oxides have been reported to be intrinsically hydrophobic. However these reports have been disputed in other publications [145,146] by arguing that environmental contamination is the main reason for apparent hydrophobicity of rare-earth oxides. The first such observation have been reported by Lawrence et al. [147] of cerium dioxide (CeO_2) membranes showing a contact angle of around 120°. Martinez et al. [148] have reported contact angle ranging from 94° to 134° for electrodeposited CeO_2.

One of the most prominent report of intrinsic hydrophobicity of rare-earth oxides has been made by Azimi et al. [149] about pressed and sintered samples of all rare-earth oxides. However, in this work the reported wetting parameter is the advancing contact angle and not the static contact angle and it must be noted that having an advancing contact angle of larger than 90° does not necessarily mean that the static contact angle is also larger than 90°. Preston et al. [150] have made a counterargument that once properly cleaned and contamination-free, rare-earth oxides are in fact hydrophilic and their apparent hydrophobicity is due to adsorption of hydrocarbon groups from exposure to ambient air. In a later publication, coauthored by Azimi, Khan et al. [151] respond to Peterson et al. [150] by claiming that rare-earth oxides demonstrate hydrophilicity due to surface oxygen content exceeding the stoichiometric ratio. They demonstrate this by showing that a freshly sputtered CeO_2 with a surface O/Ce ratio of around 3 is hydrophilic, but after being left in ultra-high vacuum, the surface O/Ce ratio reduces to around 2.2, showing hydrophobicity.

Even though the subject of intrinsic hydrophobicity of rare-earth oxides seems debatable, it could potentially offer a significant solution to the issue of durability of superhydrophobic coatings. A ceramic material such as a rare-earth oxide is naturally much more durable compared to polymeric and hydrocarbon alternatives. However, as mentioned before it is not clear whether or not rare-earth oxide demonstrate hydrophobicity at all or just in some conditions and therefore this topic is further investigated in this work in an effort to find an answer.

Methodology

Two feedstock powders were used in this research. The first powder was a samarium-doped cerium oxide (ceria) powder (Fuel Cell Materials, US) with chemical formulation of $Sm_{0.2}Ce_{0.8}O_2$ and nominal particles size of 0.1-0.4 μm. The second powder was an ytterbium oxide (ytterbia - Yb_2O_3) powder (Treibacher, Autria) with a nominal particle size of 1 μm. Two suspensions were prepared using these two powders in ethanol. These suspensions were plasma sprayed on grit-blasted in conditions similar to the TiO_2 coatings discussed in Chapter 4. Additionally, thicker coatings were made by spraying 100 passes deposition. Contact angle of these coatings were then measured. These coating were placed in the chamber of an XPS system to measure the atomic oxygen to metal ratio on their surface. After the first measurement, the surface of the coatings were sputtered by ion beam to clean their surfaces and devoid them from contamination. After sputtering, a second measurement of surface oxygen to metal ration was performed and then the samples were left in ultra-high vacuum for 20 hours after which a third test was performed on them. Then, the contact angle of the samples was measured. Also as an experiments, samples of the ceria and ytterbia coatings were put into a conventional vacuum chamber with a mechanical vacuum pump and were left there with the pump continuously working for 24 hours. The contact angle of the coatings was measured afterwards.

Furthermore, in order to assess the hydrophobicity of the feedstock powders, dry-pressed disc-shaped samples of the two powders and three combinations of the two powders with 25 at% ceria, 50 at% ceria and 75 at % ceria were made. These samples were sintered at 1800°C for 10 hours to create compact disc-shaped samples. The contact angle of these samples was measured afterwards. Also the samples were cleaned by boiling in water and air drying according to Gentleman et al. [199] to remove any potential hydrocarbon contamination and then their contact angle was measured again.

Results

Both ceria and ytterbia SPS coatings demonstrate hydrophilicity as sprayed. In fact, since both of these coatings have micro-textures with many pores, a water droplet placed on the surface spreads and wets the surface completely, making it impossible to measure the static contact angle. SEM micrographs of the two of the SPS ceria coatings is shown in Figure A.1 and Figure A.2. In Figure A.1, it is clear that the hierarchical morphology observed in SPS TiO_2 coatings is absent. This is likely due to the fact that the process parameters were not optimized for the ceria suspension feedstock. However, the type of "cauliflower-like" surface features are present but are relatively much larger than the ones previously observed in SPS TiO_2 coatings. When treated by a stearic acid solution for lowering the surface energy, both SPS ceria and ytterbia coating show superhydrophobicity with contact angles higher than 160° and sliding angles smaller than 10°.
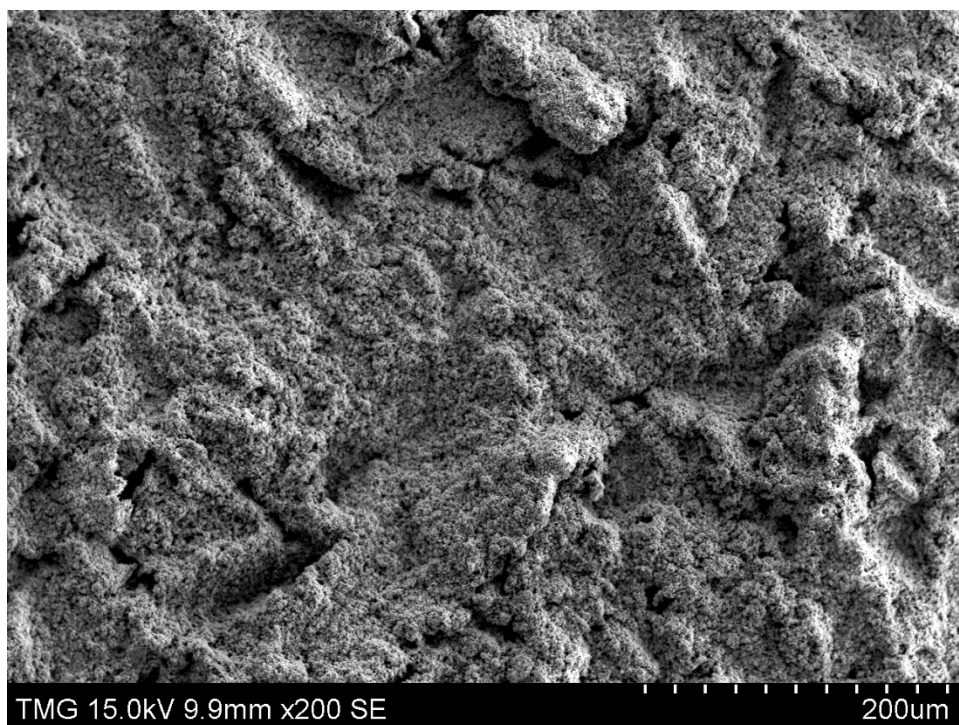
Figure A.1. SEM micrograph of the ceria SPS coating.

The XPS results indicating oxygen to metal ratio at the surface of SPS ceria and ytterbia coatings, before sputtering, after sputtering and after 24 hours in ultra-high vacuum are presented in Table A.1. This was done to investigate the claim by Khan et al. [151] that intrinsic hydrophobicity of rare-earth oxides depends on oxygen to metal ratio on the surface and if this ratio is close to the stoichiometry ratio, then rare-earth oxide demonstrate intrinsic hydrophobicity.
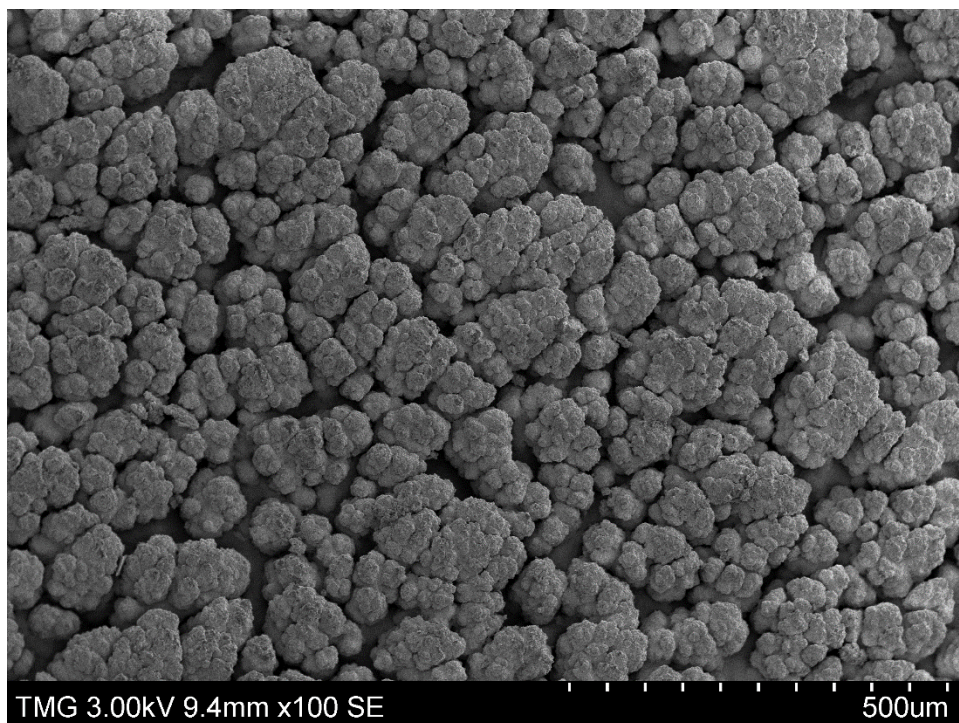
Figure A.2. SEM micrograph of the ceria SPS coating, made through depositing 100 passes.

As presented in Table A.1, for the ceria sample, initially the O/Ce is very close to the stoichiometry value i.e. 2. After sputtering the ratio decreases to 1.75 and after 24 hours in ultra-high vacuum, it increases to 1.85. Also looking at ratio of Ce^{4+} to Ce^{3+} shows that initially at the surface of the coating all cerium atoms are present in +4 oxidation state. Majority of the cerium atoms change their oxidation state to +3 after sputtering and the some of them return to +4 state after 24 hours exposure to ultra-high vacuum. It is noteworthy that the wetting behavior of the ceria coatings did not change after these tests.

For ytterbia coating, the O/Yb is higher than stoichiometry i.e. 1.5 in the beginning but decreases to the 1.5 stoichiometry value after sputtering and remains constant after 24 h in ultra-high vacuum. All ytterbium atoms are and remain in +3 oxidation state. Similar to ceria coatings, the ytterbia coating do not show any change in wetting behavior after these tests. It can be concluded that SPS ceria and ytterbia coatings do not demonstrate intrinsic hydrophobicity even after exposure to ultra-high vacuum and when the surface oxygen to metal ratio is very close to the stoichiometry ratio.

Table A.1. XPS test results for the SPS ceria and ytterbia coatings.

	SPS ceria coating		SPS ytterbia coating	
	O/Ce	$Ce^{4+}:Ce^{3+}$	O/Yb	$Yb^{3+}:Yb^{2+}$
Before sputtering	1.98	100:0	1.9	100:0
Immediately after sputtering	1.75	13:87	1.5	100:0
After 24 hours exposure to ultra-high vacuum	1.85	49:51	1.5	100:0

In Table A.2, contact angle of sintered samples of ceria, ytterbia and their mixtures is presented, as prepared and after cleaning in boiling water. None of the samples show hydrophobicity initially, but their contact angles are relatively high. However, after cleaning in boiling water, the contact angle values decrease significantly for all samples which indicates that initial contact angle values are affected by presence of contaminating hydrocarbon compounds on the surface and after these compounds are removed, all sample are unmistakably hydrophilic.

Table A.2. Water contact angle (CA) of sintered samples of ceria, ytterbia and their mixtures.

Sample	100 at% ceria	75 at% ceria − 25 at% ytterbia	50 at% ceria − 50 at% ytterbia	25 at% ceria − 75 at% ytterbia	100 at% ytterbia
CA as sintered	75°	73°	77°	82°	87°
CA after cleaning	33°	35°	41°	32°	39°

At last, the SPS ceria and ytterbia coatings were left in a vacuum chamber at a medium vacuum of about 1000 Pa for 24 hours while the vacuum pump was continuously running. After this, samples showed superhydrophobicity with contact angles higher than 160° and sliding angles smaller than 10°. It is speculated that this happens due to contamination of samples by the oil from the vacuum pump. A similar experiment but with the vacuum pump turned off after the vacuum has been reached show that the wetting behavior of coatings does not change if the pump is not

continuously working. Additionally, cleaning the superhydrophobic samples in boiling water removed their superhydrophobicity and return then to initial hydrophilic state, indicating the apparent hydrophobicity was a result of contamination.

Conclusion

No evidence was found to support the claim that rare-earth oxides demonstrate intrinsic hydrophobicity in certain condition. Any hydrophobic behavior was result of surface contamination by adsorbing hydrocarbon compounds from environment or by oil vapor from the vacuum pump. The results presented here are part of an ongoing research, and are not definitively conclusive. However, it seems that these results strongly support the hypothesis that observed and reported hydrophobicity of rare-earth oxides could be result of surface contamination and these reports require further re-examination and reaffirmation.